Journal of Engineering and Technology for Industrial Applications

ISSN 2447-0228

June 2020 Volume 06 / No 23

Editor-in-Chief: J. C. Leite

www.itegam-jetia.org

ITEGAM - JETIA ISSN 2447-0228 Online
Journal of Engineering and Technology for Industrial Applications (JETIA)

O **JETIA– Journal of Engineering and Technology for Industrial Applications (JETIA)** is a publication of the Galileo Institute of Technology and Education of the Amazon (ITEGAM), located in the city of Manaus since 2008. JETIA publishes original scientific articles covering all aspects of engineering. Our goal is the dissemination of research original, useful and relevant presenting new knowledge on theoretical or practical aspects of methodologies and methods used in engineering or leading to improvements in professional practice. All the conclusions presented in the articles It should be state-of-the-art and supported by current rigorous analysis and balanced assessment. Public magazine scientific and technological research articles, review articles and case studies.
JETIA will address topics from the following areas of knowledge: Mechanical Engineering, Civil Engineering, Materials and Mineralogy, Geosciences, Environment, Information and Decision Systems, Processes and Energy, Electrical and Automation, Mechatronics, Biotechnology and other Engineering related areas.

Publication Information:
ITEGAM-JETIA (ISSN 2447-0228), (online) is published by Galileo Institute of Technology and Education of the Amazon on a every two months (February, April, June, August, October and December).

Contact information:

Web page: www.itegam-jetia.org
Email: article@itegam-jetia.org, editor@itegam-jetia.org
Galileo Institute of Technology and Education of the Amazon (ITEGAM).

Joaquim Nabuco Avenue, No. 1950. Center. Manaus, Amazonas. Brazil.
Zip Code: 69020-031. Phone: (92) 3584-6145.

Previous Notice
All statements, methods, instructions and ideas are the sole responsibility of the authors and do not necessarily represent the view of ITEGAM -JETIA. The publisher is not responsible for any damage and / or damage to the use of the contents of this journal. The concepts and opinions expressed in the articles are the sole responsibility of the authors.

Directory

ITEGAM - JETIA
ISSN 2447-0228 Online
Journal of Engineering and Technology for Industrial Applications (JETIA)

JETIA. Vol. 06, No. 23. June of 2020. Manaus - Amazonas, Brazil. ISSN 2447-0228 (ONLINE)
https://www.itegam-jetia.org

SUMMARY

Journal of Engineering and Technology for Industrial Applications, 2020. Edition. 23. Vol: 06
https://www.itegam-jetia.org
ISSN ONLINE: 2447-0228
DOI: https://dx.doi.org/10.5935/2447-0228.20200017

RESEARCH ARTICLE OPEN ACCESS

OBJECT DEFECT DETECTION BASED ON A VISION SYSTEM WITH A MICROCONTROLLER AND AN ARTIFICIAL NEURAL NETWORK

Ingrid Martins Valente Costa[1], Lorena Cândida Mendonça[2], Miguel Gonçalves de Freitas[3], Talles Marcelo Gonçalves de Andrade Barbosa[4] and Symone Gomes Soares Alcalá[5]

[1, 2, 3, 5] Federal University of Goiás – UFG, Aparecida de Goiânia – Goiás, Brazil.
[4] Pontifical Catholic University of Goiás – PUC Goiás, Goiânia – Goiás, Brazil.

Email: ingridmvalente@gmail.com, lorena.candida12@gmail.com, miguel.goncalves.freitas@gmail.com, talles.ucg@gmail.com, symonesoares@gmail.com

Received: Jun 22th, 2019

Accepted: Jun 15th, 2020

Published: June 30th, 2020

ABSTRACT

Vision systems have been widely employed in industries to automate the inspection process in products. Their use provides standardized, reliable and accurate inspections when compared to a human operator. Vision systems pass to machines the ability to view and automatically extract features in order to indicate abnormalities in products. This paper proposes a vision system for capturing and preprocessing digital images, besides classifying objects with defect and objects without defect using an Artificial Neural Network model. As a case study, digital images of boxes are acquired and classified on a conveyor belt. Tests reveal that the proposed system is able to classify accurately a box with defect and a box without defect in real time. The main contribution of this paper is the proposal of a system that performs automated inspections in products, in order to detect abnormalities, and it can be easily coupled, modularly, to the existing industrial platforms.

Keywords: Neural network applications, Machine vision, Quality assurance, Microcontroller, Image classification.

I. INTRODUCTION

In an industry, ensuring the quality of products and processes, through the optimization and automation of production lines, is indispensable for its success. In most cases, the quality of products is mainly related to the absence of defects and their occurrence can affect the credibility of a company. In this sense, one way of verifying product conformity is by performing visual inspection.

The visual inspection allows detecting abnormalities in the products in order to attend the rules and expectations of consumers. Generally, it is performed manually, resulting in high costs, failures and difficulties in standardization. With the evolution of the new technologies, vision systems have made possible the realization of automated inspections [1, 2]. Vision systems can automatically extract characteristics and indicate abnormalities in products. For example in [3] proposed a vision system to identify humans and cars in a real time video surveillance system.

In manufacturing systems, vision systems enable accuracy and repeatability in non-contact measurements by suppressing factors such as subjectivity, fatigue, vagueness and costs inherent to the human inspection [4]. Therefore, they are more efficient, safer and faster because they certify the quality of the product, since they go beyond the human capacity for visual detection.

A vision system can be divided into the following phases: image acquisition, segmentation, image improvement, feature extraction and pattern recognition [5]. Acquisition involves capturing the digital image of product. Segmentation and improvement are employed, respectively, to highlight the relevant portion and to increase image quality. Both steps eliminate aspects such as noise, which could jeopardize later steps. Feature extraction involves capturing relevant information about the segmented image that is essential for the product classification. The last phase is done by classification algorithms, which use the characteristics extracted to classify products according to a set of categories, such as, product with defect and product without defect.

The image acquisition step can be done using microcontrollers [6]. Microcontrollers have made it possible to create low-cost computing applications. They are a kind of "computers" that can be programmed to control circuits and perform specific tasks using previously elaborated commands. In addition to being easily programmable most of the times and taking up little physical space, microcontrollers are being increasingly targeted because of the low cost.

Therefore, professionals with knowledge on the handling of these devices are being increasingly demanded. In addition, microcontrollers have been used to control apparatus, answering machines, photocopiers, medical instruments, among others. Although microcontrollers are feasible in many applications, few studies in the production engineering contemplate their use.

Classification algorithms are mainly developed using artificial intelligence methods. Through these methods, intelligent agents can be created to perform tasks that require intelligence when done by humans [7]. According to [8], the artificial intelligence methods used for pattern recognition are mainly implemented using statistical approaches, syntactic/structural approach, Artificial Neural Networks (ANNs), fuzzy logic model and hybrid models. Among these, ANNs stand out for their fault tolerance. For example, in [9] developed an ANN to classify defects in the color and texture of oranges. Currently, most vision systems recognize color patterns and few are able to recognize defects.

Thus, this paper proposes a vision system for capturing and preprocessing digital images, besides classifying objects with defect and objects without defect using an ANN model, trained by the Scaled Conjugate Gradient Backpropagation (SCGB) algorithm. For this purpose, the following phases of the vision system are performed: image acquisition using a Logitech HD Webcam C270, segmentation using the Otsu's method, improvement by median filtering, feature extraction using co-occurrence matrix, and pattern recognition by the ANN model. As a case study, digital images of boxes are acquired and classified on a conveyor belt. Experimental results reveal that the proposed system vision is able to classify accurately the box with defect and box without defect in the conveyor belt.

The main contribution of this paper is to propose a vision system that performs automated inspections in products, in order to detect abnormalities, and it can be easily coupled, modularly, to the existing industrial platforms, as it only needs to incorporate a simple Webcam to the existing machinery. For this purpose, a small scale vision system was built to simulate the environment and conditions of the conveyor belt operation. Another contribution is that the proposed system does not require calibration, since through machine learning and ANN training, it does not require human interventions for maintenance purposes. Moreover, this paper performs a survey about the use of microcontrollers in production engineering applications in Brazil.

The rest of this paper is organized as follows. Section II describes the use of microcontrollers in production engineering applications in Brazil, and details the Arduino board. Section III describes the ANN model, its main architectures and the SCGB algorithm. Section IV details the proposed vision system and its main steps. Section V shows the experimental results of the proposed vision system using images acquired from a conveyor belt. And finally, Section VI presents some concluding remarks.

II. MICROCONTROLLERS

This Section discusses the use of microcontrollers in the production engineering area in Brazil, as well as the main concepts of the Arduino board

II.1 THE USE OF MICROCONTROLLERS IN PRODUCTION ENGINEERING APPLICATIONS

Microcontrollers appeared around the 70s with the development of the Intel 4004 microprocessor [10]. Currently, Raspberry and Arduino are the most common. Raspberry and Arduino focus on teaching basic computer skills in schools, but Arduino is also used for automation applications industrial [11]. Applications that use microcontrollers are often called embedded systems, because they are programmable computers designed to perform a specific task, such as controlling the temperature of an air conditioner, printers, and other tasks [12].

According to [13], microcontrollers are basically composed of the following peripherals: initialization managers, input and output ports, serial communication, timers, analog comparators and, finally, EEPROM (Electrically-Erasable Programmable Read-Only Memory).

In Brazil, most of the production engineering applications involving the use of microcontrollers fall into the areas related to Innovation Management and Technology Management. For example, in [14] proposed the use of microcontrollers to control Automated Guided Vehicles (AGVs) in industrial transportation processes; and [15] created interfaces between microcontrollers and other software, which together can easily perform the acquisition of industrial sensor data.

Although microcontrollers are feasible in a range of applications in production engineering, in Brazil, few papers portray their use and importance, and highlight their advantages. To demonstrate this, a survey was performed on October/28/2018 on the basis of the annals of the National Meeting of Production Engineering (ENEGEP, most well-known production engineering conference in Brazil) from the years 2010 to 2017, by the website of the Brazilian Association of Production Engineering (ABEPRO), using the strings "microcontrolador" (in English, "microcontroller"), "Arduino", "Raspberry" and "sistema embarcado" (in English, "embedded system"). From the search, only 3 papers were found: one article in 2012 and two papers in 2016.

The paper of the ENEGEP 2012 was found with the string "embedded system", and it uses MINI2440 microcontroller to monitor electrical energy in industrial systems [16]. On the other hand, the two papers of the ENEGEP 2016 were found with the word ``Arduino", and the first paper optimizes the capture of light energy from solar tracking to reduce energy costs [17]; while the second paper optimizes the use of street lamps [18]. Therefore, all the papers are related to the electric power area.

Through this survey, it is noted the importance of developing this study with microcontrollers in the production engineering area, and of showing the relevance of this device that is little explored in the production engineering area in Brazil.

II.2 THE ARDUINO BOARD

According to [18], the Arduino is a prototyping board based on the Atmel AVR microcontrollers, which can be programmed from a specific programming language based on C and C++ languages. According to [19], a development platform, such as Arduino, is a physical computing platform and in it, digital

systems linked to other components measure variables in the physical environment, perform numerical calculations and can even make logical decisions, generating new variables in the environment physicist.

The abilities to control other physical devices and to receive and process data through an interface are advantages of using an electronic prototyping platform, such as Arduino. In addition, according to [20], the existence of several circuit boards, known as shields, that can be integrated with the Arduino to increase its capacity, is an advantage, since this capacity of expansion allows a range of applications of simple form and fast.

According to data from Eletrogate [21-24], Table 1 was developed. It presents the main Arduino boards available in the market and their corresponding microcontrollers, memory capacities, digital ports, analogue ports and clock speed (or CPU speed - Central Processing Unit).

As shown in Table 1, the Arduino Mega 2560 has the largest memory capacity and the largest number of digital and analog ports. Its larger number of ports, compared to the other Arduino boards, allows users to connect to a large number of devices, which can be advantageous in projects with a certain level of complexity.

Table 1: Comparison between the Arduino boards available on the market.

	NANO	**UNO**	**LEONARDO**	**MEGA 2560**
Micro-controller	ATmega 328	ATmega 328	ATmega32u4	ATmega2560
FLASH memory	32KB	32KB	32KB	256KB
EEPROM memory	1KB	1KB	1KB	4KB
SRAM memory	2KB	2KB	2.5KB	8KB
Number of digital ports	14	14	20	54
Number of analog ports	8	6	12	16
Clock velocity	16MHz	16MHz	16MHz	16MHz

Source: Author, (2019).

Therefore, this paper uses Arduino MEGA 2560 for the development of the vision system. This Arduino is based on the ATmega2560 microcontroller and has 5 volts of voltage. Figure 1 shows the Arduino MEGA 2560 board.

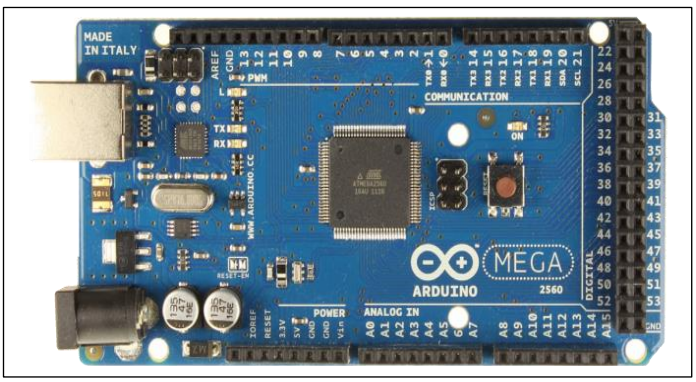

Figure 1: The Arduino MEGA 2560 board.
Source: Author, (2019).

III. ARTIFICIAL NEURAL NETWORKS

ANNs are artificial intelligence models inspired by biological neuron behaviors and have processing units, also known as neurons, and connections/weights between them, an architecture and a learning algorithm [7, 8]. After these steps, an output is generated and propagated to other neurons or to the environment [25].

The main characteristics of the ANN models are: *learning* - the ability of an ANN to initiate a learning without knowledge and be able to be trained using data; *generalization* - ability to generate the best output for an example not used in training; *massive potential parallelism* - neurons are triggered parallel throughout data processing; *robustness* - even if some neurons do not perform well, yet the whole system can work well; and *partial match* - which detonates that the known data does not exactly match with new events [26].

In literature, there are several types of ANN architectures, but Multilayer Perceptrons (MLPs), are the most popular ANN. They have one input layer, one or more hidden/intermediate layers and one output layer. In MLP, during estimation, the data propagates forward, from the input layer to the output layer. Researches have proved that MLPs are universal approximators [27]. For example, [28] demonstrated that any continuous function can be approximated by a continuous ANN having one hidden layer with neurons that use a sigmoidal non-linear activation function.

Single-hidden Layer Feedforward Networks (SLFNs) are MLPs with one hidden layer, and they have good approximation capabilities in many problems [29]. Therefore, the ANN models developed in this paper implement the SLFN architecture.

III.1 SINGLE-HIDDEN LAYER FEEDFORWARD NETWORK ARCHITECTURE

The SLFN architecture has an input layer with n_0 input neurons, an intermediate/hidden layer with n_1 hidden neurons, and an output layer with an output neuron, as shown in Figure 2.

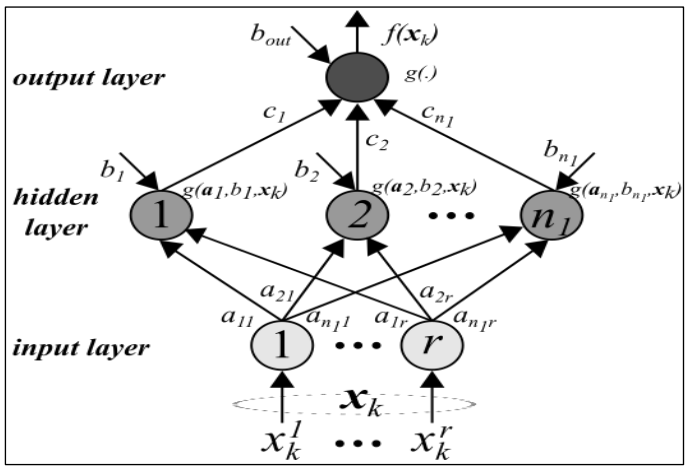

Figure 2: The SLFN architecture.
Source: Author, (2019).

Hidden neurons and output neurons have activation functions defined as $g(x)$. There are many activation functions including the *sigmoid* activation function, $g(x) = 1/(1 + \exp(-x))$, and the *linear* activation function $g(x) = x$. They perform a transformation as the last step to obtain the neuron's output value. To obtain the output value, consider a data set $\boldsymbol{D} = \{(\boldsymbol{x}_k, y_k)\}_{k=1}^{K}$ with K samples (with $x_k = [x_k^1, \cdots, x_k^R] \epsilon \mathbb{R}^R$, and

$y_k \in \{0,1\}$), a SLFN model with n_1 hidden neurons can be represented as:

SLFN model

$$f(\boldsymbol{x}_k) = g\left(\left(\sum_{j=1}^{n_1} g\left(\sum_{r=1}^{R} a_{jr}\, x_k^r + b_j\right) c_j\right) + b_{out}\right) = \hat{y}_k, \quad (1)$$

for $k = [1, \cdots, K]$; where $\boldsymbol{a}_j = [a_{j1}, \cdots, a_{jR}]^{\mathrm{T}}$ is the weight vector connecting the r input neuron and the j-th hidden neuron (for $j = [1, \cdots, n_1]$; $\boldsymbol{c} = [c_1, \cdots, c_{n_1}]^{\mathrm{T}}$ is the weights vector connecting the n_1 hidden neurons and the output neuron; b_j is the bias of the j-th hidden neuron; b_{out} is the bias in the output layer; and $\hat{y}_k$ is the output prediction. As it can be seen, the operation the neurons is guided by the introduction of the inputs, calculation of the weighted sum and application of activation functions. After these steps, an output is generated and propagated to other neurons or to the environment [25].

The weights of an ANN should be obtained using a learning algorithm in order to minimize the error in all the K samples. This process is performed in several iterations in order to obtain the final weights. This process, also known as learning process, stops when an established stop criterion is reached.

Many learning algorithms have been developed for the learning process. The most known algorithm is the Back-Propagation (BP) algorithm. It uses a gradient descent method to define the NN parameters [30]. But, in most problems, the BP algorithm may generate overfitting. To overcome this limitation, other algorithms were developed, such as the Scaled Conjugate Gradient Backpropagation (SCGB) algorithm [7]. Below, the SCGB algorithm is introduced.

III.2 THE SCALED CONJUGATE GRADIENT BACKPROPAGATION ALGORITHM

The SCGB algorithm is a faster version of the BP algorithm, where second order partial derivatives are used to change the learning rate [31]. The main objective of the SCGB algorithm is to associate the confidence region approach with the conjugate gradient approach. Thus, SCGB has a step size scaling feature, which avoids a delayed line search by learning iteration. The SCGB algorithm indicates a super linear convergence in many problems [31].

As other learning algorithms, the SCGB algorithm learns when a set of training samples (from the initial input data) is processed iteratively. The process is done by comparing the ANN's output prediction and the real output. This is performed using the mean squared error, so that to minimize the error, it is necessary to change the weights for each training sample [32].

The learning process of the SCGB neural network is performed using Equations (2) and (3):

SCGB neural network – step 1

$$Z_{i,k}^m = b_{0,i}^m + \sum_{j=1}^{n_{m-1}} w_{j,i}^m\, O_{j,k}^{m-1} \quad (2)$$

SCGB neural network – step 2

$$O_{j,k}^m = g\left(Z_{i,k}^m\right) \quad (3)$$

where $Z_{i,k}^m$ is the obtained output in the layer m and the neuron i using a sample k; $b_{0,i}$ is the threshold (bias) of a neuron i in a hidden layer m; $w_{j,i}^m$ is the weight between the layer m with the neuron j and the layer $m-1$ with the neuron i; $O_{j,k}^{m-1}$ is the output value of the layer $m-1$ and the neuron i using sample k [33].

The error between the real output and the predicted output of the ANN model can be calculated according to the formula:

ANN error

$$E = \frac{1}{2}\sum_{k=1}^{K}\sum_{j=1}^{n_2}\left(T_{j,k} - O_{j,k}^2\right)^2, \quad (4)$$

where $T_{j,k}$ is the expected/real output of the output layer in neuron j using a sample k; and $O_{j,k}^2$ is the predicted output of the output layer in neuron j using a sample k.

IV. PROPOSED VISION SYSTEM FOR DETECTING OBJECT DEFECTS

The proposed vision system automatically captures digital images of an object moving on a conveyor belt. Figure 3 shows the interaction between the components of the system. The hardware consists of a Logitech HD Webcam C270, a Notebook equipped with Intel Core i7 3.4GHz and 8GB RAM, an Arduino Mega 2560 microcontroller connected to a protoboard, conveyor belt and infrared sensor module.

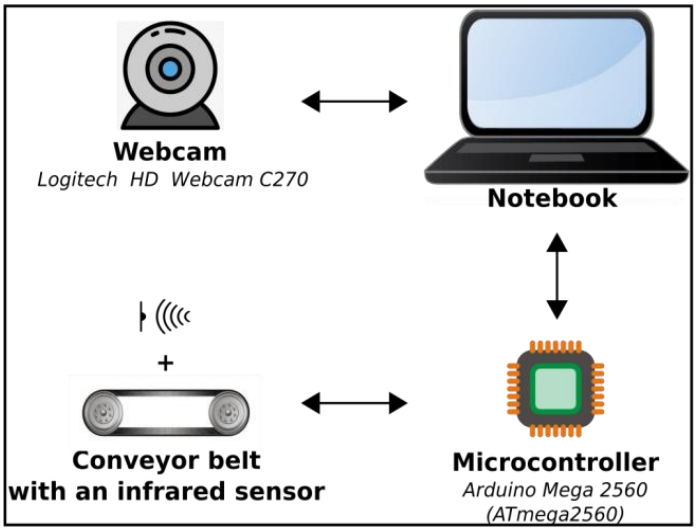

Figure 3: The main components of the proposed vision system.
Source: Author, (2019).

The software was developed in a MATLAB R2016a multi-platform environment, using the MATLAB Support Package for Arduino Hardware tool, which allows the integration and interaction between MATLAB and a microcontroller Arduino. The MATLAB R2016a also enables the processing of the acquired images of the objects, so that later they can be classified as object with defect and object without defect.

When the conveyor belt is activated, it transports an object (in this paper, a box), which is detected by an infrared sensor. When this occurs, a digital image of the object is captured and stored on the computer. If no object is on the conveyor belt, no action is performed.

Figure 4 shows the prototype of the vision system. It should be pointed that, if an object is detected, the software of the proposed vision system performs the following steps: image acquisition, segmentation, improvement, feature extraction and pattern recognition, as presented in Figure 5. The next Subsections detail each step of the proposed methodology.

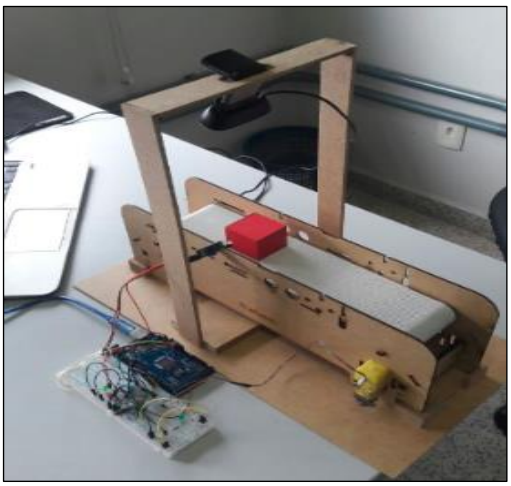

Figure 4: The prototype of the proposed vision system.
Source: Author, (2019).

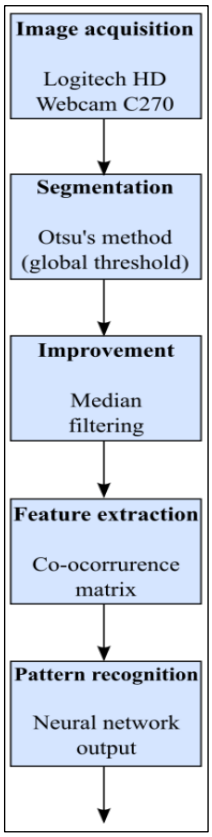

Figure 5: The steps the proposed vision system.
Source: Author, (2019).

IV.1 IMAGE ACQUISITION

The first step, *image acquisition*, obtains digital images of the boxes using the Logitech HD Webcam C270, with a resolution of 1280×960. The captured images are in the Red, Green and Blue (RGB) color system, which are then converted to the YCbCr color space.

In this case, the *Y* channel contains the luminance, the *Cb* channel contains the blue chrominance and the *Cr* channel contains the red chrominance. Moreover, the *Y* channel represents the light intensity and the *Cb* and *Cr* channels represent the colorization. The change in the color space is necessary to extract characteristics related to the luminance and chrominance of the digital images [9]. These characteristics are essential for segmenting images.

IV.2 SEGMENTATION

The *segmentation* step extracts the object from the portion considered as the background of the digital image. To do this, the Otsu's method is used [34]. It obtains a global threshold from the *Cr* channel a digital image. The threshold acts as a border, delimiting the space filled by the object and the space known as the background.

IV.3 IMPROVEMENT

The next step, *improvement*, generates digital images with higher quality, allowing a greater efficiency of the ANN learning algorithm. In this process, remaining noises of the segmentation process are eliminated using median filter, where each pixel of the image is replaced by the median of the neighborhood. In this paper, the adopted neighborhood is 5×5.

IV.4 FEATURE EXTRACTION

An efficient technique for extracting image texture information is the Gray Level Co-occurrence Matrix (GLCM), where the texture is classified by the spatial distribution of gray levels in a neighborhood. The matrix retracts the combinations of pixel brightness values (gray levels) in tabular form. It shows how often a pixel value with gray level u value occurs in relation to another pixel value, known as the neighbor pixel, with gray level v value. GLCM can be used to calculate texture characteristics such as contrast, entropy, energy and homogeneity.

The next step is to extract characteristics of the image. This is done by using GLCM, where contrast is the adopted characteristic [9]. In the GLCM method, for each channel, four co-occurrence matrices are determined employing distance equal to 1 and 4 directions, which are 0º, 45º, 90º and 135º.

Afterward, a contrast value is obtained using each matrix, totaling 12 characteristics. In addition, the average value of each channel is calculated. The calculated averages correspond to the general values of each channel in YCbCr of the segmented image. Thus, using an image, 15 characteristics (features) are obtained, and they will be used as inputs in the classification algorithm.

For the ANN training algorithm, it is necessary to create a data set consisting of two matrices, $\boldsymbol{X}$, the input matrix, and $\boldsymbol{X}$, the output matrix, where each column of them contains information about an acquired image. The input matrix $\boldsymbol{X}$ contains the features of all acquired images; while the output matrix $\boldsymbol{Y}$ contains the classes of all captured images.

The sizes of $\boldsymbol{X}$ and $\boldsymbol{Y}$ are $15 \times K$ and $2 \times K$, respectively, where K is the number of acquired images. For each image c, its 15 features, $x_{1,c}, \cdots, x_{15,c}]^{\mathrm{T}}$, are stored in a column of $\boldsymbol{X}$; and its class, $y_{1,c}, \cdots, y_{2,c}]^{\mathrm{T}}$, in a column of $\boldsymbol{Y}$. Being that, there are two distinct classes: class i - box without defect, and class ii - box with defect. For an image c belonging to the class i, the outputs are set as $y_{1,c} = 0$ and $y_{2,c} = 1$; while for an image c belonging to the class ii, the outputs are set as $y_{1,c} = 1$ and $y_{2,c} = 0$.

IV.5 PATTERN RECOGNITION

The pattern recognition step was developed using a SLFN trained with the SCGB algorithm, described in Subsection III.2. To do this, the data set was randomly divided in training data set (65%), testing data set (20%) and validation data set (15%); where the training data is used for the ANN training, the validation data is employed to verify ANN accuracy during the training and the

test data set is used to authenticate ANN accuracy after the training, using a data set which was not used in training.

After this process, the best number of neurons in the hidden layer (n_1) is determined. It was selected using the 10-fold cross-validation method that randomly divides a set of data $\boldsymbol{D}$ into 10 mutually exclusive subsets, $\boldsymbol{D}_1, \cdots, \boldsymbol{D}_{10}$. The hidden layer activation function is hyperbolic tangent sigmoid (tansing), while the output layer activation function is soft maximum (softmax).

The number of hidden neurons is selected by varying it in the interval of [2, 20]. This value is chosen based on the best performance on a 10-fold cross-validation using the training data set, where the best number of hidden neurons is chosen as the one that maximizes the mean testing performance on the 10-folds using the Mean Squared Error (MSE) [29].

For a specific value of hidden neuron, 10-fold cross-validation obtains the average of the predictive error values of the 10 subsets (each one being used as testing data set), while the other 9 sets are randomly divided into a set of data of training (75%) and validation (25%) [35, 36]. It is noted that the method selects the best number of hidden neurons that first shows the lowest percentage of incorrect classifications. Then an ANN with SLFN architecture is trained with the SCGB algorithm and the best number of hidden neurons.

V. EXPERIMENTAL RESULTS

This Section reports the main experimental results obtained with the ANN model (Subsection V.1), and the proposed vision system in real time operation (Subsection V.2).

V.1 ARTIFICIAL NEURAL NETWORK TRAINING

In this Subsection, the results described were obtained using MATLAB R2016a software. In the first step of the proposed methodology, digital images of boxes were acquired on a conveyor belt. Then, the camera (Logitech HD Webcam C270) acquired 430 images of the boxes, being that 215 images were obtained of a box with defect (defective box) and 215 images were captured of a box of without defect (nondefective box); where both boxes have shape of a cube, with edges of 3.5cm, and images captured in different angle and illumination conditions. The box with defect has paint defect on top surface.

Figures 6 and 7 show some images of the box without defect and some images of the box with defect, respectively. Figures 8 and 9 show the result of two images after the segmentation and improvement steps.

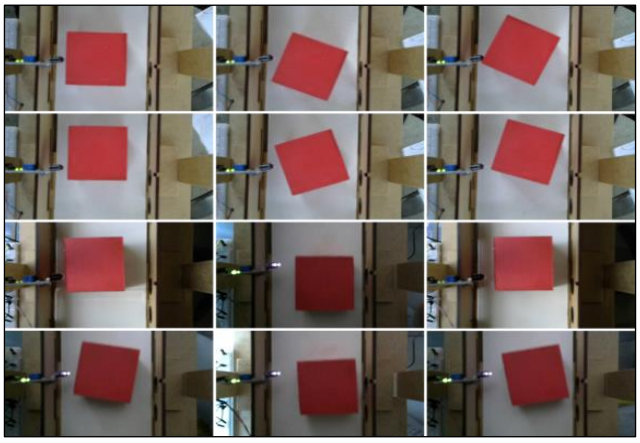

Figure 6: Some acquired images of the box without defect.
Source: Author, (2019).

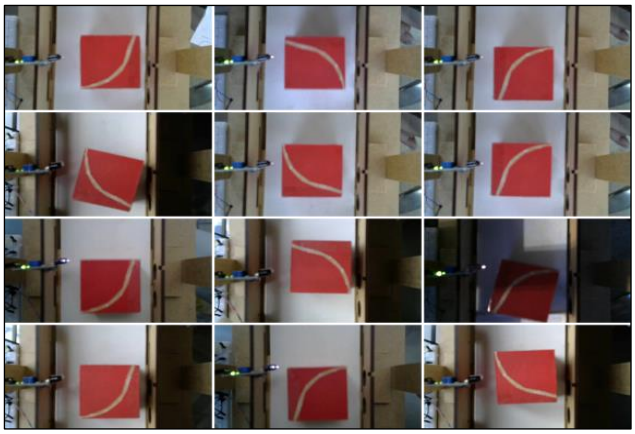

Figure 7: Some acquired images of the box with defect.
Source: Author, (2019).

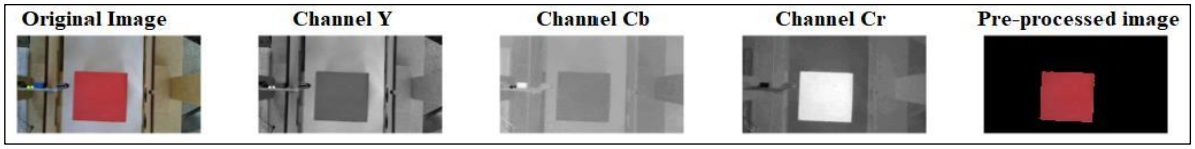

Figure 8: A preprocessed image of the box without defect.
Source: Author, (2019).

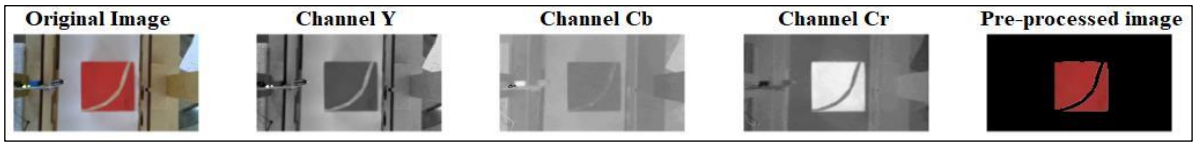

Figure 9: A preprocessed image of the box with defect.
Source: Author, (2019).

After the improvement step, the feature extraction step was performed and the data set resulting from the extraction was stored on an input matrix $\boldsymbol{X}$ of size 15×430 and an output $\boldsymbol{Y}$ matrix of size 2×430. Then, $\boldsymbol{X}$ and $\boldsymbol{Y}$ were used to training (65%), validate (15%) and test (20%) the ANN model. Furthermore, to determine the best number of hidden neurons in the hidden layer, the 10-fold cross-validation method was employed using only the training data. For further information, see Subsection IV.5.

The performance from 10-fold cross-validation method for each hidden neuron number is shown in Figure 10. The performance was measured using the average percentage (in the 10 test subsets) of incorrectly classified images.

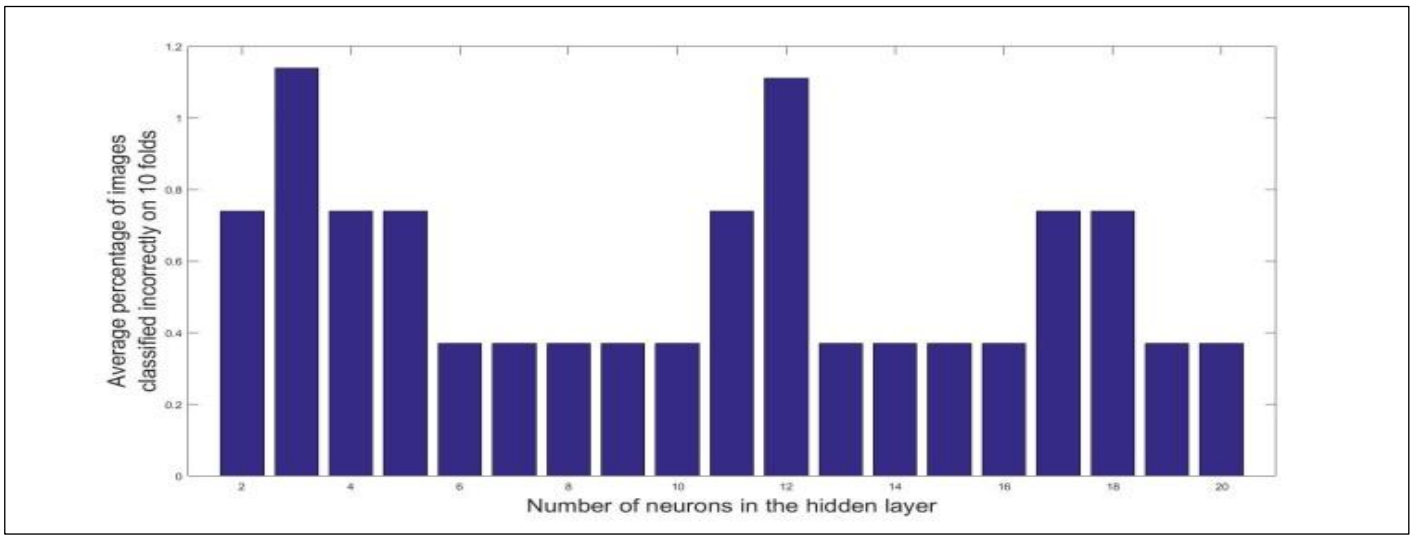

Figure 10: ANN performance in the 10-fold cross-validation method.
Source: Author, (2019).

In Figure, it was verified that the smallest error was obtained with numbers of hidden neurons equal to 6, 7, 8, 9, 10, 13, 14, 15, 16, 19, 20. Then, the smallest number of hidden neurons (i.e. 6 hidden neurons) was chosen. Figure 11 shows the architecture of the designed ANN model. As it can be seen, the ANN architecture is composed by 15 neurons in the input layer (15 features), 6 neurons in the hidden layer, and 2 neurons the output layer (2 classes in the formats of {0,1} and {0,1}).

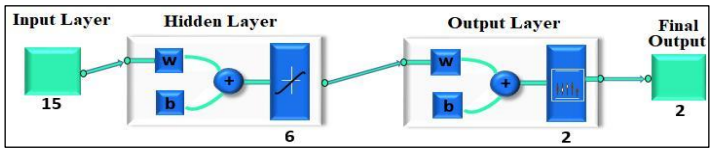

Figure 11: Architecture of the ANN model with 6 hidden neurons in the hidden layer.
Source: Author, (2019).

As described previously, the activation functions are sigmoid hyperbolic tangent (tansig) for the hidden layer and softmax for the output layer. The ANN training was done using the SCGB algorithm with the standard parameters of the MATLAB software: maximum of iterations equal to 1000, performance goal equal to 0, among others [26].

The ANN performance during the training was measured using the cross-entropy function [25]. Figure 12 shows the ANN performance in training and validation data over time. The ANN training was automatically stopped after 56 iterations.

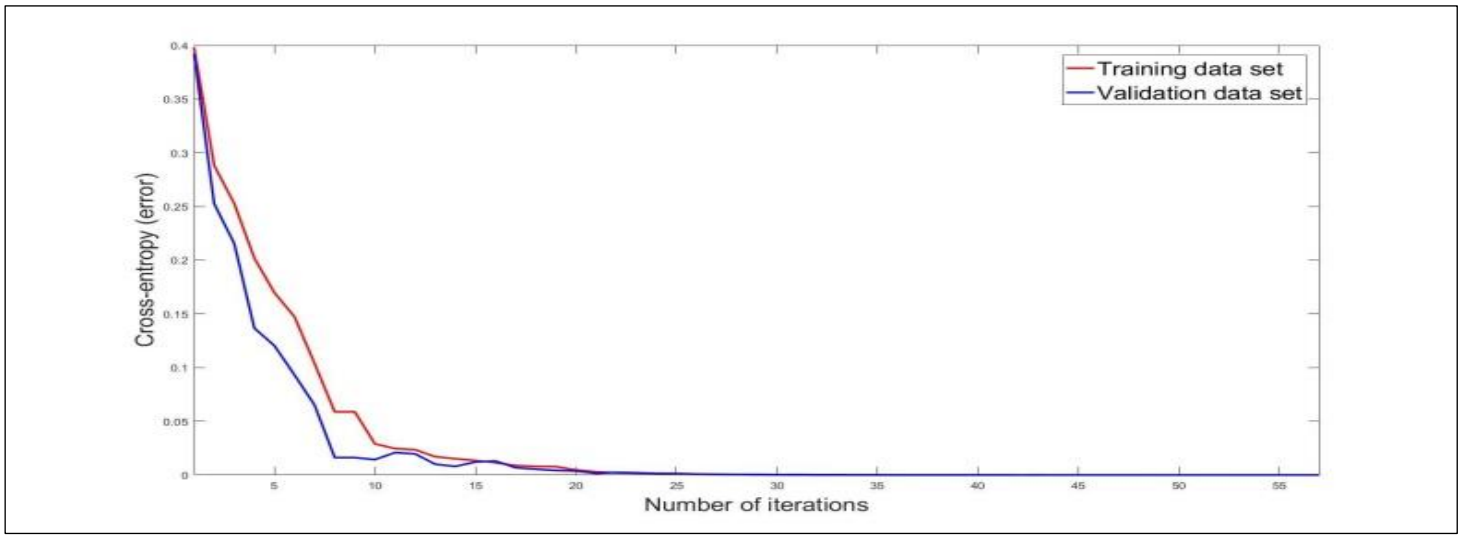

Figure 12: Performance of the ANN model in the learning process.
Source: Author, (2019).

Table 2 shows the percentage of correct and incorrect ANN classifications in training, validation, and test data. It was noticed that ANN performance was 100% in all data, such that ANN was able to classify efficiently images of the box with defect and the box without defect in all data. Therefore, the proposed methodology has effectiveness in the classification of the box without defect and the box with defect.

Table 2: Percentages of correct and incorrect classifications of the ANN model.

	Correct classifications	Incorrect classifications
Training	100%	0%
Validation	100%	0%
Test	100%	0%

Source: Author, (2019).

It should be pointed that, in this testing scenario, the boxes classifications were performed using images acquired previously, that is, the images were stored in a database. This testing scenario is necessary to create and validate the ANN model for the vision system.

V.2 REAL-TIME PERFORMANCE OF THE PROPOSED VISION SYSTEM FOR OBJECT DEFECT DETECTION

In order to analyze the real-time performance of the vision system, 60 digital images were acquired, one by one, by the proposed vision system. The acquired images consist of 30 images of a box with defect and 30 images of a box without defect, being that all the images were obtained in different angles and lighting conditions.

The main difference of this experiment (testing scenario) is that after acquiring the image of a box, it is automatically classified (with or without defect) by the vision system. While in the previous experiment (testing scenario), a set of images was simultaneously acquired and applied to train the ANN. Figure 13 shows some images acquired by the camera in this experiment.

Table 3 shows the percentages of boxes classified correctly and incorrectly by the vision system. Therefore, all the boxes were classified accurately by the proposed vision system. Thus, even in a real-time operation, the ANN model is efficient to classify boxes with and without defects in painting.

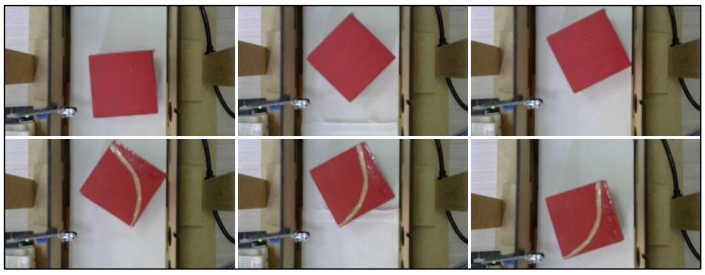

Figure 13: Some acquired images from proposed vision system in real time operation.
Source: Author, (2019).

Table 3: Percentages of correct and incorrect classifications of the proposed vision system in real time operation.

	Correct classifications	Incorrect classifications
Non-defect box	100%	0%
Defect box	100%	0%

Source: Author, (2019).

VI. CONCLUSION

The use of digital images of objects to control the quality of products is indispensable in order to avoid failures and additional costs resulting from manual inspection. This paper proposed a vision system which performs image acquisition using a Logitech HD Webcam C270, segmentation using the Otsu's method, improvement by median filtering, feature extraction using co-occurrence matrix, and pattern recognition using an ANN model. The proposed vision system was able to capture and classify accurately, in real time, images of a box with defect and a box without defect on a conveyor belt.

However, the prototype has a limitation. The used infrared sensor has problems when exposed to high level of illumination. In this situation, the infrared sensor detects an obstacle, even if an object is not in the conveyor belt. Therefore, further works should be devoted to test other infrared sensors.

Moreover, in order to make the proposed vision system more efficient, other improvements can be done, such as the integration of a Radio-Frequency Identification (RFID) model, a WiFi wireless communication module and a robotic arm in the vision system. In addition, as future work, it is expected the real application of the proposed vision system in an industry with the purpose of verifying its accuracy in a real production line.

VII. REFERENCES

[1] C. Iglesias, J. Martínez, J. Taboada. Automated vision system for quality inspection of slate slabs. Computers in Industry, vol. 99, pp. 119-129, 2018.

[2] O. Nir, Y. Parmet, D. Werner, G. Adin, I. Halachmiad. 3D Computer-vision system for automatically estimating heifer height and body mass. Biosystems Engineering, vol. 173, pp. 4-10, 2018.

[3] A. A. Shafie, A. B. M. Ibrahim, M. M. Rashid. Smart Objects Identification System for Robotic Surveillance. International Journal of Automation and Computing, vol. 11, no. 1, pp. 59-71, 2014.

[4] F. F. Feliciano, I. L. Souza, F. R. Leta. Visão Computacional Aplicada à Metrologia Dimensional Automatizada: Considerações Sobre sua Exatidão. Engevista, vol. 7, no. 2, 2010.

[5] A. R. Backes, J. J. M. S. Junior. Introdução à Visão Computacional Usando MATLAB, Rio de Janeiro: Alta Books Editora, 2016.

[6] M. Tresanchez, A. Pujol, T. Pallejá, D. Martínez, E. Clotet, J. Palacín. A proposal of low-cost and low-power embedded wireless image sensor node for IoT application. Procedia Computer Science, vol. 134, 2018.

[7] S. J. Russel, P. Norvig. Artificial Intelligence: A Modern Approach. Malaysia: Pearson Education Limited, 2010.

[8] N. Mohanan, A. Ahmad, A. A. Ghani, M. Al-Nadabi, L. Khriji, S. Al-Busaidi. A Brief Description of Pattern Recognition Techniques. Imperial Journal of Interdisciplinary Research, vol. 2, no. 8, 2016.

[9] G. Capizzi, G. L. Sciuto, C. Napoli, E. Tramontana, M. Wozniak. A Novel Neural Networks-based Texture Image Processing Algorithm for Orange Defects Classification. International Journal of Computer Science & Applications, vol. 13, no. 2, pp. 45-60, 2016.

[10] M. M. Breve, M. A. C. Bernuy. Introdução ao Desenvolvimento de Sistemas com Microcontroladores. In Seminário de Perquisa Jr., Universidade Tecnológica Federal do Paraná, Cornélio Procópio, vol. 3, 2012.

[11] N. A. Martins. Sistemas Microcontrolados. Editora Novatec, 2005.

[12] A. B. Nunes. Análise de Resultados Benchmarks para Escalonamento de Tarefas de Tempo Real em Máquinas Heterogêneas, B. Sc. dissertation, Departamento Acadêmico de Informática, Universidade Tecnológica Federal do Paraná, Ponta Grossa, PR, Brazil, 2016.

[13] U. Lopes, T. R. Bonfim. Implantação de Laboratório Acadêmico de Microcontrolador em Instituição de Ensino Superior. Revista de Ciências Exatas e Tecnologia, vol. 2, no. 2, pp. 53-61, 2007.

[14] A. D. Nogueira, V. Teixeira, W. R. de Freitas. Aplicação de Robótica em Processos de Transporte Industrial. Technical Report, Curso de Pós Graduação em Automação e Controle Industrial do Centro Universitário de Lins (Unilins), Lins, SP, Brazil, 2015.

[15] A. O. Tucci, M. J. da Cunha, A. S. de Morais, J. S. de Morais. Proposta de Desenvolvimento de uma Plataforma Computacional de Integração entre o Matlab e o Arduino Aplicado em Processos Industriais. In Conferência de Estudos em Engenharia Elétrica, vol. 12, pp. 1-4, 2014.

[16] J. A. Back, L. P. C. Tedesco. Proposta de um Sistema para Monitoração e Análise de Energia Elétrica em Ambientes Industriais. In Encontro Nacional de Engenharia de Produção (ENEGEP), vol. 32, pp. 1-13, 2012.

[17] C. A. S. de Miranda, S. L. A. Viera, A. P. C. Belem, L. F. V., N G. D. Gomes. Desenvolvimento de Sistemas Híbridos de Iluminação. In Encontro Nacional de Engenharia de Produção (ENEGEP), vol. 36, pp. 1-13, 2016.

[18] D. C. F. da Fonseca, U. E. F. Alves, F. A. G. Matos, M. K. A. Silva, I. G. A. M. da Silva. Eficiência Energética da Iluminação Pública Automatizada: Estudo de Caso na Cidade de Caruaru. In Encontro Nacional de Engenharia de Produção (ENEGEP), vol. 36, pp. 1-12, 2016.

[19] I. B. Q. da Araújo, F. V. Souto, A. G. da Costa Junior, C. P. de Sousa. Desenvolvimento de um Protótipo de Automação Predial/Residencial Utilizando a Plataforma de Prototipagem Eletrônica Arduino. In Congresso Brasileiro de Educação em Engenharia, vol. 40, pp. 1-9, 2012.

[20] A. R. da Silva. Sistema Inteligente de Controle e Monitoramento de Ambiente de Laboratórios de Análises Químicas, Master thesis, Software engineering, Instituto Metrópole Digital, Universidade Federal do Rio Grande do Norte, Natal, RN, Brazil, 2016.

[21] Eletrogate. Nano V3.0 + Cabo USB para Arduino, [Online], Available: https://www.eletrogate.com/nano-v3-0-cabo-usb-para-arduino, March 21, 2019.

[22] Eletrogate. Uno R3 + Cabo USB para Arduino, [Online], Available: https://www.eletrogate.com/uno-r3-cabo-usb-para-arduino, March 21, 2019.

[23] Eletrogate. Leonardo R3 + Cabo USB para Arduino, [Online], Available: https://www.eletrogate.com/leonardo-r3-cabo-usb-para-arduino, March 21, 2019.

[24] Eletrogate. Mega 2560 R3 + Cabo USB para Arduino, [Online], Available: https://www.eletrogate.com/mega-2560-r3-cabo-usb-para-arduino, March 21, 2019.

[25] Y. Uzun, K. Bicakci. A second look at the performance of neural networks for keystroke dynamics using a publicly available dataset. Computers & Security, vol. 31, no. 5, pp. 717-726, 2012.

[26] N. K. Kasabov. Foundations of Neural Networks, Fuzzy Systems, and Knowledge Engineering, 2nd ed., Massachusetts Institute of Technology: A Bradford book, pp. 18, 1998.

[27] K. Hornik, M. Stinchcombe, H. White. Multilayer Feedforward Networks are Universal Approximators. Neural Networks, vol. 2, no. 5, pp. 359-366, 1989.

[28] G. Cybenko. Approximation by Superpositions of a Sigmoidal Function. Mathematics of Control, Signals and Systems, vol. 2, no. 4, pp. 303-314, 1989.

[29] S. G. Soares, R. Araújo. An adaptive ensemble of on-line extreme learning machines with variable forgetting factor for dynamic system prediction. Neurocomputing, vol. 171, pp. 693-707, 2016.

[30] D. E. Rumelhart, G. E. Hinton, R. J. Williams. Learning Internal Representations by Error Propagation. Parallel Distributed Processing: Explorations in the Microstructure of Cognition, vol. 1, pp. 318-362, 1986.

[31] M. F. Moller. A Scaled Conjugate Gradient Algorithm for Fast Supervised Learning. Neural Networks, vol. 6, no. 4, pp. 525-533, 1993.

[32] S. Ekinci, K. Çarman, H. Kahramanli. Investigation and modeling of the tractive performance of radial tires using of road vehicles. Energy, vol. 93, pp. 1953-1963, 2015.

[33] D.-J. Li, Y.-Y. Li, J.-X. Li, Y. Fu. Gesture recognition based on BP neural network improved by chaotic genetic algorithm. International Journal of Automation and Computing, vol. 15, no. 3, pp. 267-276, 2018.

[34] N. Otsu. A threshold selection method from gray-level histograms. IEEE transactions on systems, man, and cybernetics, vol. 9, no. 1, pp. 62-66, 1979.

[35] S. Soares, C. H. Antunes, R. Araújo. A Genetic Algorithm for Designing Neural Network Ensembles. In Proceedings of the 14th International Conference on Genetic and Evolutionary Computation Conference (GECCO'12), p. 681-688, 2012.

[36] R. Kohavi. A Study of Cross-validation and Bootstrap for Accuracy Estimation and Model Selection. The International Joint Conference on Artificial Intelligence (IJCAI), vol. 14, no. 2, pp. 1137-1145, 1995.

Journal of Engineering and Technology for Industrial Applications, 2020. Edition. 23. Vol: 06
https://www.itegam-jetia.org
ISSN ONLINE: 2447-0228
DOI: https://dx.doi.org/10.5935/2447-0228.20200018

RESEARCH ARTICLE OPEN ACCESS

THE OUTSOURCING URBAN MOBILITY IN INDUSTRY 4.0 AND THE CHALLENGES FACED BY THE CATEGORY OF WORKERS IN SEARCH OF RIGHTS AND OCCUPATIONAL SAFETY

Fabio Junio Rodrigues da Silva[1], Adriano Silvestre Fernandes[2], Carlos Eduardo de Carvalho Costa[3], Ilidiane Correia de Oliveira[4], Robson Edgard Faria[5] and David Barbosa de Alencar[6]

[1, 2, 3, 4, 5] Blauro Cardoso de Mattos Higher Education Institute - FASERRA. Manaus – Amazonas, Brazil.
[6] Galileo Institute of Technology and Education of the Amazon - ITEGAM. Manaus – Amazonas, Brazil.

Email: f.fabiojunio28@gmail.com, silvestrekalu@gmail.com, ecarloscarvalho39@gmail.com, lidia_oliveira21@hotmail.com, robsonedfaria@yahoo.com.br, david002870@hotmail.com

Received: May 11th, 2020

Accepted: Jun 05th, 2020

Published: June 30th, 2020

ABSTRACT

This article has as its central scope to capture the challenges faced by service providers for delivery applications and urban mobility on demand such as Uber, 99POP, iFood, Rappi, among others, a profession that has emerged with innovations in technology and Industry 4.0, which with the Brazilian economic crisis, a mass of workers changed their careers out of necessity and faced new challenges, with a category that is not recognized by law, there are flaws in terms of job security, and the study will also analyze the main diseases and injuries acquired while working. In addition to highlighting other risks faced by this new category of workers, such as urban violence in large cities. For this, a descriptive research was carried out with qualitative and quantitative analysis of data using books, articles, dissertations, newspapers and magazines to support the analysis of the content extracted from the interviews that took place from January/2020 to March/2020, where it was possible to know and describe the routine, the difficulties, as well as the activities that directly affect the health and safety of this service provider's work.

Keywords: Safety, Uber, Apps.

I. INTRODUCTION

Recalling a past not far from where you had to call for taxi radio company to request a rush to place "x" at a variable rate according to the distance, and the customer had no idea how that race would cost at the beginning of it. And thinking about the times when small entrepreneurs, mainly in the food industry, they would have to hire their employees correctly through CLT (Consolidation of Labor Laws) and had obligations to that worker, ensuring the quality of services, employee safety and still bear the operating costs of that activity.

It is impossible not to notice how the current times have changed so much with the "Uberization" of work, according to the lawyer, Specialist in Individual and Collective Labor Law Tatiana Moreira Rossini, where the demands have become more frantic and the labor ties for these on-demand services have become just service delivery partnerships, where companies have the sole obligation to pay for the service provided. On-demand applications, arose from the idea of connecting idle workers to customers who needed specific services in a certain area, thus the great technology startups were born that manage the infrastructure of the most known applications in the world, such as Uber, 99POP, Cabify, InDrive [1]. In fact, it became much easier for customers to request an Uber, or any other urban mobility application on demand, to go from location "A" to "B" with flat rates, practical when requesting the service through an app (in seconds, or order your favorite snack from the comfort of your home through an iFood, Rappi, Uber Eats and have your food for a relatively low price and still have an estimated delivery time for that favorite dish. With the use of these apps from big famous startups that we know, it originated in a new working reality, where these startups have large digital platforms bringing together customers and service providers that use their labor to make a profit and deliver a demand, and the user is a mere user of the service and attributing qualification grades for the service provided. Through these simple examples we can see how we are evolving our services: greater

comfort, practicality, quality and speed, but looking through another spectrum, how does that worker live? Does he have an adequate quality of life with the service he performs? Does he have his labor rights guaranteed by law? What about your safety at work? Do companies that need your services have adequate work safety planning that can reduce risks for this worker?

The reality is that at this point raised by this article, very little have evolved, after all, is only providing service, and this developer is in an occupational dilemma where there are no laws, specific standards that compare in relation to labor laws, health and safety standards, until then they only have the right to Social Security, which through decree, classified them as individual microentrepreneurs (MEI).

II. DEVELOPMENT

It is undeniable the fact that the current technologies, advances in research and development, IoT, Industry 4.0 itself aim to facilitate work processes, efficiency and greater management control and increased productivity in all areas of a company. Speaking of applications on demand, we can analyze that startups facilitated connectivity between consumer vs. services, and in this middle there is the worker, a figure active in this process as the executor of the cheap labor offered by startups.

It can be easily noticed that it is not just a digital transformation, automation processes, but also a transformation of people, organizational methods and Work Safety is linked to this indispensable factor in labor relations, the Human Being, on how to adapt the work so that that work activity does not affect physical, cognitive and organizational health in a given daily life.

Through various literature, Industry 4.0 has the purpose of conducting research and innovating methods that can boost the effectiveness of procedures in a substantially high way, in such a way that it can help companies in their various sectors of activity, integrating them for a greater control, through automated information systems in processes ranging from manufacturing, logistics services and urban mobility, causing the complexities of these processes to be drastically reduced, reducing their costs but not their quality [2].

In the history of mankind we have important points to note in order to determine the transformation in industrial processes. The first industrial revolutions established the implantation of machines, electricity and technological information, automating repetitive processes aimed at the productivity and physical health of employees. Nowadays, with the spread of IoTs and services in manufacturing, the 4th Industrial Revolution begins.

This concept of Industry 4.0 emerged in Germany in 2011, as a means to create a new concept of that country's national economic policy based on high-tech strategies and solutions, incorporating digitization and Artificial Intelligence (AI) into industrial activity, which culminated in the concept that we know as Industry 4.0, in reference to a 4th Revolution in the world industry, characterized by integrating control information, and several interconnected processes in the network and the fusion of these means for our reality [3].

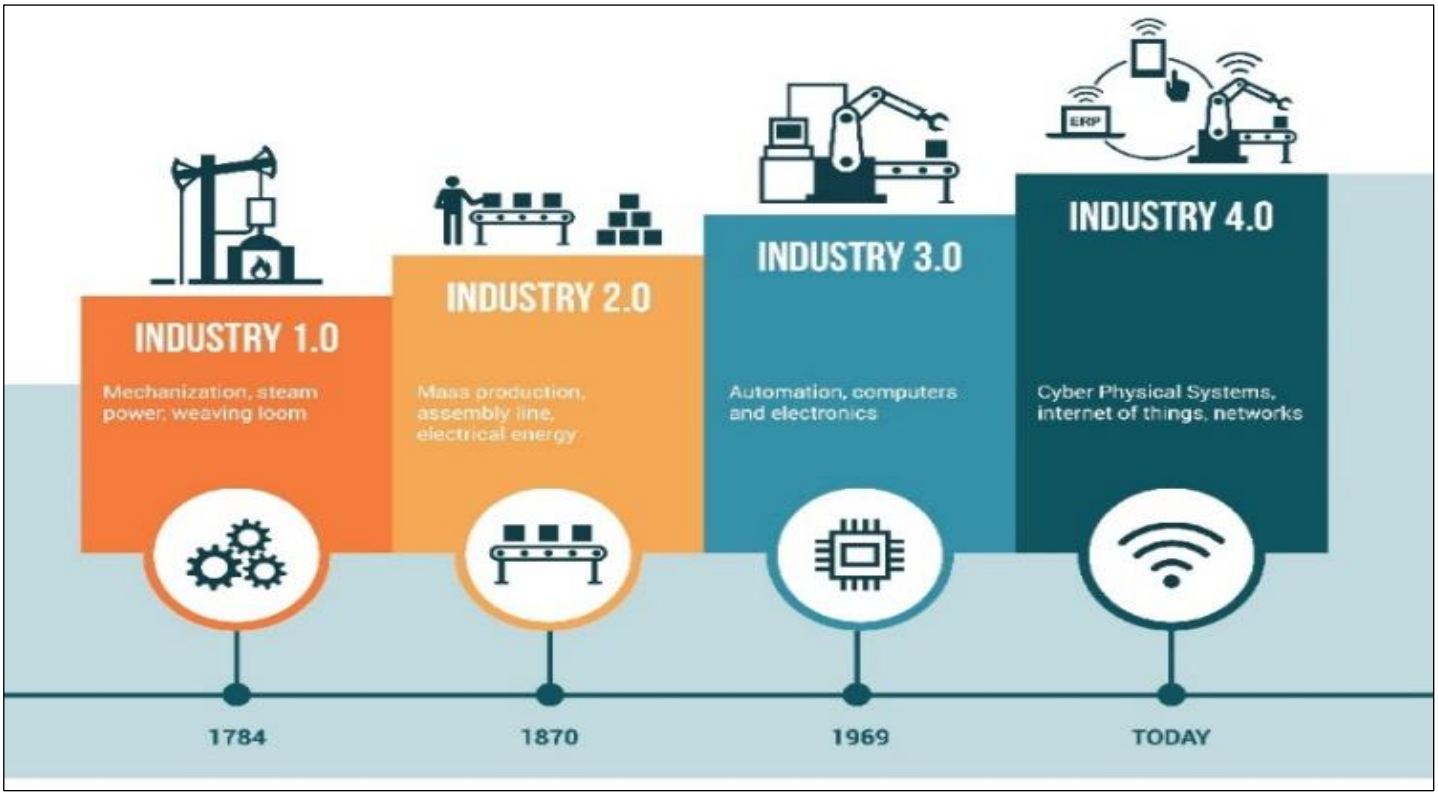

Figure 1: Timeline of Industrial Revolutions.
Source: [2].

The transformation in working methods over the years, as shown in Figure 1, became clear to our eyes, we see the replacement of human labor, by the automation of processes, the replacement of some decision making by AI, some common professions being totally shaken by the different ways of working. One of these markets are urban mobility and on-demand services.

Taxi drivers and Delivery couriers, as well as the craftsmen of the first industrial revolution, were very knowledgeable about their profession and felt great impacts due to the changes that occurred. The knowledge of paths and paths in large Brazilian cities consolidated the career of many workers who made it their livelihood for their family, and in the current times

they have come to face a tough competition from drivers and deliverers of digital platforms, and such knowledge digital has given them the facility to travel in lesser-known roads in cities by GPS, and also by the easy access of their consumers through smartphone applications, enabled this new market of mobility and service on demand bringing a higher cost benefit and quality to the sector [4].

Looking at this scenario with all these facts exposed, we can see how efficient and productive the transformations coming from Industry 4.0 are, with their flexibility, speed and ease of handling for their consumers. We cannot forget the environment in which the worker faces in his day-to-day working via apps.

The innovation that these companies brought in this new model of work is related to an amplification of freedom, where people offer their services and do it without bureaucracy and without bosses while people wish to enjoy these services for a certain period of time and paying only for the fraction that are going to use. Other determining factors explain the success of this model, in addition to unemployment, the promise of quick and easy gains, and autonomy in conducting one's own work.

What happens is that the freedom offered in this modality of work encounters a limitation of encountering practical life, where the worker needs an initial income to pay for the maintenance of basic survival needs, therefore, they are subjected to exorbitant working conditions. It is noted that such practices are shown as a new model for the appropriation of profits for large investors, leaving the workers only to contribute with their wealth and workforce, totally different from the fallacious idea of self-employed [5].

In the last decade, we lived in Brazil an economic crisis unprecedented in the history of the country, sweeping jobs from different sectors, and it was a natural way for professionals to have a means of support and adhere to applications. Of all the workers in this sector, 12% are attending or have not completed higher education and 5% have completed their degree, as cited by IBGE (Brazilian Institute of Geography and Statistics). The study does not mention whether there was an increase in this percentage [6].

When examining some studies, they can reveal the precarious aspects of this work, via applications, which mention long working hours, low remuneration, lack of labor rights, however the lack of job security is a little discussed and more harmful, both to the physical, cognitive and financial health of this worker, where he must still bear the operational costs of this work, having to make long hours to cover achieving a good monthly income [1].

All the technology apparatus of the big startups in the specific sector of work mediated by applications is the reason that companies hide their true activity. They register with regulatory agencies as "technology companies" and call themselves as a simple platform administrator and that their role is only to mediate the meeting of service providers and consumers, earning a percentage fee for each service performed by this meeting. In this way, they understand that their only obligation is to provide and maintain the adequate infrastructure for these employees to do their services and find hundreds of customers per day. And not taking responsibility for what happens before, during and after providing the service, leading drivers and delivery people to various problems and losses [6].

When workers are submitted to such working conditions, they are prone to countless occupational diseases such as stress, headaches, anxiety to meet daily goals to meet operating costs and still obtain personal profits, depression, etc. [7].

Due to the frantic routine in search of customers and races to the applications can cause Cardiovascular Diseases, due to the busy routines in the traffic, long distances, long working hours. As a result, these workers assume the risk of causing heart disease. Diabetes, due to poor diet, of course, there are cases that the genetic predisposition favors a lot, and its symptoms are mild, such as blurred vision, excessive thirst, etc.

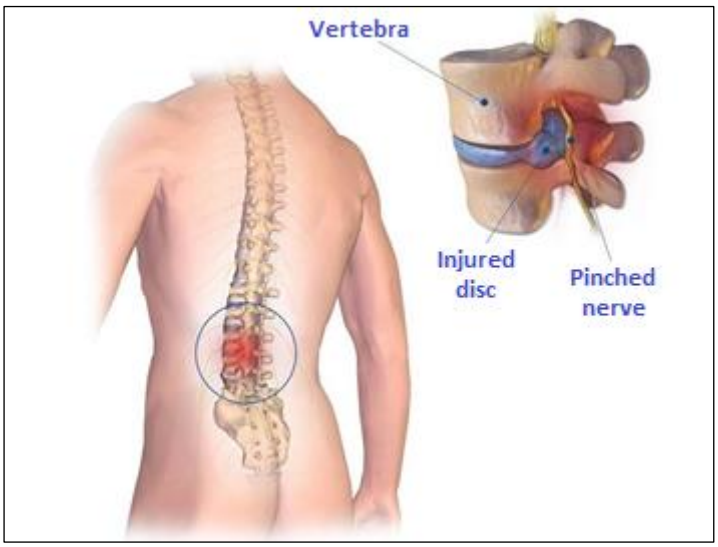

Figure 2: Spine Diseases.
Source: [8].

Spine diseases, for spending hours sitting, using repetitive movements to drive the vehicle or motorcycle, too often with the seat unregulated, which greatly favors the appearance of occupational diseases that affect the spine [9].

Experts indicate that long working hours in traffic can cause discomfort in the legs, in the quadriceps (anterior thigh muscle), in the knee cap and even in the cervical spine, whose force on the discs is stronger when the person is sitting [10].

Professional drivers are more likely to develop herniated discs. This is because, spending many hours sitting, the tendency of drivers is to relax the trunk, placing all their weight on the bones of the lumbar spine and pelvis. The discs are like 'shock absorbers' that exist between the vertebrae. They are composed of an outer ring, which covers the soft center (core), almost all composed of water. Disc injuries can result from a rupture of the disc. This causes the soft center to be forced outward or to break, sometimes even pressing on the nerves of the spinal channels. This is called a herniated disc [11].

Figure 3: Achilles tendonitis.
Source: [12].

In these cases, it is common for a person to have tendonitis in the achilles tendon and pain in the calf, as shown in Figure 3. Achilles tendinitis (also called Achilles tendinopathy or calcaneus tendinitis) is an inflammatory condition that affects the Achilles tendon. The Achilles tendon is a large tendon that connects the calf muscle (calf) to the heel bone. Achilles tendonitis can be diagnosed

based on symptoms and physical examination of the ankle and tendon. It particularly affects drivers, who are workers who use repetitive effort in the area of the feet and legs to execute commands to accelerate, clutch and brake the car [13].

Motorcyclists are also not free from occupational injuries that likewise happen due to repetitive effort due to long working hours, braking, changing gears, acceleration, movements to turn the handlebars, muscular force applied to these movements and incorrect posture (postural vices). Carpal tunnel syndrome in the wrists or other parts of the body such as elbow tenosynovitis and supraspinatus tendonitis (shoulder) are the most common for motorcyclist workers. It is necessary to remember that there is a risk factor that accelerates these degenerative processes which is the segmental vibration (arms) and the whole body. The vehicle vibrates due to its softness and on uneven floors [14].

As in any other profession, stress is strictly linked to the activity of drivers and app deliverers. A 2011 survey by Detran/RS (Traffic Department of Rio Grande do Sul) reported that professional drivers diagnosed with stress and involved in accidents are due to lack of attention and sleep, it is noted that there is a strict connection with the long working hours. The interaction between the worker and the chaotic environment in which he remains during his work routine is the determining factor for the development of stress, and the negative effects of stress only tend to worsen when there are no resources to adapt the routine, or to solve personal problems. reflected in all areas of the individual's life.

The stress generated by stress causes discomfort, tiredness, insomnia, decreased pace of life and the ability to maintain physical and mental balance in daily activities, generating catastrophic health effects and personal and family relationships [15].

It is undeniable that the routine of these workers has a high propensity to acquire stress, especially because they have to bear all the operational costs and still take risks with traffic and urban violence, it raises a high propensity to suffer from a high burden. mental, high cognitive and psychic burdens arising from personal concerns, pressure to hit daily goals for their livelihood, as well as getting rid of assaults in large cities [16].

In addition to occupational diseases that these employees are predisposed to suffer, they are at serious risk with the violence of the streets of the great cities of Brazil, where they can be assaulted, assaulted, stolen their profits obtained from their work, but also have their vehicle (car/motorcycle) stolen by bandits, this situation is even more alarming when there are cases of collaborators, women are at risk, and may be harassed, raped, stolen or any other type of violence.

Brazil still suffers from a deficiency in social protection of application regulation, and employees also lack security, be it labor, occupational or legal, generating dependency. And there is also a lack of public policies that regulate such deficiencies, it is noted that for the leaders of these large startups, the growth of this type of work precarious in rights and duties does not lose strength and there is no prospect that this will change if there is no action regulatory powers. Promoting forms of work that are not precarious and harmful to workers is fundamental in our society today.

It can be noted that for the time being the state strives to adapt itself to the contemporary and national economy, without worrying about the fundamental rights of workers (providing a kind of insurance for drivers, limitation of hours worked, establishment of a minimum salary ceiling for employees, medical assistance and training in routine job security, etc.) by these companies to their so-called "partners", and corporate thinking is only about capital accumulation. Abandoning their collaborators under the law, where they should be at the same level [17].

III. MATERIALS AND METHODS

The instruments used for data collection were the individualized interview with workers combined with on-site observation of the routine, data collection tools and search filters such as Google Forms, and messaging platforms such as Skype and WhatsApp for communicating with drivers and application deliverers.

In the stage of preparing and applying the interview with these workers, the typology of deductive research was used, so that it was not invasive and did not reach the privacy and individuality of each group, but that it obtained results and concise answers to what the research requires. It is noteworthy that informal questions were asked where drivers and couriers could be comfortable with the questions and answers were spontaneous and realistic.

The interviews took place from January/2020 to March/2020. These workers are from several cities in the country, such as: Manaus/AM, Iranduba/AM, São Paulo/SP, Diadema/SP, Itapevi/SP, Cubatão/SP, Santos/SP, São Bernardo do Campo/SP, São Vicente/SP, Rio de Janeiro/ RJ, São João de Meriti/RJ, Campos dos Goytacazes/RJ, Teresópolis/RJ, Belo Horizonte/MG, Juiz de Fora/MG, Divinópolis/MG, Curitiba/PR, Maringá/PR, Cuiabá/MT, Teresina/PI and Brasília/DF.

Table 1: Number of respondents by Brazilian state.

State	Number of respondents
Amazonas	5 people
Distrito Federal	4 people
Mato Grosso	1 person
Minas Gerais	4 people
Paraná	5 people
Piauí	1 person
Rio de Janeiro	8 people
São Paulo	14 people
TOTAL	**42 people**

Source: Authors, (2020).

The only criterion used to choose the interviewees was the experience and daily performance as a service provider partner (Drivers and Deliverers) of on-demand service applications.

The following questions were asked of workers:

- Name and Age?
- Genre?
- Education level?
- Which applications does the worker provide services for?
- Total or partial financial dependence on work for applications?
- How many hours do you work a day?
- How much do you need to earn per day to have a minimum income to cover operating costs of work and basic needs of the home?
- Have you been in pain in any part of your body since you started working for apps?
- Do you agree with job safety training for apps drivers and delivery couriers?

• Would you like the profession to be regulated and have more labor rights?
• Have you suffered any kind of urban violence? Describe it.

The questionnaire method is the most used among the methodologies of collecting data. Today, people are more familiar with approaching interviewers at any time of the day. It is a versatile tool, almost all research problems can be addressed through a questionnaire. It is usually faster and more practical than observation [18].

The author values ethics as a differential factor in the performance of the research, the questions had a neutral character, as a way of not influencing the answers.

IV. RESULTS AND DISCUSSION

This is a descriptive, cross-sectional research with quantitative and qualitative data analysis. The present study has a descriptive character, as it aims to know the worker's routine, the difficulties that he faces every day, as well as the activities performed that directly affect the health and safety of work in this category.

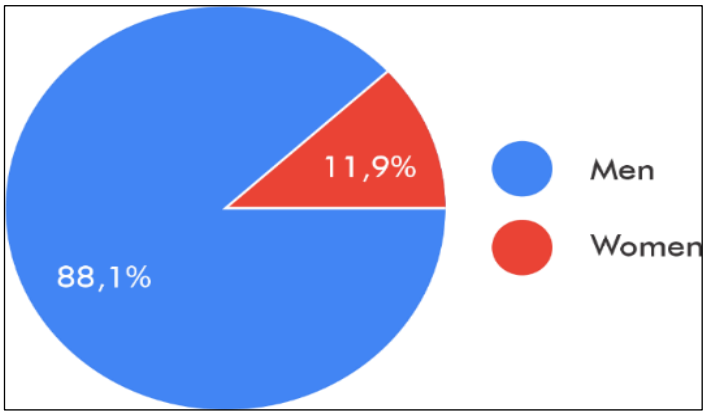

Figure 4: Population Gender.
Source: Authors, (2020).

According to this study, the sample of verified population that works via on-demand applications is mostly men than women, in the scenario of this article Figure 4 shows that 88.1% of the interviewees claim to be men, and 11.9% are women.

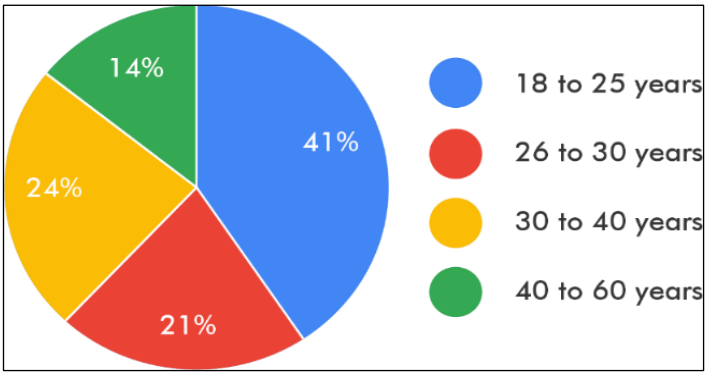

Figure 5: Population Age.
Source: Authors, (2020).

This present study mentions that in the last decade Brazil has suffered an unprecedented economic crisis, sweeping jobs, which is why it has opened new markets, such as on-demand application startups, which has led a mass of workers to look for a new type of family income for their livelihood.

The Figure 5 shows that 41% of the population verified in this study is between 18 and 25 years old, this can be translated with the loss of jobs of people, unemployed individuals, or who are starting their professional career and have not yet had a job. job opportunities, which can be equivalent to the first job, those support positions such as: production assistants, machine operators, call center attendant, receptionist, etc., and these people saw in this application service market on demand a means to stay financially and enter the market without so much bureaucracy to start.

The other ages shown have a certain balance as some have higher education and managed to remain in their positions, and those who did not keep on working for applications on demand, as they face difficulties for professional replacement in their area of origin, either due to lack vacancies, lack of professional qualification or old age.

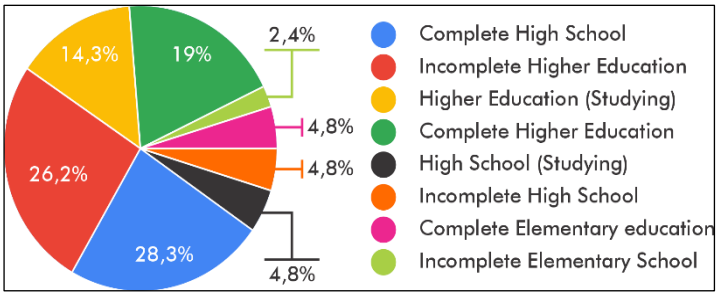

Figure 6: Education level.
Source: Authors, (2020).

The Figure 6 shows that the majority of drivers and delivery couriers of on-demand apps have Incomplete Higher Education, 26.2%, due to the remuneration from the activity having to be shared with the operational costs all in charge of the worker, they reported that they had to lock up their Higher Education courses so that they could reallocate their financial resources to the areas of basic needs of their families. The Figure 6 also shows that all classes, regardless of education, were affected and depend on this activity.

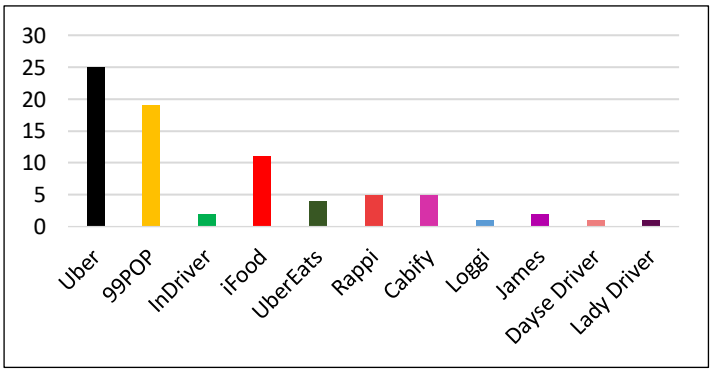

Figure 7: Applications used by the interviewees as a means of work.
Source: Authors, (2020).

From the universe of on-demand service applications, respondents mentioned that they work for Uber, for being a pioneer in the country in this modality and for offering a greater number of customers per hour. For on-demand delivery applications we have iFood as a reference, using the same argument as Uber, offering a greater number of restaurants registered on the platform, in other

words, giving fluidity to a greater number of customers per hour, as exposed by the frequency of use of applications in Figure 7.

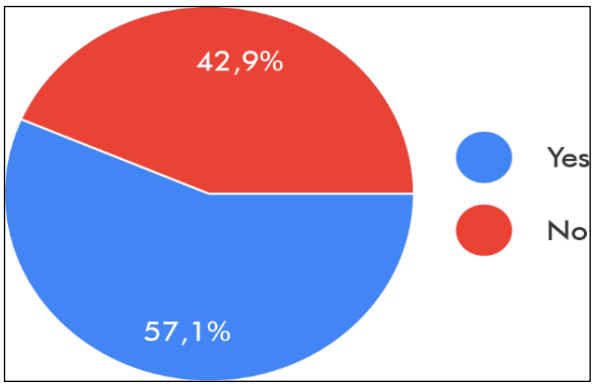

Figure 8: Financial dependence on income from applications.
Source: Authors, (2020).

Respondents were asked whether the income collected from driving and delivering work for on-demand applications was unique and necessary, or just a financial supplement for the family, 57.1% reported that it depends only on this income, being this only source of financial resources for your basic monthly needs. The other party reported that the work reported that the provision of services for applications was only to increase the family's monthly income, complementing the other type of work that the person does, according to what is shown in Figure 8.

Respondents were encouraged to describe their work routines, so most described that they usually work every day, from Monday to Sunday to obtain an adequate monthly income at the end of the month, some stated that they work 12 to 15 hours a day to collect between R$ 200.00 to R$ 300.00 per day to meet operating costs, such as maintenance, fuel, and to meet the needs of their homes.

Most of them said they get up early and sleep an average of 6 hours a day, leaving early and returning home late, they described the routine as being tiring and stressful, due to the constant and busy traffic in their cities. A large part of the interviewees reported being harassed by customers, being accused of stealing from their customers, either due to the high rate indicated in the application, or the food arriving cold, due to the difficulty of access to the delivery place, which greatly increases the degree of stress on workers who depend on this service to survive, customers assign grades to the service, if low grades occur the worker can be blocked from the application, thus preventing him from working normally.

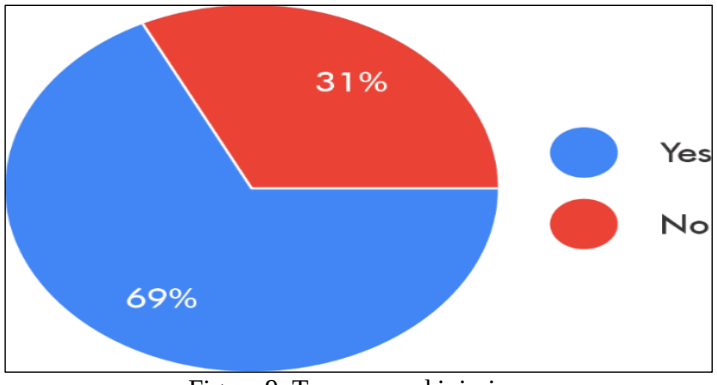

Figure 9: Traumas and injuries.
Source: Authors, (2020).

The workers were asked if they feel pain in the body due to working for on-demand applications, 69% of them stated that Yes, according to Figure 9. Then they were asked what types of pain they feel, which describe where and how the pain is and how long have they been experiencing these symptoms. They said they felt pain in the feet, legs, calf, hands, back pain, low back pain, pain in the arms, pain in the neck, headache. We can see that these are the regions where the greatest repetitive efforts occur due to labor activity. One person claimed to have developed depression due to work stress and financial concerns.

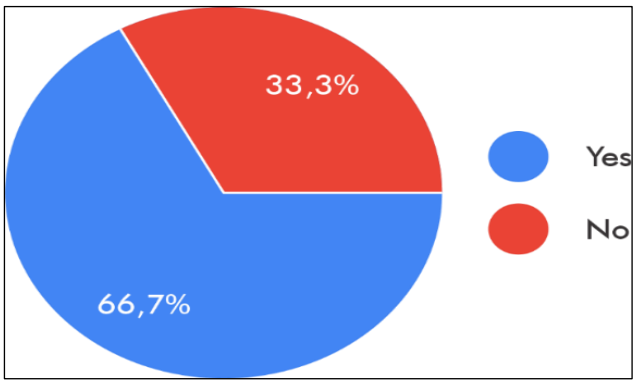

Figure 10: Work Safety and Labor Rights.
Source: Authors, (2020).

Respondents were asked what they thought about having work safety rights and training when exercising the activity and their guaranteed labor rights. The majority of 66.7% stated that they wished to have access to worker safety training on the part of application companies, so they would avoid the profession's risks when performing the activity, regarding labor rights, in addition to the majority agreeing that they should have labor rights guaranteed by law, as shown in Figure 10.

Workers informed that they should be better recognized by labor laws, have health insurance coverage, fixed working hours, limited daily workload, operating allowance or fuel vouchers, annual profit sharing, some type of health insurance for exposure to urban violence, guarantee fund and unemployment insurance. They reported that just being MEI does not guarantee much quality of life, as it only contributes a percentage of their Social Security to the INSS (National Institute of Social Security), but they live and work as if they were informal workers.

Drivers and delivery couriers were asked about urban violence, they reported having been robbed, having their goods taken away, such as a work vehicle and smartphone. Only 5% of the interviewees reported having suffered physical aggression, which increased the pathology of injuries acquired at work.

V. CONCLUSIONS

This article concludes that special attention is needed for this new work niche that has emerged with advances in industry and new technologies through on-demand service applications. When analyzing the facts exposed in this study, it can be noted that there is still a lack of improvement in regulations and health and safety at work for the category of apps drivers and deliverers, they live in a scenario of false protection of the law through the MEI (Individual Microentrepreneur), but with working conditions as if they were informal workers. And so they develop injuries, traumas, and stress itself, which is the general factor of all the difficulties together in the profession.

It is possible to affirm that there is a precarious scenario in this category of workers and there is much to be done, recent legal decisions still rule out the possibility of regulation of the profession and improvements being made. Workers and society

need to claim their rights and make them recognize that this modality is essential nowadays, we have gone through a pandemic period of SARS-CoV-2, named by WHO (World Health Organization) as COVID-19 (Corona Virus Desease - 2019), and these workers were still one of the few who were in full activity making the country's economy work and many businesses, mainly restaurants and stores were not totally paralyzed, and other sectors benefited from the activity of these workers, with transportation and delivery of goods, enabling all sectors to reinvent themselves, with the fundamental participation of this sector studied in this article.

There is a lot that needs to be done to ensure that work health and safety is effectively guaranteed for this category, but at least we can highlight some initiatives by the big startups that are already starting to change this situation, where Uber limits the maximum workload to 12 hours. performance in the application [19], or iFood that announced that it will have insurance, courses and health insurance discounts for its partners [20].

VI. REFERENCES

[1] Moraes, R. B. S.; Oliveira, M. A. G.; Accorsi, A. Uberização do trabalho: a percepção dos motoristas de transporte particular por aplicativo. Revista Brasileira de Estudos Organizacionais – v. 6, n. 3, p. 647- 681, dez/2019.

[2] Industry 4.0 and Industrial IoT in Manufacturing: A Sneak Peek. Available in: <https://www.aberdeen.com/opspro-essentials/industry-4-0-industrial-iot-manufacturing-sneak-peek/>. Accessed on 06/03/2020.

[3] Becker, A. Schneider, A. Ercico, J. Werlang, R. Os Conceitos da Indústria 4.0 Associados a Abordagem da Capacidade Dinâmica. ANAIS - Engenharia de Produção. UCEFF. 2018.

[4] Souza. M. A indústria 4.0 e os artesãos da era digital. Available in: <https://www.industria40.ind.br/artigo/19652-a-industria-40-e-os-artesaos-da-era-digital>. Accessed on 29/03/2020.

[5] Rubenich, R. S. A Possibilidade de Configuração da Relação de Emprego Entre a Uber e os Seus Motoristas. Âmbito Jurídico. 2020. Available in: <https://ambitojuridico.com.br/cadernos/direito-do-trabalho/a-possibilidade-de-configuracao-da-relacao-de-emprego-entre-a-uber-e-os-seus-motoristas/>. Accessed on 06/03/2020.

[6] Uber com diploma. Available in: <https://economia.uol.com.br/reportagens-especiais/profissionais-com-faculdade-viram-uber/#uber-com-diploma>. Accessed on 06/03/2020.

[7] Pina, J. A. Intensificação do trabalho e saúde dos trabalhadores na indústria automobilística: estudo de caso na Mercedes Benz do Brasil, São Bernardo do Campo. Tese apresentada para obtenção do título de Doutor em Ciências na área de Saúde Pública. Escola Nacional de Saúde Pública Sérgio Arouca - ENSP. FIOCRUZ. 2012.

[8] Hérnia de Disco. Available in: <https://www.bauerfeind.com.br/blogs/news/hernia-de-disco>. Accessed on 05/05/2020.

[9] Almeida, L. M. Ideias de Negócio - Transporte por aplicativo. Empreendedorismo. SEBRAE. 2019.

[10] Rodrigues. E. O peso da embreagem: Para e arranca no trânsito pode virar doença crônica. 2014. Available in: <http://www.diariogaucho.clicrbs.com.br/rs/dia-a-dia/noticia/2014/06/para-e-arranca-no-transito-pode-virar-doenca-cronica-4519338.html>. Accessed on 01/05/2020.

[11] Motoristas têm mais chances de desenvolver Hérnia de Disco. Available in: <https://www.transaltransportes.com.br/dicas/motoristas-tem-mais-chances-de-desenvolver-hernia-de-disco>. Accessed on 01/05/2020.

[12] O que é tendinite de Aquiles? Available in: <https://www.saudebemestar.pt/pt/clinica/ortopedia/tendinite-tendao-aquiles/>. Accessed on 01/05/2020.

[13] Tendinite de Aquiles. Available in: <https://ada.com/pt/conditions/achilles-tendonitis/>. Accessed on 01/05/2020.

[14] Brito, P. Movimentos repetitivos no trânsito causam doenças em motociclistas. Available in: < http://www.perkons.com.br/pt/noticia/1301/movimentos-repetitivos-no-transito-causam-doencas-em-motociclistas>. Accessed on 01/05/2020.

[15] Martins, F. F.; Lopes, R. M. F.; Farina, M. Nível de estresse e principais estressores do motorista de transporte coletivo. Bol. Acad. Paulista de Psicologia, São Paulo, Brasil - V. 34, no 87, p. 523-536.

[16] Costa, E. A. V. G. Estudo dos Constrangimentos Físicos e Mentais Sofridos pelos Motoristas de Ônibus Urbano da Cidade do Rio de Janeiro. Dissertação de Mestrado apresentada ao Programa de Pós-Graduação em Design da PUC-Rio. 2006.

[17] Firmino. V. H. Como a Uber contribui para a precarização do trabalho na modernidade. Available in: <https://vitorfirmino.jusbrasil.com.br/artigos/534725925/como-a-uber-contribui-para-a-precarizacao-do-trabalho-na-modernidade>. Accessed on 06/03/2020.

[18] Guimarães, P. R. B. Estatística e pesquisa de opinião. Departamento de Estatística - Universidade Federal do Paraná, UFPR, 2020. Available in: <https://docs.ufpr.br/~prbg/public_html/ce020/estatística%20E%20pesquisa%20de%20opinião%201a%20parte.pdf>. Accessed on 08/05/2020.

[19] Uber lança ferramenta que limita o tempo online do motorista dirigindo usando o aplicativo para promover segurança viária. Available in: <https://www.uber.com/pt-BR/newsroom/uber-lanca-ferramenta-que-limita-o-tempo-online-do-motorista-dirigindo-usando-o-aplicativo-para-promover-seguranca-viaria/>. Accessed on 02/05/2020.

[20] iFood Delivery de Vantagens. Available in: <https://entregador.ifood.com.br/regulamento-ifood-delivery-de-vantagens/>. Accessed on 02/05/2020.

Journal of Engineering and Technology for Industrial Applications, 2020. Edition. 23. Vol: 06
https://www.itegam-jetia.org
ISSN ONLINE: 2447-0228
DOI: https://dx.doi.org/10.5935/2447-0228.20200019

RESEARCH ARTICLE OPEN ACCESS

ESTIMATION OF THERMOPHYSICAL PROPERTIES OF VEGETABLE OILS FOR CREATION DATABASE TO ENGINEERING CALCULATIONS

Gisele Cristina Rabelo Silva[1] and Maria Helena Caño de Andrade[2]

[1] Federal University of São João del-Rei – UFSJ, Divinópolis – Minas Gerais, Brazil.
[2] Federal University of Minas Gerais – UFMG, Belo Horizonte – Minas Gerais, Brazil.

Email: giselec@ufsj.edu.br, cano@ufmg.br

Received: Apr 14th, 2020

Accepted: Jun 24th, 2020

Published: June 30th, 2020

ABSTRACT

Researches focusing on the development of biofuel production processes have increased significantly in recent years, mainly for environmental and economic issues. The identification of low-cost raw materials and the development of simulation models able to predict the conditions of production and the properties of the components may be the way to optimize these processes. Biodiesel is an alternative renewable fuel to petroleum-based diesel departing from vegetal oils (fresh or reused) as well as some kinds of animal tallows. The knowledge of thermophysical properties of the components of the feed is crucial for optimization this process. The experimental determination of these properties is complex and high costs, as can occur chemical degradation during analysis or it is impossible to have them this like pure components. Thus, the objective of this study was to evaluate methods for predicting physical and thermodynamic properties, in order to develop a database of the compounds involved in the biofuels production's process and to recommend appropriate methods based on accuracy and consistency of data obtained. In view of that, this work investigated the performance of groups contribution methods and fragment-based approach in the calculation of as normal boiling temperature, critical temperature, critical pressure, critical volume, acentric factor, heat capacity, vapor pressure, enthalpy of vaporization liquid density and enthalpy of formation. At the end of this work, the most viable models were recommended for each property evaluated, comparing the estimated values to the experimental data available in the literature. Finally, a database with physical and chemical properties of vegetable oils was created to use in engineering calculations.

Keywords: Vegetable oils, Biodiesel, Thermophysical properties.

I. INTRODUCTION

The decline in available oil reserves and stricter environmental regulations has motivated global interest in studies for the discovery and improvement of renewable energy sources, especially biofuels.

Vegetable oils and fats animal's types used in the manufacture of biofuel, can cause changes in their properties. In other words, biodiesel can present different properties by the chemical composition of raw materials, for example, a low performance in relation to the properties of cold flow [1].

The literature reveals that there is a large volume of researches conducted in the design of processes and manufacture of biofuels from vegetable oils, but the experimental data available for thermodynamic properties of vegetable oils and/or predict methods are limited [2-6].

The scarcity of data on the thermophysical properties of biodiesel components and vegetable oils can be related to the difficulty in obtaining them in pure form and in the performance of experiments, as these substances can degrade under severe conditions [7], [8]. However, vegetable oils aren't composed only by a triacylglycerol. Oils and fats can contain dozens of different triacylglycerols (TAG), as tripalmitin, tristearin and triolein.

Diacylglycerols (DAG), monoacylglycerols (MAG) and free fatty acids (FA) are also components of vegetable oils and have few properties reported in the databases, as well as methyl and ethyl esters [4], [9-12].

Group Contribution (CG) methods have been used in recent years to estimate some physicochemical properties of organic substances, such as normal boiling point, critical properties and acentric factors [3], [11], [13]. The GC considers that the properties of molecules depend on the nature of atoms and the types of chemical bonds within molecules [14]. In addition to GC, methods with the principle of contributor fragments have been used for calculations that consider that the properties of molecules are established from the contributions of their functional groups [8]. These methodologies need only small amounts of information about the substances in order to obtain a reliable estimate. Although there are many methods in the literature, each of them has built-in premises and practical limits that must be applied. Therefore, selecting the most appropriate models for predicting thermophysical properties is extremely important for achieving realistic results in a process simulation.

II. METHODOLOGY

II.1 MODELING OF PREDICTING THERMOPHYSICAL PROPERTIES

For the development of property estimates, electronic spreadsheets were created in MS-Excel® with equation sequences for the calculations of the methods.

For the application of the methods of estimating properties, the molecules of the compounds of interest (TAGs, DAGs, MAGs and FA) were drawn and, then, the functional groups identified and quantified.

Example: A molecule of triacylglycerol PLO, formed by the junction of palmitic fatty acids (P), linoleic (L) and oleic (O) in a glycerol molecule. Its chemical formula is represented by $C_{55}H_{100}O_6$. Figure 1 represents the triacylglycerol PLO molecule.

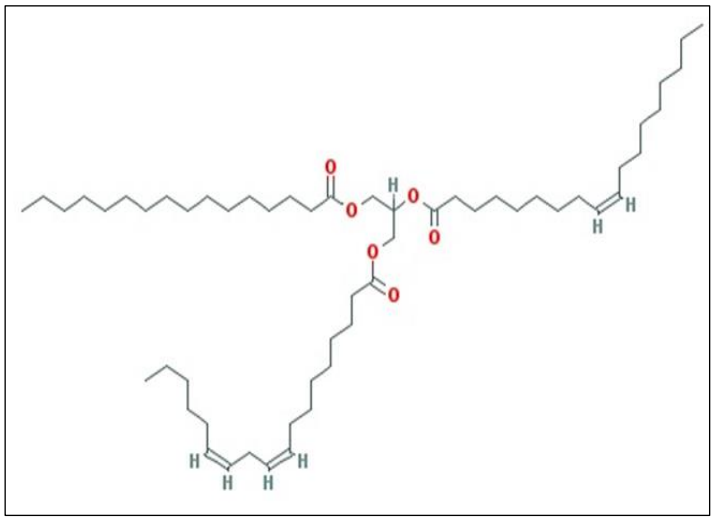

Figure 1: Chemical structure of triacylglycerol PLO.
Source: Authors, (2020).

The groups present in the molecular structure represent in Figure 1 were counted for the methods of contribution of groups showed in Table 1, JOBACK [15] and GANI [16].

Table 1: Occurrence of the groups for the JOBACK and GANI method for the PLO triacylglycerol.

JOBACK groups	Score	GANI groups	Score
CH_3	3	**CH_3**	3
$>CH_2$	42	**$>CH_2$**	40
>CH-	4	**>CH-**	1
-COO-	3	**$-CH_2-COO-(C)$**	2
=CH-	3	**-COO-**	1
		-CH=CH-	3

Source: Authors, (2020).

Each of these groups has a contribution value depending on the property to be calculated and method used. Thus, it's possible to use the equations of the methods safely to predict the properties.

Equations necessary for the calculations of GC methods and fragments approach are described below.

Normal boiling temperature (T_b): T_b is the temperature at which the vapor pressure equals the external or atmospheric pressure.

Developed an advanced method of group contribution based on the groups of the thermodynamic model *Universal Functional Activity Coefficient* (UNIFAC) [16-17]. In addition, the authors added the so-called "second order" contributions that allow differentiating molecules from isomers, molecules that have the same groups, located together or not, resonance structures, among others [8].

The equations of the JOBACK and GANI models for Tb estimation are represented by equations 1 and 2.

JOBACK:

$$T_b = 198 + \sum_k N_k(T_{bk}) \quad (1)$$

GANI:

$$T_b = 204.359 \times \ln(\sum_k N_k T_{bk}) \quad (2)$$

where N_k represents the number of groups of type k and T_{bk} the contribution to the normal boiling temperature of groups k.

The semi-empirical approach of [18], [19] was also used to calculate of boiling temperature of TAGs, DAGs and MAGs is implemented the basis of fragments of the constituents. A relationship between the boiling temperature of each of the fragments of the TAGs (fatty acids and glycerol) and pressure was applied. Therefore, the experimental data of [20], [21] on the temperature of each of the fragments were adjusted to Equation 3.

ZONG:

$$T_b^a = a \times \ln(P) + b \quad (3)$$

where a and b are the adjustment parameters of each fragment, T_b^a is the boiling temperature of fragment a (K) and P is the vapor pressure (mmHg). Knowing the value of T_b^a for each of the fragments, it was possible to calculate the value of T_b^{TAG} using Equation 4:

$$T_b^{TAG} = \frac{\sum N_{Frag,a} \times T_b^a}{3} \quad (4)$$

T_b^{TAG} represents normal boiling temperature of triacylglycerol (K) and N_{Frag} number of fragments of a.

Critical properties (P_c, V_c, T_c and Z_c): Pressure (P_c),volume (V_c),temperature (T_c) and compressibility factor (Z_c) critical are parameters used in many volumetric, thermodynamic and transport correlations based on the theory of corresponding states to estimate gas and liquid properties.

According to [8], the experimental determination of these properties is difficult, as chemical degradation can occur at high temperatures, especially for long chain components.

The critical point of glycerol was defined by [22] through an unconventional methodology called *pulse-heating*, being the only experimental measure available in the literature. The critical temperature obtained was 850 K and the critical pressure was 75 bar. As glycerol begins to undergo thermal degradation from 510 K (DIPPR, 2019), the critical parameters of this molecule can be included in predictive calculations.

The estimation methods evaluated in this study were: [15], [16], [23], [24]. The first method requires only information on the structure of the compound, while the other methods require values of molar mass and boiling temperature. The methods are represented by Equation 5 to Equation 16.

JOBACK:

$$T_c = T_b[0.584 + 0.965\sum_k N_k(T_{ck}) - \left(\sum_k N_k(T_{ck})\right)^2]^{-1} \quad (5)$$

$$P_c = [0.113 + 0.0032N_{at} - \sum_k N_k(P_{ck})]^{-2} \quad (6)$$

$$V_c = 17.5 + \sum_k N_k(V_{ck}) \quad (7)$$

GANI:

$$T_c = 181.28 \times \ln(\sum_k N_k T_{ck}) \quad (8)$$

$$P_c = [\sum_k N_k P_{ck} + 0.10022]^{-2} + 1.3705 \quad (9)$$

$$V_c = \left(\sum_k N_k(V_{ck}) - 0.00435\right) \times 1000.0 \quad (10)$$

AMBROSE:

$$T_c = T_b\left[1 + \left(1.242 + \sum_k N_k(T_{ck})\right)^{-1}\right] \quad (11)$$

$$P_c = M_M\left[0.339 + \sum_k N_k(T_{ck})\right]^{-2} \quad (12)$$

$$V_c = 40 + \sum_k N_k(V_{ck}) \quad (13)$$

LYDERSEN:

$$T_c = \frac{T_b}{0.567 + \sum N_k(T_{ck}) - (\sum N_k(T_{ck}))^2} \quad (14)$$

$$P_c = \frac{M_M}{(0.34 + \sum N_k(P_{ck}))^2} \quad (15)$$

$$V_c = 40 + \sum N_k(V_{ck}) \quad (16)$$

T_{ck}, P_{ck} and V_{ck} represent the contributions of each functional group and that vary numerically depending on the method of contribution of groups. N_{at} is the number of atoms in the molecule, in the critical pressure equation for the JOBACK method. M_M the molar mass, N_k is the number of times the group "k" appears in the molecule. T_c is given in Kelvin, P_c in bar and V_c in cm³/mol.

Acentric factor (ω): The acentric factor was introduced by Kenneth Sunborn Pitzer in 1955. It's associated with the sphericity of the molecule force field and polarity [8]. Originally defined by Equation 17:

$$\omega = -log\left[\lim_{\left(\frac{T}{T_c}\right)=0.7}\left(\frac{P_{vp}}{P_c}\right)\right] - 1.0 \quad (17)$$

where P_{vap} is vapor pressure, T_c critical temperature and P_c critical pressure.

The definition of the equation (Equation 17) arose because monoatomic gases (Air, K-r, Xe) have ω ~ 0, except for noble gases (He, Ne) and some others (e.g. Rn). All other species have positive values up to 1.5. To obtain ω values is necessary to know the constants T_c, P_C and the property P_{vap} at reduced temperature, T/T_c =0.7.

Pitzer rule (PITZER) and Kesler-Lee (LEE) were selected in this work to determined ω. Equation 18 was presented by [25] for ω calculation:

$$Z_c = 0.291 - 0.080\omega \quad (18)$$

According to [8], Equation 18 can be used to predict the acentric factor of strongly polar substances and associative substances. However, the authors indicate that if the critical parameters were not adequately estimated for the substance there isn't guarantee of the accuracy of the desired property.

A set of equations was developed by [26] to evaluate properties of chemical compounds such as molecular mass, normal boiling temperature, critical pressure, critical temperature and acentric factor. For the latter, the following correlations were developed (Equation 19 and Equation 20). Such models depend on the reduced boiling temperature (T_{br}=T_b/T_c) and the characterization factor of Watson (K_w).

For T_{br} > 0,8:

$$\omega = -7.904 + 0.1352K_w - 0.007465K_w^2 + 8.359T_{br} + \frac{(1.408 - 0.01063K_w)}{T_{br}} \quad (19)$$

For $T_{br} < 0,8$:

$$\omega = \frac{-lnP_c - 5.92714 + \frac{6.09648}{T_{br}} + 1.28862 lnT_{br} - 0.169347 T_{br}^6}{15.2518 - \frac{15.687}{T_{br}} - 13.4721 lnT_{br} + 0.43577 T_{br}^6} \quad (20)$$

The Watson factor can be defined by Equation 21:

$$K_w = \frac{MT_b^{1/3}}{d_{15°C}} \quad (21)$$

where MT_b is the average of the normal boiling temperature given in °R and d is the relative density measured at 15°C.

Enthalpy formation and Gibbs free energy of formation in the standard state: The knowledge of standard enthalpy of formation (ΔH_f^0) is important to provide the enthalpy reaction for the formation of a mol of a substance from the chemical elements that constitute it, in its reference states.

The Gibbs free energy formation (G_f^0) is defined as Gibbs' energy reaction for the formation of a mol of a substance from the chemical elements that constitute it in its reference states. According to [27], Gibbs free energy can be obtained from calorimetric data (enthalpy and entropy, from calorific capacities), equilibrium constants in chemical reactions, electrochemical measurements and spectroscopy data, when in the gas phase.

Rarely values for the calculation of the reaction Gibbs energy are found. Methods of contributions from groups such as [15], [28],[16] and others, have been of great help in predicting reliable estimates of values of formation enthalpy, absolute entropy and Gibbs free energies.

Groups contribution to G_f (298.15 K) and H_f (298.15 K) were obtained by [16] through equations (Equation 22 and Equation 23).

GANI:

$$H_f^0 = 10.835 + \sum_k N_k \left(H_{fk}\right) \quad (22)$$

$$G_f^0 = -14.828 + \sum_k N_k \left(G_{fk}\right) \quad (23)$$

N_k represents the number of groups and H_{fk} and G_{fk} the group's contribution to enthalpy and Gibbs energy, respectively.

The method of [28] can also be used to estimate formation enthalpy and absolute entropy of chemical compounds in the gas phase, considering the standard state. In this method, contributions are given only to atoms with valence greater than one. Groups are linked to key atoms with specific nomenclature (Equation 24, Equation 25, and Equation 26). For example, group C-(C)$(H)_3$ is a reference to the carbon atom (key atom) bound to another carbon and three hydrogens.

BENSON:

$$\Delta H_f^0(298{,}15K) = \sum_k N_k \left(\Delta H_{fk}^0\right) \quad (24)$$

$$\Delta G_f^0(298{,}15K) = \Delta H_f^0(298{,}15K) - 298{,}15 \Delta S_f^0 \quad (25)$$

$$\Delta S_f^0(298{,}15K) = \sum_k N_k \left(\Delta S_{fk}^0\right) - Rln\sigma + ln\eta \quad (26)$$

where σ is the symmetry of the molecule and η the number of isomers. R is the universal constant of gases.

The Joback and Reid method [15] is an extension of the Lydersen method [24]. It's a method that uses additive contributions and no contribution to interactions between groups. According to the authors, it is not a high-precision method, but works well for many chemical species. Among these properties, those of interest for this work are Gibbs free energy estimates of standard formation and enthalpy of standard formation. Equation 27 and Equation 28 are used by this method to estimate these two properties.

JOBACK:

$$H_f^0 = 68.29 + \sum_k N_k \left(H_{fk}\right) \quad (27)$$

$$G_f^0 = 53.88 + \sum_k N_k \left(G_{fk}\right) \quad (28)$$

N_k represents the number of groups, H_{fk} contribution to enthalpy formation and G_{fk} contribution to Gibbs free energy of formation of groups k.

The highlight the similarity of Equation 22 and Equation 27, for the calculation of the enthalpy of formation in the GANI and JOBACK methods, respectively. The main difference in these equations lies in the identification of group k. It's known that the GANI method considers second-order interactions, consequently, the groups identified by this method may be different from that obtained by JOBACK. Similarly, it happens in Equation 23 and Equation 28 for Gibbs energy calculation.

Vapor pressure (p_{vap}): The fragment-based method [19] and the Clausius-Clapeyron equation were applied to estimate vapor pressures of TAGs using Equation 29. As it wasn't possible to find experimental data for vapor pressures of unsaturated TAGs, then was considered that the chains of saturated and unsaturated fatty acids have identical vapor pressures when they have the same number of carbon atoms for the fragment approach.

ZONG:

$$\log P\,(T) = \frac{-\Delta G_\theta^{vap}}{R\theta ln10} + \frac{\Delta H_\theta^{vap}}{R\theta ln10}\left(\frac{1}{\theta} - \frac{1}{T}\right) \quad (29)$$

where P is the vapor pressure (Pa), T is the absolute temperature (K), R is the constant of the gases, θ is the reference temperature (θ=298.15 K), ΔH_θ^{vap} is the vaporization enthalpy at the reference temperature θ, and ΔG_θ^{vap} is the Gibbs energy of vaporization at the reference temperature θ.

A group contribution method was proposed to estimate vapor pressure and heats of vaporization as a function of the temperature of organic liquids found in the oil and biofuel industries [29]. The regression of the parameters was based on an extensive database, composed of fatty acids, esters of methyl, ethyl, propyl and butyl, tri-, di- and monoacylglycerols and hydrocarbons. This methodology improved the predictions obtained by [18] method, due to the inclusion of new experimental data of esters and acylglycerols (in addition to hydrocarbons) and critical points. Like this, the equation 30 was used to calculated of vapor pressure (P_{vap}). The pressure is in Pa and temperature in K.

CERIANI:

$$\ln(P^{vap}) = A + \frac{B}{T} + C \cdot \ln(T) \quad (30)$$

$$A = \sum_k N_k(A_{1k} + M_M \cdot A_{2k}) + (s_0 + N_{Cs} \cdot s_1) + \alpha(f_o + N_C \cdot f_1)$$

$$B = \sum_k N_k(B_{1k} + M_M \cdot B_{2k}) + \beta(f_o + N_C \cdot f_1)$$

$$C = \sum_k N_k(C_{1k} + M_M \cdot C_{2k})$$

N_k is the number of k groups in the molecule, MM is the molecular mass of the component, N_{Cs} is the number of carbons of the alcoholic part of methyl and ethyl esters ($N_{cs\ equals}$ 1 and 2, respectively), NC is the total number of carbon atoms in the molecule. A_{1k}, B_{1k}, C_{1k}, A_{2k}, B_{2k}, C_{2k}, α, β, s_0, s_1, f_0 and f_1 are the parameters obtained by regression.

The model for predicting vapor pressure and heat of vaporization from organic compounds to the critical point using the same sets of functional groups as proposed in [18] was improved by [29], but with another dependence on temperature. The authors' proposal was a consequence of the works of [30] and [31], which indicated the limitation of the equation of determination of vaporization enthalpies at a temperature range.

Vaporization enthalpy (H_{vap}): A model to predict vaporization heat from the Clausius-Clapeyron equation (Equation 31) was developed by [30] and the group contribution method of [18] (Equation 32). After substitution and manipulating in the Clausius-Clapeyron equation, an equation for ΔH_{vap} was obtained as a function of temperature (Equation 33).

$$\frac{dP_i^{vap}}{dT} = \frac{P_i^{vap}\Delta H_i^{vap}}{RT^2} \quad (31)$$

$$P_i^{vap} = exp\left(A_i + \frac{B_i}{T^{1.5}} - C_i lnT - D_i T\right) \quad (32)$$

$$\Delta H_i^{vap} = -R\left(\frac{1.5B_i}{\sqrt{T}} + C_i T + D_i T^2\right) \quad (33)$$

R represents the universal constant of gases and B_i, C_i and D_i are the parameters of the same contribution group used to estimate the vapor pressure in [18]. In high temperature and high vapor pressure conditions, the ideal gas condition made in the equation (Equation 33) isn't valid. Therefore, [30] included a correction term, which originated Equation 34.

$$\Delta H_i^{vap} = -R\left(\frac{1.,5B_i}{\sqrt{T}} + C_i T + D_i T^2\right)\left(1 - \frac{T_c^3 P_i^{vap}}{T^3 P_c}\right)^{0.5} \quad (34)$$

P_i^{vap} is the vapor pressure of component i and Tc and Pc are critical temperature and critical pressure respectively.

Changes in the previous prediction model for calculating heat of vaporization were made by [29] to obtain a wider range of compounds. Thus, the authors studied several compounds available in the databases so that the parameters of the equation for the calculation of vaporization heat were updated.

A linear equation to estimate heat of vaporization was used by [25]. ΔH_{vap}, as a function of reduced temperature (Tr) and acentric factor ω. This expression was derived in an analytical equation [31], through an approximation of the correlation of 0.6 <Tr <1.0 (Equation 35).

$$\frac{\Delta H_{vap}}{RT_c} = 7.08(1 - T_r)^{0.354} + 10.95\omega(1 - T_r)^{0.456} \quad (35)$$

[32] applied another group contribution method to estimate vaporization heat for several substances as a function of reduced temperature (Equation 36).

$$\Delta H_{vap} = A(1 - T_r)^{\alpha}\exp(-\alpha T_r) \quad (36)$$

ΔH_{vap} represents vaporization heat, T_r at reduced temperature, and A and α are contributing parameters of the group.

[19] used Equation 29 to predict vaporization enthalpy. The vaporization heat appears from the correlation of vapor pressure by Antoine's equation. Temperature dependence with vaporization heat was not evaluated.

Density (ρ): Rackett's modified equation was used to estimate the density of liquid vegetable oils [33]. First, the density of the liquid mixture of free fatty acids was estimated and then a correction factor was added to describe the shape of the TAGs (Equation 37). No correction factors were presented for DAGs and MAGs.

$$\rho = \frac{\sum x_i MM_i}{R\left(\frac{\sum x_i T_{ci}}{P_{ci}}\right)(\sum x_i Z_{RAi})^{\left[1+(1-T_r)^{\frac{2}{7}}\right]}} + F_c \quad (37)$$

where x_i, MM_i, Tc_i, Pc_i, and Z_{RAi} are molar fractions, molecular mass, critical temperature, critical pressure and Rackett parameter, respectively, of each fatty acid i. T_r is the reduced temperature. The density is given in kg/m3.

The fragment-based approach was proposed by [19] to estimate the molar volume of each fragment with dependence on temperature, and then estimated the molar volume of the liquid based on the composition and contribution of each fragment (Equation 38).

$$v^L = \sum_A N_{frag,A} v_A^L(T) \quad (38)$$

v_A^L is the molar volume of the liquid of each fragment and $N_{frag,A}$ is the number of fragments A in a component.

[34] extended the method of group contribution developed by [35] to predict the densities of pure liquid compounds (Equation 39).

$$\rho = \frac{MM}{v} = \frac{MM}{\sum n_i \Delta v_i} \quad (39)$$

where MM molecular mass and ν molar volume.

Heat capacity (c_P): The fragment-based method to estimate the heat capacity of TAGs, DAGs and MAGs was described by [19]. Fragments of FAs and MAGs were expressed as linear temperature-dependent equations (Equation 40). Unsaturated fatty acid fragments were assumed to be identical.

$$C_p^L = \sum_A N_{frag,A} C_{p,A}^L(T) \quad (40)$$

where $N_{frag,A}$ the number of fragments A in the component and $C_{p,A}^L$ is the contribution of the calorific capacity of the fragment in component A (J/kmol. K).

Ceriani *et al*. [30] extended their method of contribution of groups previously used for the prediction of vapor pressure of organic liquids to develop a heat capacity model with the same set of functional groups in addition to a new linear relationship as a function of the contribution of the group (Equation 41).

$$C_{pi}^L = \sum_k N_k (A_k + B_k T) \quad (41)$$

N_k represents the number of K groups in the molecule, A_k and B_k are obtained from regression parameters.

Heat capacities for TAGs and vegetable oils was estimated by [36], primarily by Rowlinson-Bondi equation [37][38]. Equation 42 estimated the heat capacities of pure fatty acids. They then added a correction factor, based on study of [33], to predict the density of triacylglycerols. Resulting in an expression with dependence on the molecular mass of the oil (Equation 43).

$$\frac{C_{p(AG)} - C_{p(AG)}^0}{R} = 1.45 + 0.45(1 - T_r)^{-1} + 0.25\omega\left[17.11 + 25.2(1 - T_r)^{1/3} T_r^{-1} + 1.742(1 - T_r)^{-1}\right] \quad (42)$$

$c_{p(AG)}$ is the liquid specific heat of fatty acids, $c_{p(AG)}^0$ the specific heat of the ideal gas, R the universal constant of gases, T_r the reduced temperature and ω the acentric factor.

$$C_{p(estimado)} = C_{p(AG)} + F_c \quad (43)$$

F_c correction factor dependent on the molecular mass of the oil.

II.2 CHARACTERIZATION OF VEGETABLE OILS

To evaluate the methods of prediction of properties correctly, one should make the choice of consistent data, that is, the composition of the studied oil sample should be as real as possible, in order to ensure that the conclusions are effective.

For soybean, sunflower and palm oil, which were used as raw material in this work, the composition used in triacylglycerols was that obtained by [39], [40], [41], respectively. These authors determined the oil profile in TAGs by high performance liquid chromatography (HPLC).

For macauba pulp oil, as the composition in TAGs, DAGs and MAGs was not found in the literature, two characterization methodologies were proposed. The first is an approach in which oil is represented by a mixture of Mixed TAG, either by (A) high resolution gas chromatography or (B) computational methodology proposed by [42]. The second approach characterizes vegetable oil as a mixture of fatty acids.

Approach 1:

(A) High Performance Gas Chromatography Analysis (GC)

The sample of macauba pulp oil was diluted in toluene at the final concentration of 0.7%. GC analysis was performed without derivatization on a thermo stabilized fused silica capillary column of TG-5 HT from Thermo brand of 15 meters x 0.25 mm x 0.10 micrometers. The analysis was performed with hydrogen flow from 1.5 mL to 50ºC under constant pressure. The initial temperature of the column was 50ºC, with a temperature increase schedule of 15ºC/minute to 180ºC, with ramps of 7ºC/minute up to 230ºC and up to 350ºC with programming of 10ºC/min, remaining at this temperature for another 25 minutes. The injector was maintained at 320ºC, in the flow division mode of 1:50 and 1 microliter of solution was injected. The detector was maintained at 380ºC.

Internal normalization was performed to quantify triacylglycerols. Standards of palmitic acid, linoleic, monoolein, monopalmitin, diolein, dipalmitin, tripalmitin and triolein from Sigma and Nu Chek brands were used for identification. They were dissolved in toluene PA.

(B) Computational Analysis

The computer program was assembled in Microsoft Excel based on equations to calculate the molar percentage of triacylglycerols according to the distribution and molar composition of fatty acids present in vegetable oil.

For the characterization of the pulp oil of the macauba to be performed, the fatty acid profile was necessary. Thus, the mass composition obtained by [43].

For the construction of the oil profile studied in TAGs, 33 triacylglycerol molecules with 99 fatty acid radicals were considered, and the number of each radical in these 33 molecules was proportional to the percentage shown in composition [43]. These FA radicals were randomly distributed among the 33 molecules of TAGs.

Thus, the thermophysical properties were estimated for each mixed TAG by applying the specific prediction method and then the mixing rule was used to estimate the oil property according to the composition of mixed triacylglycerols.

Approach 2: The second approach is based on the characterization of vegetable oil as being a mixture of fatty acids. That is, the fatty acid composition of the oil is used to determine the properties of interest. This methodology has been the most used by researchers, because there is a greater amount of experimental data on the properties of pure fatty acids.

III. RESULTS AND DISCUSSIONS

Three statistical parameters have been used to determine the accuracy of the performed predictions: absolute deviation (AD), relative deviation (%RD) and absolute average relative deviation (%AARD):

$$Absolute\ deviation\ (AD) = \left|x_{exp,i} - x_{calc,i}\right| \quad (44)$$

$$\%RD = \frac{\left|x_{exp,i} - x_{calc,i}\right|}{X_{exp,i}} \quad (45)$$

$$\%AARD = \frac{\sum_i^N \frac{\left|X_{exp,i} - X_{calc,i}\right|}{X_{exp,i}}}{n} \quad (46)$$

X is the property to be evaluated, n is the number of experimental data, and the subscripts “exp” and “calc” indicate the experimental and calculated property, respectively.

III.1 ESTIMATION OF THERMODYNAMIC PROPERTIES

The estimated properties for TAGs, DAGs, MAGs and FAs, which will be discussed below, are available in the supplementary materials.

Normal boiling temperature (Tb): First, normal boiling temperatures for triacylglycerols were estimated, whose experimental data were found in the literature. The contribution methods of JOBACK and GANI groups, and the method based on ZONG fragments were evaluated and the estimated data are represented in Figure 2.

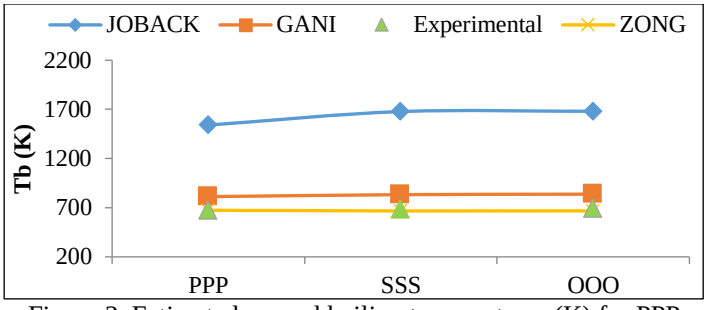

Figure 2: Estimated normal boiling temperatures (K) for PPP (tripalmitin), SSS (tristearin) and OOO (triolein).
Source: Authors, (2020).

Figure 2 shows the t_b estimated for three simple triacylglycerols, PPP, SSS and OOO, compared to experimental data obtained in [44], [45] [38]. The results show that the T_b values calculated by the JOBACK method have high deviations (AARD>100%). The lowest absolute average relative deviation was reached when the ZONG method was used (AARD=1.9%), followed by 21% for GANI. Thus, the ZONG method was used in this work to calculate T_b for vegetable oils, in the TAG approach.

Since no experimental data from The MAGs and DAGs were found in the literature, the method adopted for the determination of T_b was the ZONG method, which observed lower deviations for the TAGs analyzed, as shown above.

The relative deviations of the estimate of T_b for fatty acids according to JOBACK and GANI are presented in Figure 3. The experimental data used are found in [21] and [46]. It's noteworthy that it wasn't possible to apply the fragment-based methodology proposed by [19] for these compounds.

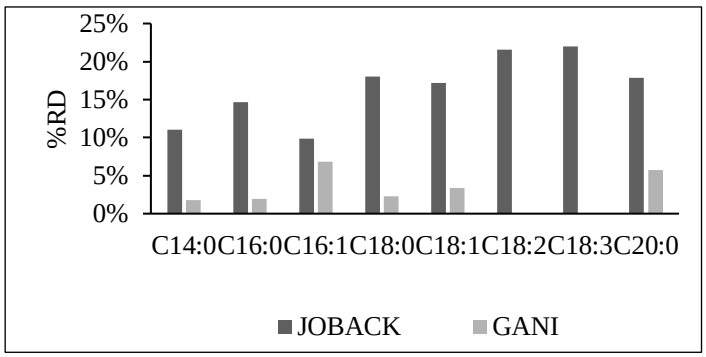

Figure 3: Relative deviations (%) for normal boiling temperature for fatty acids in the JOBACK and GANI methods.
Source: Authors, (2020).

By the analysis of Figure 3, it is observed that the greatest deviation of the GANI method occurred in unsaturated fatty acid C16:1. The absolute average relative deviation (AARD) found for saturated fatty acids was 15.4% for the JOBACK method and 2.9% for GANI. On the other hand, unsaturated FAs gave AARD equal to 17.6% and 2.5% for the same methods, respectively. This analysis shows the agreement of the estimation of T_b by the GANI method for both saturated and unsaturated AGs.

A T_b curve as a function of the molar mass of saturated and unsaturated FAs was constructed to improve previous analysis (Figure 4). In this figure, the boiling points of saturated fatty acids (continuous line) show an almost linear characteristic. In addition, it can be noted the proximity of the experimental data with the values estimated by the GANI method.

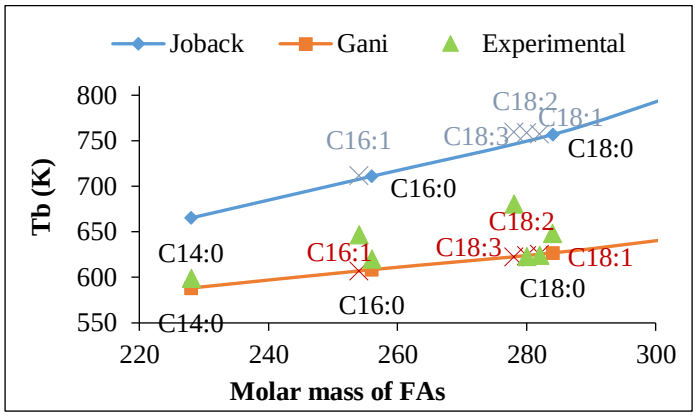

Figure 4: Normal boiling temperatures (K) estimated as a function of molar mass for fatty acids. X represents unsaturation.
Source: Authors, (2020).

It's important to highlight that, in a simulation study of biodiesel production, an error in the value of T_b will imply in the erroneous prediction for other properties, such as critical properties. This fact leads to erroneous results when properties, such as viscosity and density, are calculated using equations and correlations incorporated into commercial simulators.

Critical properties (P_c, V_c, T_c and Z_c): Critical properties were estimated for TAGs, DAGs and MAGs for AMBROSE [23], JOBACK [15], GANI [16] and LYDERSEN [24] methods.

It's important to mention that only critical temperature data from some AGs were found [46]. No values were available for TAGs, DAGs and MAGs. However, they were considered enough to point out the most precise method.

The AARD obtained for the predicted critical temperatures for the AGs compared to the experimental data are 3.31%, 0.52%, 3.57% and 2.40%, respectively, for the JOBACK, GANI, LYDERSEN and AMBROSE methods.

It's noted that the GANI method presented an average of the smaller relative deviations for fatty acids (AARD=0.52%). In addition, this method is the only one among those evaluated that requires, as input, only the molecular structure (ASPEN TECH, 2014). Thus, this methodology was chosen to predict the critical properties of the components of vegetable oils.

Critical properties were estimated for several compounds involved in biodiesel production by [47]. Fatty acids, triacylglycerols and methyl esters were analyzed. The authors compared the data obtained with experimental data and pointed to GANI as the most accurate method, compared to the other two studied, [15] and [48].

The critical properties were estimated using the methods of [23] and [15] by [49]. According to the authors, in these two methods the critical temperature estimation is dependent on the normal boiling temperature. Therefore, the critical temperature was also evaluated by the authors by [50], in which the critical temperature is independent of the normal boiling temperature. According to [49], the Joback method presented the lowest

deviations for critical volume and Ambrose's method presented the smallest deviations from the data available in [46] for critical temperature and pressure.

[51] evaluated the critical temperature by the methods of [50], [15] and [24]. Comparing the results with predicted values in [46], the authors selected the Lydersen and Joback groups and highlighted the success of these methods because they considered the experimental value of normal boiling temperature in the prediction of critical temperature.

Acentric factor (ω): The data estimated by [25], [26] and [26] showed similar results, as can be seen in Table 2.

Table 2: Estimated data of the acentric factor for trilinolinin (LLL), dilinolein (LL) and monolein (L).

Components	Pitzer	Kesler-Lee
LLL	-0.6524	-0.6343
LL	-0.3183	-0.3183
L	1.0146	1.0692

Source: Authors, (2020).

In this work, the Pitzer rule was adopted for the determination of the acentric factors of all compounds, as it's the most used method according to [37].

Enthalpy of formation and Gibbs free energy formation in the standard state (H_f^0 e G_f^0): Initially, the formation enthalpy data were evaluated for TAG (triolein-OOO), DAG (diolein-OO) and MAG (monoolein-O) compared to data available in the literature [52], [53].

Table 3 shows the absolute deviations obtained for each method used in estimating this property. It is noted that the evaluated methods presented relative mean deviations below 3%. The lowest AARD was observed when GANI (0.75%) was used, followed by JOBACK (0.95%). However, the GANI method requires normal boiling temperature as input. Thus, to avoid the error associated with a previously estimated measurement, the method chosen in this work was JOBACK. This requires as input only the molecular structure of the compounds. The Gibb's free energies also were calculated by JOBACK for TAGs, DAGs and MAGs.

Table 3: AD and AARD of the standard energy of formation of TAG, DAG and MAG.

	DIPPR 801(kJ/mol)	Absolute deviation (kJ/mol)		
		JOBACK	GANI	BENSON
OOO	-2161	14.415	1.078	35.053
OO	-1670	14.844	16.090	44.916
O	-1175	15.345	14.681	45.660
	AARD(%)	***0.954***	***0.754***	***2.733***

Source: Authors, (2020).

For the FAs, only data from stearic acid formation enthalpy (-884.7 kJ/mol) were obtained in the literature. The absolute deviations (AD) found for the methods of JOBACK, GANI and BENSON, respectively, were 119.58, 121.14 and 389.22 kJ/mol. Therefore, the first method was chosen to predict the formation energy for fatty acids.

For Gibbs free energy, the method chosen for fatty acids was BENSON [37]. According to [54], this is more accurate in estimating this property compared to GANI and JOBACK methods, considering the effects of neighboring atoms on calculations.

Vapor pressure (P_{VAP}): The vapor pressure was initially evaluated for simple TAGs by the group contribution method [29] and fragment-based method [19], [55]. Figure 5 compares the estimated P_{vap} data compared to experimental data for tristearin (SSS) and tripalmitin (PPP), obtained in [56].

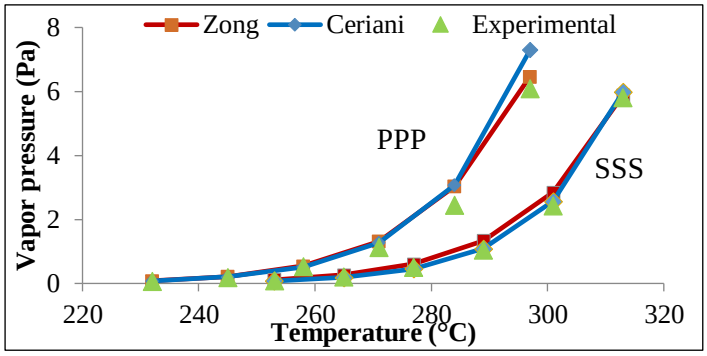

Figure 5: Experimental and estimated steam pressure (Pa) data for tripalmitin (PPP) and tristearin (SSS).
Source: Authors, (2020).

The methods of [29], [19], [55] showed similar predictions for TAGs as shown in Figure 5. The means of the deviations of the estimated steam pressures, in the temperature range of 230 to 313°C, for the simple triacylglycerols tripalmitin (PPP) and tristearin (SSS) were respectively 15.01 and 20.04 for ZONG and 6.63 and 19.58 for CERIANI. This resulted in AARDs for the ZONG method of 17.52% and for CERIANI 13.11%. By the analysis of the AARDs, the method of [29] showed higher accuracy, so it was pointed to the estimation of steam pressure for TAGs.

Moreover, according to [29], the proposed method can represent any number of fatty and hydrocarbon compounds with the lowest number of parameters and can extrapolate the temperature (critical point), by correctly describing the vapor pressures and vaporization heats.

Enthalpy of vaporization (H_{VAP}): Table 4 shows the estimated values for enthalpy of vaporization compared to data obtained from [46].

According to the analysis in Table 4, the lowest AARD was observed for the Basarova method (AARD=2.68%), followed by Ceriani (AARD=10.05%) and Pitzer (AARD=25.55%). It is noteworthy that, for the methods of [25] and [32], it is necessary to inform the critical temperatures and pressures, and the acentric factors of the TAGs.

Table 4: Relative deviations (RD) and absolute average relative deviation (AARD) of enthalpy of vaporization.

	Temp. (°C)	Exp. (kJ/mol)	RD (%)		
			[29]	[25]	Basarova [32]
SSS	247-314	164.63	13.84	27.74	2.89
PPP	232-300	158.53	6.27	23.36	2.47
		AARD(%)	***10.05***	***25.55***	***2.68***

Source: Authors, (2020).

For [31] indicated Basarova and Svoboda method to predict enthalpy of vaporization values when the Ceriani and Meirelles method (2004) was used [31]. In turn, [29] corrected the temperature limitations of the previously proposed method [18]. So, the method adopted in this study to predict Δhvap of TAGs, DAGs and MAGs was Ceriani [29].

Density (ρ): Table 5 compares density predictions by [19], [33], [34], [55] to experimental data of simple TAGs [57-59].

Table 5: Densities estimated for simple TAGs.

Components	*AARD (%)*		
	HALVROSEN	**ZONG**	**IHMELS**
PPP	0.3	0.2	1.1
SSS	3.6	4.0	2.7
OO	2.8	2.1	1.5
LLL	1.2	0.1	1.4

Source: Authors, (2020).

All four methods evaluated ensure accuracy by predicting density for TAGs in the temperature range from 80°C to 100°C. The means of the deviations found were low, not exceeding 4.0%.

The method described in [33] doesn't have adequate correction factors for the DAGs and MAGs of the Rackett equation to estimate the density of vegetable oils. In addition, the method of contribution of groups showed in [34] isn't particularly designed for predictions of lipid compound density. In other words, there isn't specific group to describe the portion of glycerol in TAGs, DAGs, MAGs and oils. Therefore, groups CH2, CH, CH2OH, and CHOH should be used as substitutes when describing the portion of glycerol. To improve the accuracy of the method, data should be developed for the glycerol group.

While the methods described by [19], [55] were based on fragments, generally more accurate than group contribution methods. Also, can be to observe an increasing order to AARDtotal of densities estimated like: ZONG (1.6%) < IHMELS (1.7%) < HALVROSEN (2.0%). Then, the ZONG method was chosen to predict the densities of TAGs, DAGs and MAGs

Figure 6 illustrates the good agreement of the [34] method for the calculation of the density of fatty acids. For this comparison, experimental data from [60] were used and [61]. In this, continuous lines are estimated data and points are experimental values, equal colors mean the same fatty acid.

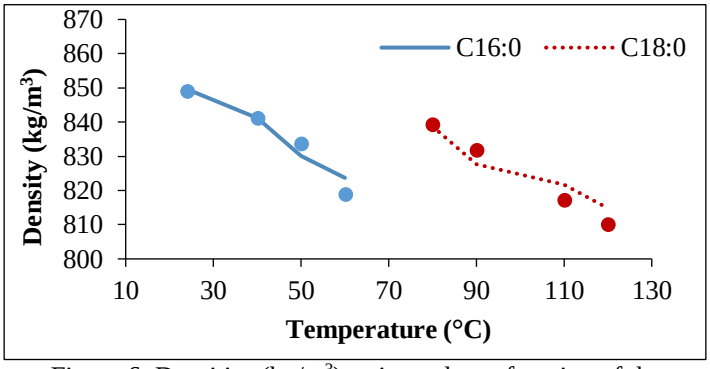

Figure 6: Densities (kg/m^3) estimated as a function of the temperature of FAs. Continuous lines represent the estimated data and the points experimental values obtained from the literature.
Source: Authors, (2020).

The AARD (%) obtained for fatty acids for the [34] method was low (0.30%). Showing that the method is accurate when estimating the density for these compounds.

Heat capacity (cp): The deviations of estimated heat capacities compared to experimental data from [58] and [36] can be seen in Table 6. The data were estimated in the temperature range of 60-180°C.

The results obtained, as shown in Table 6, showed that the method [19] have greater accuracy than [30] and [36]. In this specific case, the AARD for the ZONG method was 0.88%, while for [30] and [36] were 3.26% and 1.51%, respectively. It is worth mentioning that the method of [36] is applicable only to TAGs.

Table 6: Heat capacities estimated for simple TAGs.

Components	**AARD (%)**		
	MORAD [36]	**ZONG** [19]	**CERIANI** [30]
PPP	2.74	1.24	2.21
SSS	1.10	1.24	1.33
OOO	0.68	0.15	6.25
AARD$_{total}$ (%)	**1.51**	**0.88**	**3.26**

Source: Authors, (2020).

Therefore, the methodology proposed by [19] was adopted. for the calculations of this property for TAGs, DAGs and MAGs.

III.2 CHARACTERIZATION OF OILS

Approach 1:

(A) High Performance Gas Chromatography Analysis (GC)

The results of chromatographic analysis can be seen in Table 7.

As in this technique a non-polarized capillary column was used, the analysis is qualitative and simplified, because the TAGs are separated into groups having the same number of carbon atoms, not being possible the determination of unsaturation.

Table 7: Composition of macauba pulp oil obtained by GC.

Sample	**Macauba pulp oil**		
TAGs	**Rep. 1**	**Rep. 2**	**Examples of possible TAGs**
C48	0.77924	0.80121	PPP
C50	9.96296	9.79972	PPS, PPO, PPL, PPLn
C52	42.1804	41.928	SSP
C54	47.077	47.471	SSS, OOO, LLL

Source: Authors, (2020).
Note: There isn't differentiation between C18:0, C18:1 e C18:2.

A more refined separation of TAGs occurs when a polarized column is used in chromatographic analysis. Thus, in a polarized column, the separation of TAGs, such as POO and PLS, which are TAGs with the same number of carbons and degree of unsaturation, but with different polarity, can be achieved. In both non-polar and polarized columns, there is no discrimination between isomeric triacylglycerols such as POO and OPO [42].

(B) Computational Analysis

Table 8 shows the proportions of triacylglycerols through the composition of fatty acids obtained from the computational program created in this work according to the methodology cited by [42].

Table 8: Characterization of macauba pulp oil in TAGs.

Groupss	**TAGs**	**%m/m**	**Groupss**	**TAGs**	**%m/m**
C50:1	POP	8.0	C52:4	PLnO	4.0
C50:1	PPoS	2.0	C54:2	SOO	4.0
C52:2	POO	28.0	C54:3	OOO	26.0
C52:3	OPoO	4.0	C54:4	OOL	14.0
C52:3	PLO	2.0	C54:5	OLL	2.0
C52:4	LOPo	6.0			

Source: Authors, (2020).

The identification of triacylglycerols by groups with different numbers of carbon atoms and by different combinations of saturated and unsaturated fatty acids were made by comparing the percentage data obtained from the GC with those provided by the program created on the computer. The data in Table 9 show that the proportions of each component calculated by the computer (PC) are close to the average obtained by chromatographic analysis (GC).

Table 9: Composition of macauba pulp oil in triacylglycerols by GC and using a program elaborated on the computer (PC).

Number of Carbons	Composition (%)	
	PC	GC
C48	0.00	0.79
C50	10.00	9.88
C52	44.00	42.05
C54	46.00	47.27

Source: Authors, (2020).

Thus, the list of triacylglycerols presented in Table 8, obtained by the computer program, will be considered as the composition of the macauba pulp oil for this present study. Since the mixed triacylglycerol approach is closer to reality, and the results of chromatographic analysis show that the program used for the distribution of mixed TAGs meets the data obtained experimentally.

III.3 SELECTION OF THE MACAUBA OIL CHARACTERIZATION METHOD

The choice of the appropriate characterization method is important in the prediction of thermophysical properties. Some criteria to be considered in the adoption of the method are ease of use, rigorous characterization, and satisfactory predictions. Table 8 and [43] showed the composition of macauba oil in terms of TAGs and fatty acids, respectively.

Predictions of some properties were made to compare the two approaches to oil characterization. Table 10 shows predictions of density and calorific capacity of macauba pulp oil for the approach in mixed TAGs and fatty acids.

Table 10: Densities and heat capacities by the two approaches of characterization of macauba pulp oil.

	Method	TAG-Mixed	Fatty acids
Density	[33]	0,17	0,16
	[19]	0,97	ND
	[34]	1,79	1,83
Heat capacity	[36]	2,17	2,50
	[19]	2,20	ND
	[30]	0,56	0,47

Source: Authors, (2020).

According to the analysis of Table 10, it can be observed that the two approaches had similar estimates, with small average of relative deviations. However, it's recommended to use the characterization of oils in mixed TAGs, because it is closer to the real.

III.4 PROPERTIES OF VEGETABLE OILS

It's known that vegetable oil is a mixture of various TAGs, DAGs, MAGs and free FAs. In this work was adopted that vegetable oils were composed only of TAGs and DAGs. To determine the properties of vegetable oils, their compositions presented above, and the predicted properties of the compounds present in the mixture were used, using the ideal mixing rule (equation 47).

$$P_{mixture} = \sum_{i=1}^{n} x_i P_{pure,i} \quad (47)$$

The methods adopted to predict the thermophysical properties of TAGs, DAGs and MAGs, consequently of vegetable oils, are summarized in Table 11.

Table 11: Methods adopted to predict the thermophysical properties of vegetable oils.

Properties	Methods
T_b	Zong *et al.* (2010a and 2010b)
Tc, *Pc* e *Vc*	Constantinou and Gani (1994)
Acentric factor(ω)	Pitzer (1995)
Enthalpy formation(H_{f0})	Joback and Reid (1987)
Gibbs Energy(G_{f0})	Joback and Reid (1987)
P_{vap}	Ceriani *et al* (2013)
H_{vap}	Ceriani *et al* (2013)
ρ	Zong *et al.* (2010[a] e 2010[b])
c_p^L	Zong *et al.* (2010[a] e 2010[b])

Source: Authors, (2020).

Therefore, the estimated properties for vegetable oils were compared with experimental data available in the literature. The representation of temperature-dependent thermophysical properties, such as vaporization enthalpy (H_{vap}), heat capacity (c_{pL}), density (ρ) and vapor pressure (P_{vap}) is shown in Figure7(a), Figure 7(b), Figure 7(c) and Figure 7(d), respectively.

By the analysis of Figure 7 (a), it is observed that the enthalpy of vaporization of vegetable oils decreases with increasing temperature. Heat of vaporization for soybean oil was determined by [62], H_{vap}=184.9 kJ/mol. The predicted value for soybean oil in this study was in the range of 216 to 174 kJ/mol, showing that there is agreement of the predicted given with the experimental. By the analysis of Figure 7 (b), it can be observed that the calorific capacities of the analyzed vegetable oils increased linearly with the increase in temperature from 20 to 80°C. Similar behavior was observed by [63].

Density and viscosity for babassu, buriti, Brazil nut, macadamia and grape seed oils were obtained by [38]. The densities found were from 912 to 876 kg/m^3, in the temperature range of 20-70°C. [64] determined the density of palm oil, ρ=888 kg/m^3 at 50°C, close to the value found in this study (880 kg/m^3). For sunflower oil, these authors found density in the range of 880 to 945 kg/m^3 in the temperature range of -20 to 80°C. Similar values were found, as shown in Figure 7 (c) [65] determined for the pulp oil of macauba densities in the range of 918.5 to 925.3 kg/m^3,showing again that the estimates calculated in this study reached good precision.

Vapor pressure of various vegetable oils was determined by [66]. The authors found vapor pressures for soybean oil in the range of 2.6kPa to 73.5kPa, ranging from 250-330°C. Similar values were observed, as can be seen in Figure 7 (d).

Table 12 shows the rest of the thermophysical properties that were estimated for the different vegetable oils under study, which can be able to use as input data for engineering calculations like simulations and optimize process.

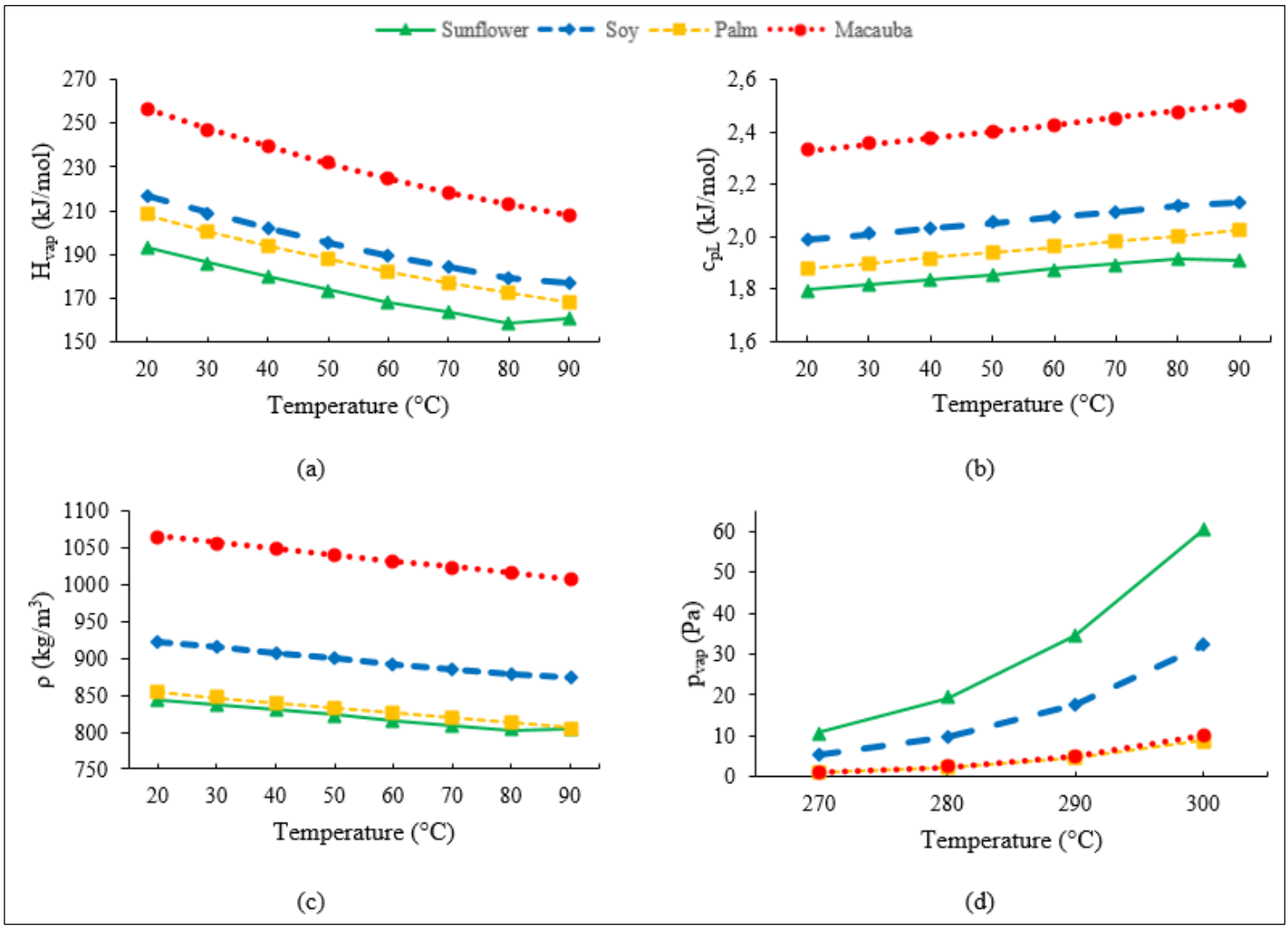

Figure 7: Estimated properties dependent on temperature (a) Vaporization enthalpy, (b) Heat capacity, (c) Density and (d) vapor pressure for sunflower (▲), palm (■), soybean (♦) and macauba pulp (●) oil.
Source: Authors, (2020).

Table 12: Estimated properties for vegetable oils by the methods adopted in this work.

Properties	**Sunflower**	**Soy**	**Palm**	**Macauba**
T_b *(K)*	583.34	662.40	615.54	739.08
T_C *(K)*	836.34	950.30	879.71	1051.57
P_C *(N/m²)*	2.95x10^5	3.36 x10^5	3.17 x10^5	3.86 x10^5
V_C *(m³/kmol)*	2.80	3.18	2.91	3.48
Z_C	0.04	0.05	0.03	0.03
H_f *(J/kmol)*	-1.40 x10^9	-1.76 x10^9	-1.84 x10^9	-2.09 x10^9
G_f *(J/kmol)*	-6.95 x10^7	-2.16 x10^8	-3.99 x10^8	-3.73 x10^8
ω	-0.59	-0.66	-0.62	-0.75

Source: Authors, (2020).

Finally, the values predicted in this study are in acceptable ranges when compared with experimental data of similar vegetable oils. The difference in the composition of oils, especially in the number of unsaturation, causes changes in thermodynamic properties, as seen in the previous analyses.

IV. CONCLUSIONS

This work showed that the modeling of properties of TAGs, DAGs, MAGs and fatty acids is closely linked to the estimation of base parameters, such as normal boiling temperature, critical temperature, pressure and volume and acentric factor. In addition, it was shown that the use of experimental data to validate the method should be carried out with caution, considering that the nature of many available data is predicted.

Prediction models of properties such as group contribution and fragment approach were evaluated to determine the normal boiling point, critical properties, vapor pressure, liquid density, calorific capacity and vaporization enthalpy of fatty acids, triglycerides, diacylglycerols and monoacylglycerols. It was possible to arrive at values similar the experimental values of the properties to vegetable oils with the application of selected methods for each property.

The estimation of the thermophysical properties of vegetable oils is of paramount importance when one wishes to evaluate biofuel production processes by simulation technique. This is because experimental data of these raw materials are scarce in the literature. Therefore, a database with values close to the actual is required for the use of simulators to have correct predictions. Thus, in this work a database was created that can be used as input parameters in simulation projects.

V. REFERENCES

[1] A. E. Atabani, A. S. Silitonga, I. A. Badruddin, T. M. I. Mahlia, H. H. Masjuki, and S. Mekhilef, “A comprehensive review on biodiesel as an alternative energy resource and its characteristics,”

Renewable and Sustainable Energy Reviews, vol. 16, no. 4. pp. 2070–2093, May 2012, doi: 10.1016/j.rser.2012.01.003.

[2] N. S. Evangelista, F. R. do Carmo, and H. B. de Sant'Ana, "Estimation of Vapor Pressures and Enthalpies of Vaporization of Biodiesel-Related Fatty Acid Alkyl Esters. Part 2. New Parameters for Classic Vapor Pressure Correlations," Industrial and Engineering Chemistry Research, vol. 56, no. 29, pp. 8349–8357, Jul. 2017, doi: 10.1021/acs.iecr.7b01539.

[3] N. S. Evangelista, F. R. do Carmo, and H. B. de Sant'Ana, "Estimation of Vapor Pressures and Enthalpies of Vaporization of Biodiesel-Related Fatty Acid Alkyl Esters. Part 1. Evaluation of Group Contribution and Corresponding States Methods," Industrial and Engineering Chemistry Research, vol. 56, no. 8, pp. 2298–2309, Mar. 2017, doi: 10.1021/acs.iecr.6b04772.

[4] N. S. Evangelista, F. R. do Carmo, and H. B. de Sant'Ana, "Estimation of Physical Constants of Biodiesel-Related Fatty Acid Alkyl Esters: Normal Boiling Point, Critical Temperature, Critical Pressure, and Acentric Factor," Industrial and Engineering Chemistry Research, vol. 57, no. 25, pp. 8552–8565, Jun. 2018, doi: 10.1021/acs.iecr.8b01310.

[5] M. García, J. J. Alba, A. Gonzalo, J. L. Saínchez, and J. Arauzo, "Comparison of methods for estimating critical properties of alkyl esters and its mixturesaa," Journal of Chemical and Engineering Data, vol. 57, no. 1, pp. 208–218, Jan. 2012, doi: 10.1021/je201039n.

[6] E. D. Nikitin and A. P. Popov, "Vapor–liquid critical point measurements of fifteen compounds by the pulse-heating method," Fluid Phase Equilibria, vol. 380, pp. 11–17, Oct. 2014, doi: 10.1016/J.FLUID.2014.07.038.

[7] T. Wallek, J. Rarey, J. O. Metzger, and J. Gmehling, "Estimation of pure-component properties of biodiesel-related components: Fatty acid methyl esters, fatty acids, and triglycerides," Industrial and Engineering Chemistry Research, vol. 52, no. 47, pp. 16966–16978, Nov. 2013, doi: 10.1021/ie402591g.

[8] J. P. POLING, B. E; PRAUSNITZ, J. M.; O'CONNELL, The Properties of Gases and Liquids, 5th ed. New Yord: McGraw-Hill, 2001.

[9] Y. Nannoolal, J. Rarey, and D. Ramjugernath, "Estimation of pure component properties: Part 3. Estimation of the vapor pressure of non-electrolyte organic compounds via group contributions and group interactions," Fluid Phase Equilibria, vol. 269, no. 1–2, pp. 117–133, Jul. 2008, doi: 10.1016/J.FLUID.2008.04.020.

[10] B. Moller, J. Rarey, and D. Ramjugernath, "Estimation of the vapour pressure of non-electrolyte organic compounds via group contributions and group interactions," Journal of Molecular Liquids, vol. 143, no. 1, pp. 52–63, Sep. 2008, doi: 10.1016/J.MOLLIQ.2008.04.020.

[11] T. Wallek, J. Rarey, J. O. Metzger, and J. Gmehling, "Estimation of pure-component properties of biodiesel-related components: Fatty acid methyl esters, fatty acids, and triglycerides," Industrial and Engineering Chemistry Research, vol. 52, no. 47, pp. 16966–16978, Nov. 2013, doi: 10.1021/ie402591g.

[12] L. P. Cunico, A. S. Hukkerikar, R. Ceriani, B. Sarup, and R. Gani, "Molecular structure-based methods of property prediction in application to lipids: A review and refinement," Fluid Phase Equilibria, vol. 357, pp. 2–18, Nov. 2013, doi: 10.1016/j.fluid.2013.04.004.

[13] M. García, J.-J. Alba, A. Gonzalo, J. L. Sánchez, and J. Arauzo, "Comparison of Methods for Estimating Critical Properties of Alkyl Esters and Its Mixtures," Journal of Chemical & Engineering Data, vol. 57, no. 1, pp. 208–218, 2012, doi: 10.1021/je201039n.

[14] F. R. do Carmo, N. S. Evangelista, F. A. N. Fernandes, and H. B. de Sant'Ana, "Evaluation of Optimal Methods for Critical Properties and Acentric Factor of Biodiesel Compounds with Their Application on Soave-Redlich-Kwong and Peng-Robinson Equations of State," Journal of Chemical and Engineering Data, vol. 60, no. 11, pp. 3358–3381, Oct. 2015, doi: 10.1021/acs.jced.5b00638.

[15] K. G. Joback and R. C. Reid, "Estimation of Pure-Component Properties from Group-Contributions," Chemical Engineering Communications, vol. 57, no. 1–6, pp. 233–243, Jul. 1987, doi: 10.1080/00986448708960487.

[16] L. Constantinou and R. Gani, "New Group Contribution Method for Estimating Properties of Pure Compounds," AIChE Journal, vol. 40, no. 10, pp. 1697–1710, 1994.

[17] A. Fredenslund, R. L. Jones, and J. M. Prausnitz, "Group-contribution estimation of activity coefficients in nonideal liquid mixtures," AIChE Journal, vol. 21, no. 6, pp. 1086–1099, 1975, doi: 10.1002/aic.690210607.

[18] R. Ceriani and A. J. A. Meirelles, "Predicting vapor-liquid equilibria of fatty systems," Fluid Phase Equilibria, vol. 215, no. 2, pp. 227–236, Feb. 2004, doi: 10.1016/j.fluid.2003.08.011.

[19] L. Zong, S. Ramanathan, and C. C. Chen, "Fragment-based approach for estimating thermophysical properties of fats and vegetable oils for modeling biodiesel production processes," Industrial and Engineering Chemistry Research, vol. 49, no. 2, pp. 876–886, Jan. 2010, doi: 10.1021/ie900513k.

[20] R. M. Matricarde Falleiro, L. Y. Akisawa Silva, A. J. A. Meirelles, and M. A. Krähenbühl, "Vapor pressure data for fatty acids obtained using an adaptation of the DSC technique," Thermochimica Acta, vol. 547, pp. 6–12, Nov. 2012, doi: 10.1016/J.TCA.2012.07.034.

[21] "DDB. DORTMUND DATA BANK." Available http://www.ddbst.com/ddb.html. Access: February 2019.

[22] E. D. Nikitin, P. A. Pavlov, and P. V. Skripov, "Measurement of the critical properties of thermally unstable substances and mixtures by the pulse-heating method," The Journal of Chemical Thermodynamics, vol. 25, no. 7, pp. 869–880, Jul. 1993, doi: 10.1006/JCHT.1993.1084.

[23] D. Ambrose, "Correlation and Estimation of Vapour-Liquid Critical Properties. I Critical Temperatures of Organic Compounds," NPL Rep. Chem, no. 92, 1980.

[24] A. L. Lydersen, "Estimation of critical properties of organic compounds," 1955.

[25] K. S. Pitzer, "The Volumetric and Thermodynamic Properties of Fluids. I. Theoretical Basis and Virial Coefficients1," Journal of the American Chemical Society, vol. 77, no. 13, pp. 3427–3433, Jul. 1955, doi: 10.1021/ja01618a001.

[26] M. G. KESLER and B. I. LEE, "Improve Predictions of Enthalpy of Fractions.," Hydrocarbon Processing, no. 55, pp. 153–158, 1976.

[27] P. W. ATKINS, J. PAULA, and J. Keeler, Physico-chemical, Eleventh Edition. Oxford University Press, 2017.

[28] S. W. BENSON et al., "Additivity rules for the estimation of thermochemical properties," Chemical Reviews, vol. 69, no. 3, pp. 279–324, 1969.

[29] R. Ceriani, R. Gani, and Y. A. Liu, "Prediction of vapor pressure and heats of vaporization of edible oil/fat compounds by group contribution," Fluid Phase Equilibria, vol. 337, pp. 53–59, 2013, doi: 10.1016/j.fluid.2012.09.039.

[30] R. Ceriani, R. Gani, and A. J. A. Meirelles, "Prediction of heat capacities and heats of vaporization of organic liquids by group contribution methods," Fluid Phase Equilibria, vol. 283, no. 1–2, pp. 49–55, Sep. 2009, doi: 10.1016/j.fluid.2009.05.016.

[31] Y. C. Su, Y. A. Liu, C. A. Diaz Tovar, and R. Gani, "Selection of prediction methods for thermophysical properties for process modeling and product design of biodiesel manufacturing," Industrial and Engineering Chemistry Research, vol. 50, no. 11, pp. 6809–6836, Jun. 2011, doi: 10.1021/ie102441u.

[32] P. Basařová and V. Svoboda, "Prediction of the enthalpy of vaporization by the group contribution method," Fluid Phase Equilibria, vol. 105, no. 1, pp. 27–47, Mar. 1995, doi: 10.1016/0378-3812(94)02599-V.

[33] J. D. Halvorsen, W. C. Mammel, and L. D. Clements, "Density estimation for fatty acids and vegetable oils based on their fatty acid composition," Journal of the American Oil Chemists' Society, vol. 70, no. 9, pp. 875–880, 1993, doi: 10.1007/BF02545346.

[34] E. C. Ihmels and J. Gmehling, "Extension and revision of the group contribution method GCVOL for the prediction of pure compound liquid densities," Industrial and Engineering Chemistry Research, vol. 42, no. 2, pp. 408–412, 2003, doi: 10.1021/ie020492j.

[35] H. S. Elbro, A. Fredenslund, and P. Rasmussen, "Group contribution method for the prediction of liquid densities as a function of temperature for solvents, oligomers, and polymers," Industrial & Engineering Chemistry Research, vol. 30, no. 12, pp. 2576–2582, Dec. 1991, doi: 10.1021/ie00060a011.

[36] N. A. MORAD, A. A. M. KAMAL, F. PANAU, and T. W. YEW, "Liquid specific heat capacity estimation for fatty acids, triacylglycerols, and vegetable oils based on their fatty acid composition," Journal of the American Oil Chemists' Society, vol. 77, no. 9, pp. 1001–1005, 2000, doi: 10.1007/s11746-000-0158-6.

[37] R. C. REID, J. M. PRAUSNITZ, and B. E. POLING, The properties of gases and liquids., 4th ed. New York: McGraw-Hill, 1987.

[38] R. Ceriani, F. R. Paiva, C. B. Gonçalves, E. A. C. Batista, and A. J. A. Meirelles, "Densities and viscosities of vegetable oils of nutritional value," Journal of Chemical and Engineering Data, vol. 53, no. 8, pp. 1846–1853, Aug. 2008, doi: 10.1021/je800177e.

[39] S. C. Cunha and M. B. P. P. Oliveira, "Discrimination of vegetable oils by triacylglycerols evaluation of profile using HPLC/ELSD," Food Chemistry, vol. 95, no. 3, pp. 518–524, Apr. 2006, doi: 10.1016/j.foodchem.2005.03.029.

[40] F. Ma and M. A. Hanna, "Biodiesel production: a review 1." Bioresource Technology; 70, - 1-15, 1999, https://doi.org/10.1016/S0960-8524(99)00025-5.

[41] M. N. DUNKLE, F. DAVID, and P. SANDRA, Analysis of triglycerides in vegetable oils using the Agilent 1260 Infinity Analutical SFC System with evaporative light scattering detection, 5991st–0987EN ed. Agilent Technologies Publication, 2012.

[42] N. R. Antoniosi Filho, O. L. Mendes, and F. M. Lan, "Computer Prediction of Triacylglycerol Composition of Vegetable Oils by HRGC." Chromatographia, 40, 557-562, 1995.

[43] J. C. del Río, A. B. Evaristo, G. Marques, P. Martín-Ramos, J. Martín-Gil, and A. Gutiérrez, "Chemical composition and thermal behavior of the pulp and kernel oils from macauba palm (Acrocomia aculeata) fruit," Industrial Crops and Products, vol. 84, pp. 294–304, Jun. 2016, doi: 10.1016/J.INDCROP.2016.02.018.

[44] J. W. Goodrum and D. P. Geller, "Rapid thermogravimetric measurements of boiling points and vapor pressure of saturated medium-and long-chain triglycerides." Bioresource Technology, 84, 75-80, 2002.

[45] C. M. García Santander, S. M. Gómez Rueda, N. de Lima Da Silva, C. L. de Camargo, T. G. Kieckbusch, and M. R. Wolf MacIel, "Measurements of normal boiling points of fatty acid ethyl esters and triacylglycerols by thermogravimetric analysis," Fuel, vol. 92, no. 1, pp. 158–161, Feb. 2012, doi: 10.1016/j.fuel.2011.08.011.

[46] "NIST. National Institute of Standards and Technology." Available https://www.nist.gov/. Access: February 2019.

[47] M. Sales-Cruz, G. Aca-Aca, O. Sánchez-Daza, and T. López-Arenas, "Predicting critical properties, density and viscosity of fatty acids, triacylglycerols and methyl esters by group contribution methods," 20th European Symposium on Computer Aided Process Engineering, 2010.

[48] J. Marrero and R. Gani, "Group-contribution based estimation of pure component properties," Fluid Phase Equilibria, 183–184, 2001, pp. 183-208.

[49] H. An, W. M. Yang, A. Maghbouli, S. K. Chou, and K. J. Chua, "Detailed physical properties prediction of pure methyl esters for biodiesel combustion modeling," Applied Energy, vol. 102, pp. 647–656, Feb. 2013, doi: 10.1016/J.APENERGY.2012.08.009.

[50] R. F. Fedors, "Relationship between Chemical Structure and the Critical Temperature," Chem. Eng. Comm., 1982.

[51] K. Anand, R. P. Sharma, and P. S. Mehta, "A comprehensive approach for estimating thermo-physical properties of biodiesel fuels," Applied Thermal Engineering, vol. 31, no. 2–3, pp. 235–242, Feb. 2011, doi: 10.1016/j.applthermaleng.2010.09.003.

[52] "DIPPR. National Institute of Standards and Technology." Available: https://www.nist.gov/. Access: February 2019.

[53] A. Vatani, M. Mehrpooya, and F. Gharagheizi, "Prediction of Standard Enthalpy of Formation by a QSPR Model," Int. J. Mol. Sci, vol. 8, pp. 407–432, 2007, [Online]. Available: www.mdpi.org/ijms/.

[54] "ASPEN TECH." Available: http://www.aspentech.com/products/aspen-plus.aspx. Access: March 2020.

[55] L. Zong, S. Ramanathan, and C. C. Chen, "Predicting thermophysical properties of mono- and diglycerides with the chemical constituent fragment approach," Industrial and Engineering Chemistry Research, vol. 49, no. 11, pp. 5479–5484, Jun. 2010, doi: 10.1021/ie901948v.

[56] E. S. PERRY, W. H. WEBER, and B. F. DAUBERT, "Vapor Pressures of Phlegmatic Liquids. I. Simple and Mixed Triglycerides," J. Am. Chem. Soc., vol. 71, no. 11, pp. 3720–3726, 1949.

[57] M. A. Eiteman and J. W. Goodrum, "Density and Viscosity of Low. Molecular Weight Triglycerides and Their Mixtures," Journal of the American Oil Chemists' Society, 71 (11), pp: 1261, 1994.

[58] J. C. PHILLIPS and G. J. MATTAMAL, "Effect of Number of Carboxyl Groups on Liquid Density of Esters of Alkylcarboxylic Acids.," Journal Chemical Engineering, vol. 23, pp. 1–6, 1978.

[59] A. K. Sum, M. J. Biddy, J. J. de Pablo, and M. J. Tupy, "Predictive Molecular Model for the Thermodynamic and Transport Properties of Triacylglycerols," Journal of Physical Chemistry B, vol. 107, no. 51, pp. 14443–14451, Dec. 2003, doi: 10.1021/jp035906g.

[60] H. Noureddini, B. C. Teoh, and D. Clements, "Densities of Vegetable Oils and Fatty Acids." [Online]. Available: http://digitalcommons.unl.edu/chemeng_biomaterialshttp://digitalcommons.unl.edu/chemeng_biomaterials/14.

[61] M. J. Pratas, S. Freitas, M. B. Oliveira, S. C. Monteiro, A. S. Lima, and J. A. P. Coutinho, "Densities and viscosities of fatty acid methyl and ethyl esters," Journal of Chemical and Engineering Data, vol. 55, no. 9, pp. 3983–3990, Sep. 2010, doi: 10.1021/je100042c.

[62] E. G. HAMMOND, L. A. JOHNSON, C. SU, T. WANG, and P. J. WHITE, Soybean Oil. In: Bailey's Industrial Oil and Fat Products, Sixth Edition. John Wiley & Sons, 2005.

[63] O. O. Fasina and Z. Colley, "Viscosity and specific heat of vegetable oils as a function of temperature: 35°C to 180°C," International Journal of Food Properties, vol. 11, no. 4, pp. 738–746, Oct. 2008, doi: 10.1080/10942910701586273.

[64] L. R. STRECKER, M. A. BIEBER, A. MAZA, T. GROSSBERGER, and W. J. DOSKOCZYNSKI, Bailey's Industrial Oil and Fat Products, Fifth Edition. New York: Wiley, 1996.

[65] H. S. RODRIGUES, "Obtenção de ésteres etílicos e metílicos, por reações de transesterificação, a partir do óleo da palmeira Latino Americana macaúba - Acrocomia aculeata.," 2007.

[66] K. Murata, Y. Liu, M. Inaba, and I. Takahara, "Production of Synthetic Diesel by Hydrotreatment of Jatropha Oils Using Pt−Re/H-ZSM-5 Catalyst," Energy & Fuels, vol. 24, no. 4, pp. 2404–2409, Apr. 2010, doi: 10.1021/ef901607t.

Journal of Engineering and Technology for Industrial Applications, 2020. Edition. 23. Vol: 06
https://www.itegam-jetia.org
ISSN ONLINE: 2447-0228
DOI: https://dx.doi.org/10.5935/2447-0228.20200020

RESEARCH ARTICLE OPEN ACCESS

ANALYSIS AND OPTIMIZATION OF TRAFFIC CONGESTION AT SINGLE INTERSECTION USING MATLAB AND ARENA SIMULATION

Rakesh Roy[1], Sourav Kumar Ghosh[2], Naurin Zoha[3] and Mohammad Arif-Ul-Islam[4]

[1] Jashore University of Science and Technology (JUST). Jashore-7408, Bangladesh.
[2] Bangladesh University of Textiles (BUTEX). Dhaka-1208, Bangladesh.
[3] Bangladesh University of Engineering and Technology (BUET). Dhaka-1000, Bangladesh.
[4] Noakhali Science & Technology University (NSTU). Noakhali-3802, Bangladesh.

Email: rakeshroy996@gmail.com, sourav@butex.edu.bd, naurin.zoha@gmail.com, arif.rahad@gmail.com

Received: Apr 22th, 2020

Accepted: Jun 18th, 2020

Published: June 30th, 2020

ABSTRACT

Traffic jam is one of the most widespread problems commonly seen all over the world that causes loss of billions of dollars and useful hours per annum. Traffic lights are used at the intersections to manage the traffic flow, but one problem of those traffic lights is that the color changes at constant intervals irrespective of the traffic density or time of the day. As a result, the measure fails to keep the optimal traffic flow throughout the day at every convergence. This study describes a possible and effective method to systemize traffic lights by considering the traffic density for a specific time of the day. The range of idle time or waiting time within the queue is identified as a function of cycle time, effective green time and traffic arrival rate. After plotting the values within the graph, the trend is observed for idle time with reference to these variables. The lower and upper bound for these independent variables like cycle time, effective green time and traffic arrival rate are decided from observed data sets. As the idle time comes in the form of a range, an estimation of traffic congestion at a particular time is yielded from the method. This traffic flow is analyzed using Arena. The result of idle time using Arena is analogous with the previously analyzed model using MATLAB. Also, at the end of the study, a simulation video is generated that gives practical visual experience.

Keywords: Traffic Congestion, MATLAB, ARENA Simulation, Traffic Flow.

I. INTRODUCTION

With emerging economic development, vehicles maintain a substantial increase in quantity and as a result queuing phenomenon is so common in road traffic. The intersection is the main concentrated area of a stream of people and vehicles. It is one infrastructure construction of connecting the roads to make it work as an interconnected network. Generally, traffic congestion corresponds to the intersection directly which makes it evident that road intersections play a prime role in determining the traffic congestion situation depending on the road capacity and time of the day. Traffic control in an optimal manner at these intersections can be an effective way to reduce traffic congestions.

Traffic congestion has nowadays become one of the main hindrances in the big cities like Dhaka and Chittagong in Bangladesh. Mostly because of the high density of population and uncontrolled numbers of vehicles, the productive time loss due to congestion is counted in billions every year. There are many intersections in Dhaka, some of which are more important than others to control the overall jam in the city as those lie in the locus of the town. Traffic everywhere in Dhaka is controlled by the traditional way where the time of signaling is constant. It may not be the right approach as the traffic flow is not constant throughout the day and timing of the day must be considered as a variable. For example, usually, the entrance roads of educational institutes may be busy at the early hours of the day whereas in the evening the exits of office roads may be busy. This study focuses on an important intersection of Dhaka city to minimize the queue based on a simulation result. Here traffic flow analysis is done using MATLAB and Arena. MATLAB is used to find out the range of the waiting time and Arena, discrete event simulation and

automation software, which is used to develop the optimized result and simulation of the traffic flow.

For accurate analysis of our data, it is important to know the distribution of the data set as the outcome of simulation highly depends on the nature of the distribution. In this study, after analysis, it is observed that the relevant data follow the Poisson distribution and the process utilizes Poisson Experiment that helps in getting outcomes occurring with this data set during a given time interval or in a specified region.

II. LITERATURE REVIEW

Level of service (LOS) can be measure by traffic delays and queues. [1] Signal timings can be derived by considering either a single or a set of intersections. These methods are called isolated methods and coordinated methods, respectively [2]. Delay minimization and capacity maximization are the most common objective functions used by pre-existing methods. Delay may be directly measured, leading to a data-driven approach, or estimated (model-based approach). The first approximate expression for the delay at an intersection was given by Webster [3], this expression is still widely used. Other expressions include those of Newell [4] Miller [5] and McNeil [6]. Viti [7] provides a review of delay models. Dion [8] compares the performance of different delay models. Arena simulation is used to suggest several optimal solutions to manage the traffic queue in the most densely traffic intersection in the Malang city, Indonesia [9]. Existing traffic was estimated and a preassigned speed was proposed to synchronize the traffic signal [10]. Fuzzy logic was developed to solve a linear programming traffic model to efficiently control the intelligent traffic lights [11]. Deep reinforcement learning is used to analyze the traffic flow. Three different methodologies are developed for comparative analysis [12]. A fuzzy c-means clustering algorithm was applied to classify the traffic flow pattern which eventually ameliorated the signal control and traffic capacity [13]. Vehicle to vehicle (V2V) and vehicle to infrastructure (V2I) was integrated into three simulation models to compare the system efficiency, total time, waiting time and WIP [14].

III. METHODOLOGY

Here Webster equation is used to find out the range of waiting time as a function of cycle time, effective green time and arrival rate. These independent variables are found by observation in six different distinct times in the day. Their lower and upper bound is used as a limit and using MATLAB maximum and minimum of waiting time is determined.

This new way to control traffic lights takes into consideration the arrival rates of vehicles at an intersection from different directions at different times. For this purpose, an area is chosen where the traffic flow needs to be optimized, all the mean arrivals rates at the intersections in that area are calculated and the nature of the distribution of the arrival rates is found out using the help of Chi-square formula. Then the Arena program is created showing the network, using the values as input and necessary logics so that the traffic flow is optimal and cars don't get piled up at any intersection and the resulting animation visually proves that. The way (duration of red and green lights) the traffic lights change in the animation is the proposed optimal way of controlling the traffic lights without the help of traffic police for that area for that particular time and it corresponds to the waiting time obtained from the simulation result. For the data collection, a fairly busy area (center at Latitude- 23.73688613, Longitude- 90.38740754) is chosen where a traffic jam is a common occurrence. At first, the widely used approximate delay formula is developed by Webster [3] from a combination of theoretical and numerical simulation approaches:

$$d = \frac{c\left(1-\frac{g}{c}\right)^2}{2[1-\left(\frac{g}{c}\right)x]} + \frac{x^2}{2q(1-x)} - 0.65\left(\frac{c}{q^2}\right)^{\frac{1}{3}} x^{2+5\left(\frac{g}{c}\right)} \quad (1)$$

where,
d = average delay per vehicle (sec)
c = cycle length (sec)
g = effective green time (sec)
x = degree of saturation (flow to capacity ratio) = $\frac{q}{c}$
S = departure (saturation) flow rate from queue during effective green (veh/sec)
C = capacity rate (veh/sec, or veh/cycle, or veh/h)
q = arrival rate (veh/sec)

For this equation and from obtained data at different segments of the daily minimum and maximum waiting time at that segment is obtained. MATLAB is used to find the maximum and minimum waiting time for the range of arrival rate, effective green time and cycle length. Departure rate is assumed to be constant from different observations as all vehicles depart at the same rate when a green signal is on. Afterward, simulation is done to find the consistency of this result with the arena.

The probability distribution of the Poisson random variable X, representing the number of outcomes occurring in a given time interval or specified region denoted by t, is:

$$p(x;\lambda t) = \frac{e^{-\lambda t}(\lambda t)^x}{x!} \quad (2)$$

For x =0,1, 2…
where λ is the average number of outcomes per unit time, distance, area, or volume, and e = 2.71828…

The mean values of arrival rates are calculated using the weighted mean method and its distribution is determined with the help of the Chi-square formula.
The mean arrival rate:

$$\lambda = \frac{\sum_n^k = 1 f_n * x_n}{\sum_n^k = 1 f_n} \quad (3)$$

The test statistic follows the chi-square distribution, designated as $\chi 2$ Chi-square test statistic:

$$x^2 = \sum [\frac{(f_0 - f_e)^2}{f_e}] \quad (4)$$

With k-1 degrees of freedom, where:
k is the number of categories
f_0 is an observed frequency in a particular category
f_e is an expected frequency in a particular category

$$f_e = 45p \quad (5)$$

Now, it's needed to find the critical value corresponding to the chosen level of significance and degrees of freedom.

If the value of chi-square is less than the critical value, the null hypothesis is accepted, otherwise, its rejected. Here, the null hypothesis is that there is no difference between the observed and expected value.

After knowing the input data distribution and its mean value, the input is given to the Arena module and according to that, the output is achieved. The data follows the Poisson distribution as per the calculations mentioned above. The following assumptions are made in the intended model:

Only two kinds of vehicles are available on the roads, vans, and trucks having an equal length.

All the vans/trucks have an equal uniform velocity of 25 km/h.

Vehicle switching to each of the three routes is given by assumption.

The full Arena model (Figure 1) is developed for simulation. Here four individual networks denote four routes that meet at an intersection.

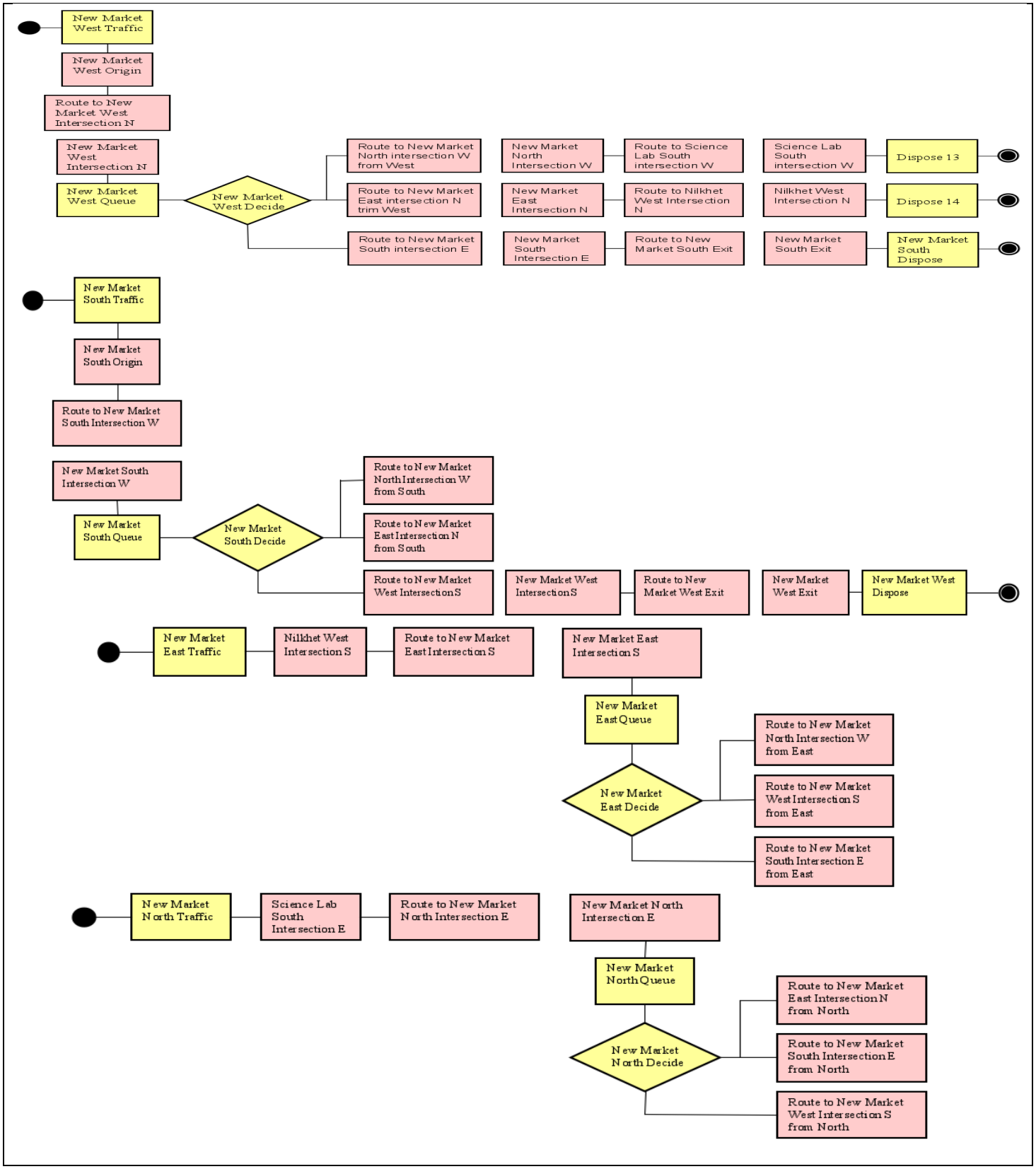

Figure 1: Full Arena Model.
Source: Authors, (2020).

The Poisson Mean of arrivals (interarrival time) is. So, the interarrival time of the vehicle comes from the science lab intersection is 1/2 sec = 0.00833 min.

The Poisson Mean of other arrivals is as follows.

Table 1: Poisson Mean of arrivals.

Location	New Market North Traffic	New Market East Traffic	New Market South Traffic	New Market West Traffic
Poisson mean of interarrival (min)	0.01425	0.0111	0.00833	0.01030

Source: Authors, (2020).

For calculating route time (the time is taken for an entity to move from one station to another), Given:

The velocity of an entity = 25 km per hour.

Distance between New Market East Intersection to Nilkhet West Intersection = 0.2 km.

So, route time from New Market intersection to Nilkhet intersection = 0.2/25*60 = 0.48 min.

The parameters of the create modules of the top part are as follows (As the model considers two types of vehicles in the road so here two types of the entities are exhibited).

Table 2: The parameters of the create modules.

Name	Entity Type	Time between arrivals			Entities per arrival	Max Arrival	First creation
		Type	Expression	Units			
New Market East Traffic	Entity 1	Expression	POIS (0.0111)	Minutes		Infinite	0
New Market South Traffic	Entity 2	Expression	POIS (0.00833)	Minutes	1	Infinite	0

Source: Authors, (2020).

The parameters of the route modules of the top part are as follows.

Table 3: The parameters of the decide modules.

Name	Route time	Units	Station name
New market west origin	0.48	Minutes	New market west intersection
New market north intersection	0.4	Minutes	Science lab south intersection
New market east intersection	0.48	Minutes	Nilkhet west intersection
New market south intersection	0.15	Minutes	New market south exit

Source: Authors, (2020).

Table 4: The parameters of the route module.

Name	Type	Percentage	Destination
New Market West Decide	N-way by chance	60	Nilkhet west intersection
		30	Science Lab South Intersection
		10	New market south exit

Source: Authors, (2020).

Here percentage indicates the priority of respective routes while switching from the intersection. Other decide module is made in the same fashion. All other modules are made in the same fashion.

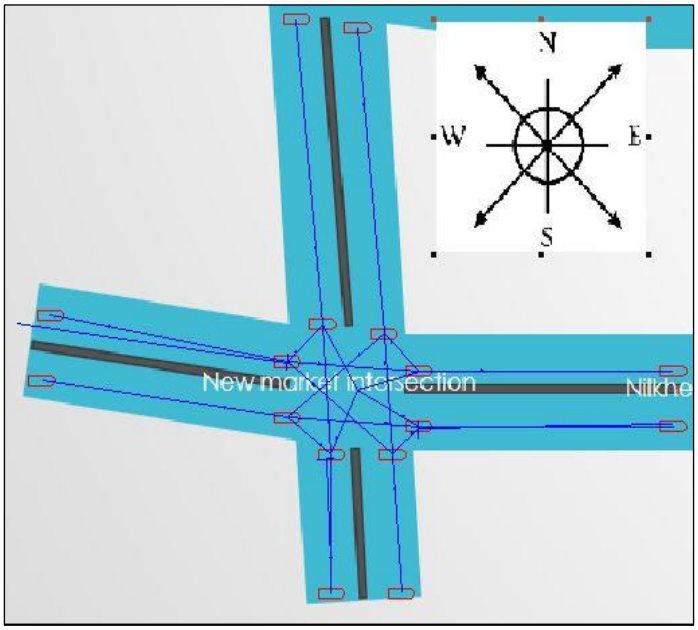

Figure 2: Route diagram of Arena simulation.
Source: Authors, (2020).

To represent this module combination or Arena flow chart in a practical scenario for visual representation a route is drawn (Figure 2) based on the concept of the module diagram. The program is allowed to run with an animation speed factor (Time Units Per Frame) of 0.00066736.

IV. RESULTS

From this data, a graph (Figure 3) for identifying how idle time varies at different periods of the day is plotted. The graph shows the upward trend which indicates as the time proceeds towards the evening, vehicles wait longer and it becomes evident that vehicles are more likely to stack at a traffic jam at this hour. From this data, it can be estimated how much time one should keep in hand to reach a destination on time.

Another graph (Figure 4) for waiting times against arrival rates was plotted. From the data and graph, it is evident that waiting times increase with the arrival rates. Another graph (Figure 5) was also plotted for waiting time against cycle length. From the data and graph, it is evident that waiting time increases as cycle length increases.

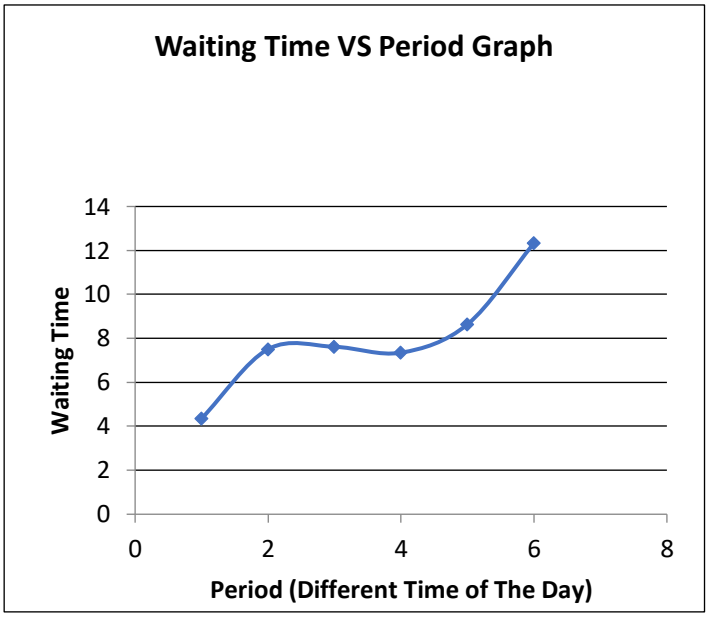

Figure 3: Waiting time at different period of the day.
Source: Authors, (2020).

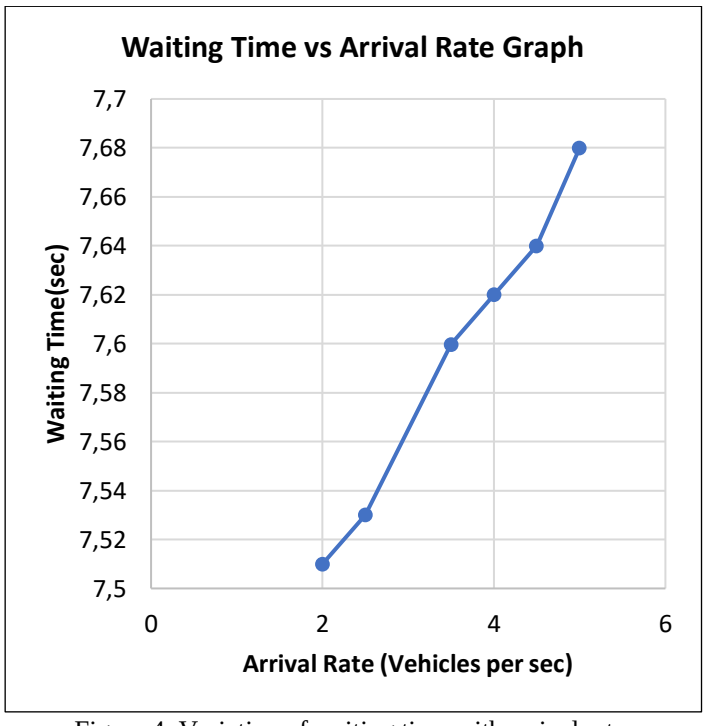

Figure 4: Variation of waiting time with arrival rate.
Source: Authors, (2020).

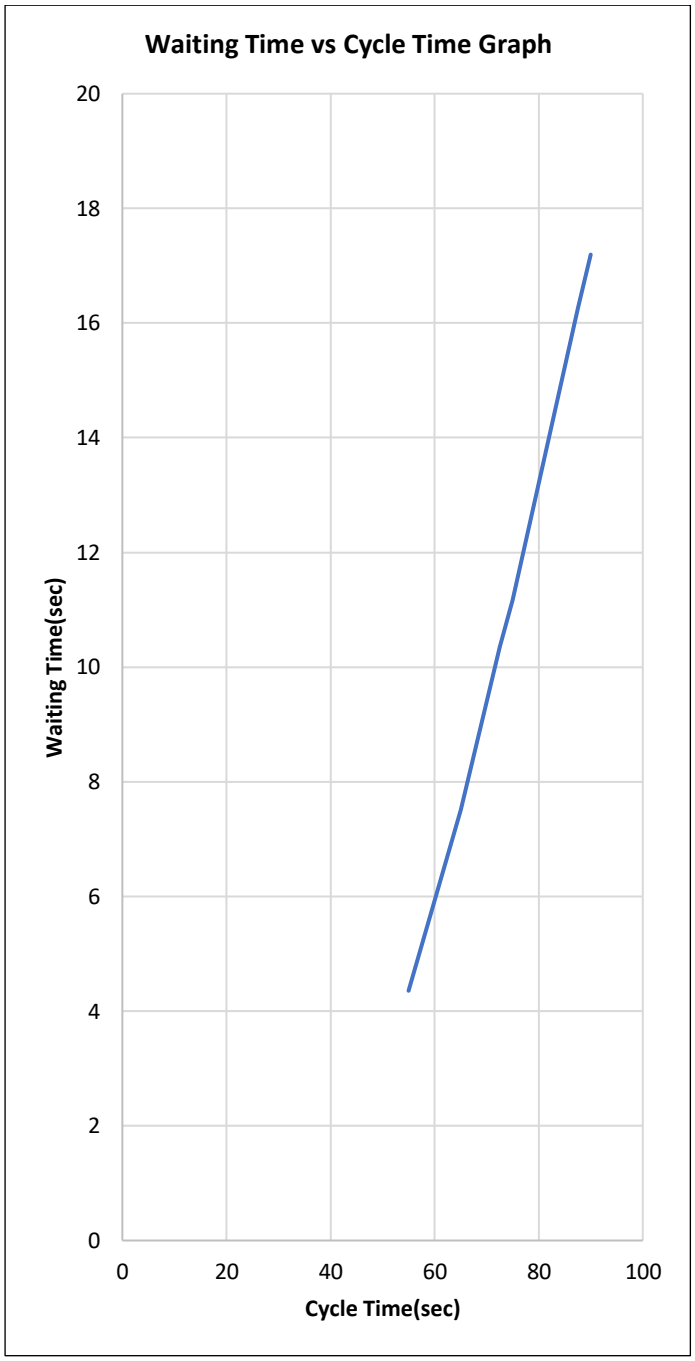

Figure 5: Variation of waiting time with a cycle length.
Source: Authors, (2020).

In another graph(Figure-06) for change of waiting time against effective green time, it is evident that waiting for time decrease as an effective green time increase. Next, the analysis of traffic flow and waiting time using Arena was done (Figure-07) and it was found that for a particular arrival rate, waiting time is quite analogous for both the cases.

For entity 1, the Poisson Mean of arrivals (interarrival time) is 1/λ. So the interarrival time of vehicle comes from New Market East Traffic (From Nilkhet west intersection)is 1/1.5 sec = 0.0111 min. For entity 1 from Arena simulation, we have found that it has minimum tends to zero min per vehicle and a maximum of 0.06998177 min per vehicle. This means it has to wait time minimum tends to zero sec per vehicle and maximum 4.1989062 sec per vehicle. This value has quite a similarity with.

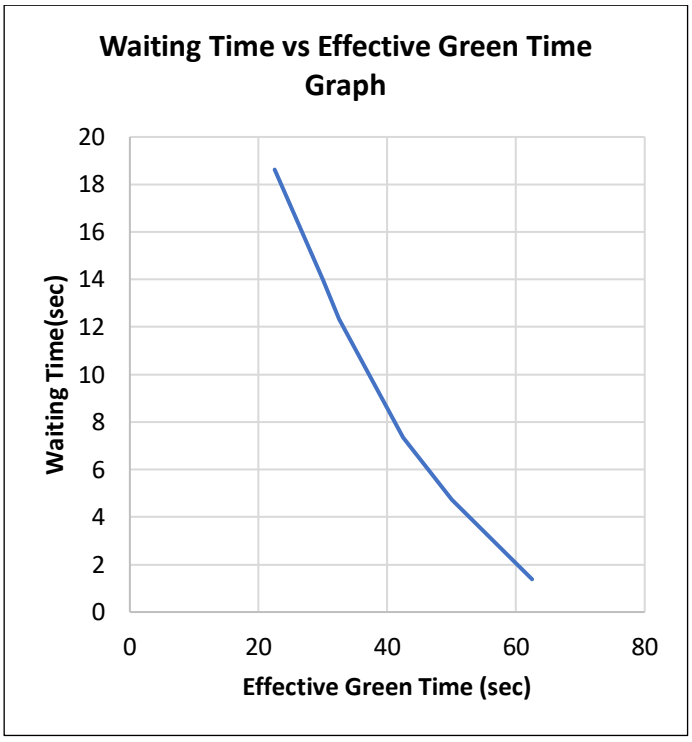

Figure 6: Variation of waiting time with a cycle length.
Source: Authors, (2020).

Webster's equation as it is found for an arrival rate of between 1 and 2 vehicles per second waiting time is min 1.016464 and max 7.69274625. The arrival rate of between 1 and 2 vehicles per second means an interarrival time of two vehicles is 1/1.5 sec = 0.0111 min which is similar to the mean of Poison distribution for entity 1. For Arena simulation, all other parameters are kept as usual as in simulating Webster's equation in MATLAB. The ratio of effective green time to cycle length is given as 35/55 = 0.6363 in the arena simulation module. Here 35 is mean of effective green time range [30,40] and 55 is mean of cycle length range [50,60].

For entity 2, the Poisson Mean of arrivals (interarrival time) is 1/λ. So the interarrival time of vehicle from New Market South Traffic (From Azimpur north intersection) is 1/2 sec = 0.00833min.

For entity 2 from Arena simulation, it is found that it has a minimum 0.0111667 min per vehicle and a maximum of 0.112 min per vehicle. Which means has a waiting time minimum of 0.67 sec per vehicle and a maximum of 6.672 sec per vehicle.

This value has quite a similarity with Webster's equation as it was observed for an arrival rate of between 1 and 3 vehicles per second waiting time is min 1.62549051 and max 7.82147255.

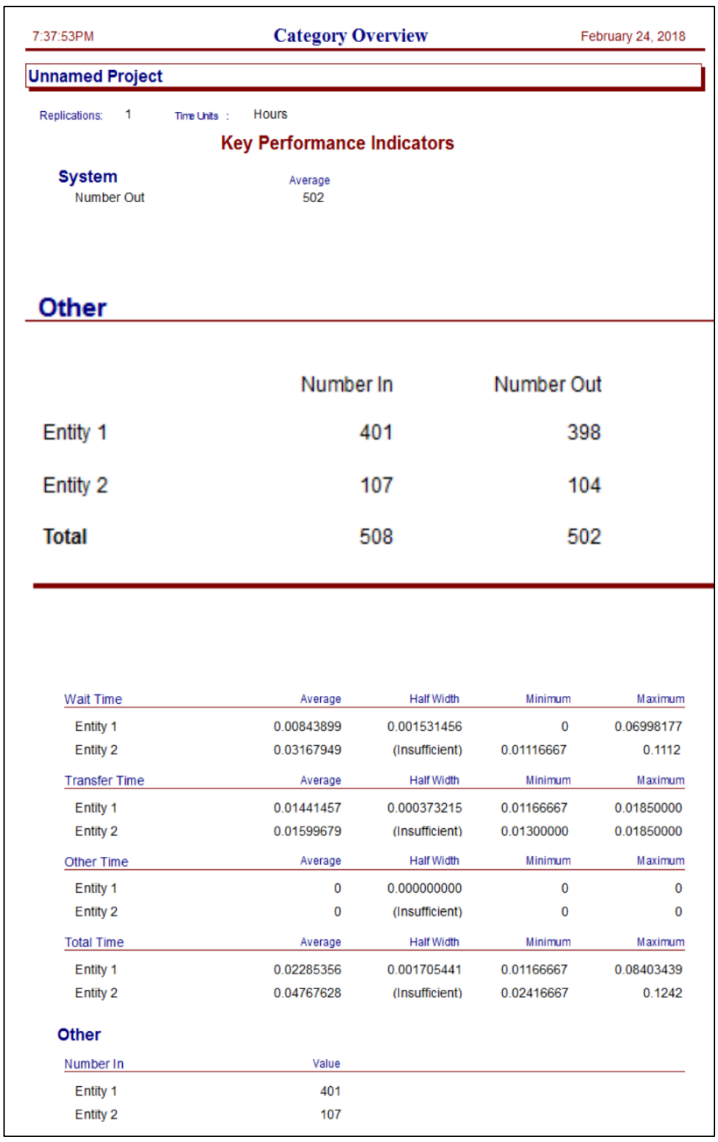

7:37:53PM — Category Overview — February 24, 2018

Unnamed Project

Replications: 1 Time Units : Hours

Key Performance Indicators

System
Number Out — Average: 502

Other

	Number In	Number Out
Entity 1	401	398
Entity 2	107	104
Total	508	502

Wait Time	Average	Half Width	Minimum	Maximum
Entity 1	0.00843899	0.001531456	0	0.06998177
Entity 2	0.03167949	(Insufficient)	0.01116667	0.1112
Transfer Time	**Average**	**Half Width**	**Minimum**	**Maximum**
Entity 1	0.01441457	0.000373215	0.01166667	0.01850000
Entity 2	0.01599679	(Insufficient)	0.01300000	0.01850000
Other Time	**Average**	**Half Width**	**Minimum**	**Maximum**
Entity 1	0	0.000000000	0	0
Entity 2	0	(Insufficient)	0	0
Total Time	**Average**	**Half Width**	**Minimum**	**Maximum**
Entity 1	0.02285356	0.001705441	0.01166667	0.08403439
Entity 2	0.04767628	(Insufficient)	0.02416667	0.1242

Other

Number In	Value
Entity 1	401
Entity 2	107

Figure 7: Arena output.
Source: Authors, (2020).

For Arena simulation, all other parameters are kept as usual as in simulating Webster's equation in MATLAB. The ratio of effective green time to cycle length is given as 50/75 = 0.6666 in the arena simulation module. Here 50 is mean of effective green time range [45,55] and 75 is mean of cycle length range [70,80]. For Arena simulation, the video link is given below "https://drive.google.com/file/d/1LCHi1Vcju0xrqlk8ECcuZA4hLNbG6Tht/view?usp=sharing".

Table 5: Comparison of MATLAB and Arena output.

Entity Type	Interarrival Time (1/λ) (min)	Arena Input	Arena Output		MATLAB Input (Range of vehicle arrival rate)	MATLAB Output	
			Minimum waiting time per vehicle	Maximum waiting time per vehicle		Minimum waiting time per vehicle (Sec)	Maximum waiting time per vehicle (Sec)
Entity-1	0.011	POIS(0.0111)	Tends to zero	0.0699817min	[1,2]	1.016464	7.6927462
			Tends to zero	4.1989062 sec			
Entity-2	0.00833	POIS(0.0083)	0.011166 min	0.112 min	[1,3]	1.625490	7.821472
			0.67 sec	6.672 sec			

Source: Authors, (2020).

V. CONCLUSION

This study shows how waiting time varies as a function of arrival rate, effective green time and cycle length. Webster's equation is used to illustrate this analysis and Arena simulation finds the consistency of the analysis and finds the optimal way to control traffic. But this model is not flawless, there are some limitations:

• Here, the student version of Arena was used, which didn't allow adding many modules in the model which could make the simulation more realistic and descriptive. It can only accommodate 150 entities.

• This model is not a generic one irrespective of the area analyzed. For other areas, different traffic networks and arrival rates would have to be used.

• Again, in Webster's equation, to find the effect of arrival rate, effective green time and cycle length with waiting time one parameter is taken as variable and the rest are kept constant for every case for simplicity of analysis.

Although there are some drawbacks, this model gives a good scenario of traffic congestion and provides a method to optimize it. Further study can be done by taking larger areas into consideration, giving priority to the roads in a more realistic manner and, of course, considering a range of values for the different variables instead of its crisp mean value.

VI. REFERENCES

[1] Tay, A. C., and H. H. Lee. "Traffic condition with road upgrading during construction and operation stages based on level-of-service (LOS)." *IOP Conference Series: Materials Science and Engineering*. Vol. 344. No. 1. IOP Publishing, 2018.

[2] M. Papageorgiou, C. Diakaki, V. Dinopoulou, A. Kotsialos e Yibing Wang, "Revisão de estratégias de controle de tráfego rodoviário", em *Proceedings of the IEEE* , vol. 91, n. 12, pp. 2043-2067, dez. 2003, doi: 10.1109/JPROC.2003.819610.

[3] Webster, F. V. "Traffic signal settings, road research technical paper no. 39." *Road Research Laboratory* (1958).

[4] Newell, Gordon Frank. "Approximation methods for queues with application to the fixed-cycle traffic light." *Siam Review* 7.2 (1965): 223-240.

[5] Miller, Alan J. "Settings for fixed-cycle traffic signals." *Journal of the Operational Research Society* 14.4 (1963): 373-386.

[6] McNeil, Donald R. "A solution to the fixed-cycle traffic light problem for compound Poisson arrivals." *Journal of Applied Probability* 5.3 (1968): 624-635.

[7] Viti, Francesco. "The dynamics and the uncertainty of delays at signals." (2006).

[8] Dion, Francois, Hesham Rakha, and Youn-Soo Kang. "Comparison of delay estimates at under-saturated and over-saturated pre-timed signalized intersections." *Transportation Research Part B: Methodological* 38.2 (2004): 99-122.

[9] Yuniawan, Dani, et al. "Traffic queue modeling using arena simulation software (a case study of Mergan 4-Way intersection in Malang City)." *MATEC Web of Conferences*. Vol. 204. EDP Sciences, 2018.

[10] Goliya, H. S., and Nitin Kumar Jain. "Synchronization of traffic signals:"A case study—eastern ring road, Indore"." International *Journal of Advanced Technology in Civil Engineering* 1.2 (2012): 1-7.

[11] de Queiróz Lamas, Wendell, Giorgio Eugenio Oscare Giacaglia, and Eliana Campos de Oliveira. "Intelligent Urban Traffic Flow Control: A Case Study on Fuzzy Logic Application." International *Journal of Transportation Engineering and Technology* 3.3 (2017): 25.

[12] Tewari, Ujwal Padam, et al. "Intelligent Coordination among Multiple Traffic Intersections Using Multi-Agent Reinforcement Learning." *arXiv preprint arXiv:1912.03851* (2019).

[13] Zhu, Yun, et al. "Study on traffic flow patterns identification of single intersection intelligent signal control." *Procedia engineering* 137 (2016): 452-460.

[14] Benzaman, Ben, and Deepak Sharma. "Discrete event simulation of a road intersection integrating V2V and V2I features to improve traffic flow." 2017 *Winter Simulation Conference (WSC)*. IEEE, 2017.

Journal of Engineering and Technology for Industrial Applications, 2020. Edition. 23. Vol: 06
https://www.itegam-jetia.org
ISSN ONLINE: 2447-0228
DOI: https://dx.doi.org/10.5935/2447-0228.20200021

RESEARCH ARTICLE OPEN ACCESS

REDUCING ENVIRONMENTAL NOISE IN THE MOTORCYCLE TEST SECTOR

João Cláudio Ferreira Soares[1] and Rebeca Pereira Soares[2]

[1, 2] Research and Innovation Analysis Center Foundation – FUCAPI, Manaus – Amazonas, Brazil.

Email: claudio.ueabm@gmail.com, rebecapsoares01@gmail.com

Received: May 08th, 2020

Accepted: Jun 15th, 2020

Published: June 30th, 2020

ABSTRACT

The noise pollution is currently the third biggest environmental problem, affecting many people. When exposed to a high level of noise, the people can show occupational, social, physical and/or psychological problems. The noise is part of people's daily lives and work environments, so research projects and proposals that aim to improve this difficult reality are justified. Personal protection is an immediate measure. However, the control should aim mainly at the emitting source, whether in the noise generation mechanism or in the containment of the propagation. The general objective of this work is the developing of an acoustic booth proposal to reduce environmental noise from the motorcycle test area. The specific objectives are: to map the environmental noise level in the motorcycle testing area; propose an acoustic booth design. In the methodology sought practical results oriented to the problem of controlling environmental noise at the emitting source. An inductive approach is chosen when collecting noise data in the test sector and developing a design as a result of analysing that data. An exploratory, descriptive and explanatory study was developed. Exploratory in data collection, descriptive and explanatory in the development of the acoustic cabin. The investigation strategy uses a case study focused on specifying all qualitative aspects that allow the total reproduction of the results. So, the sound sources that generate noise from the motorcycle test area were verified; area noise levels were measured; the area with the highest noise level was evaluated; the place of installation of the cabin was evaluated; the noise absorbing material was defined; each item used to make the cabin was listed; the costs for making the cabin were defined; the way the panels were assembled was defined; and; The final design of the acoustic booth was designed. The highest noise level found was the motorcycle horn, which when performing the functional test reached an average of 100.91 dB. With the implementation of acoustic booth in the test area, it is proposed to reduce environmental noise in the areas of people circulation.

Keywords: Sounds, Noises, Acoustic Booth.

I. INTRODUCTION

Sound is part of our daily lives and can come in many forms; noise is a type of sound, but unpleasant. The noise pollution is currently the third biggest environmental problem, affecting many people, because when exposed to a high level of noise it can cause, in addition to occupational problems, social problems, physical and/or psychological [1,2].

The main sources of noise and noise pollution from large cities and environments are motor vehicles [3,4]. Which leads us to study solutions to reduce the noise level in a motorcycle test environment, since the tests performed generate high noise levels.

The general objective of this research is to develop an acoustic booth to reduce the environmental noise in the test area of a motorcycle manufacturer.

The specific objectives are: to map the level of environmental noise in the motorcycle testing area; and propose an acoustic booth project.

The methodology sought practical results oriented to the problem. An inductive approach is chosen when collecting data and developing a project as a result of data analysis. In the nature of the investigation, an exploratory, descriptive and explanatory study is combined. Exploratory in data collection, descriptive and explanatory in the development of the proposed solution to the

problem. The investigation strategy uses a case study focused on qualitative aspects [5,6].

Initially, the work presents a literature review that addresses the main concepts related to noise, its effects and necessary controls. Then he develops a case study carried out in a motorcycle industry. It presents the technical aspects of the collection of environmental noise in a test sector and concluded with the elaboration of an acoustic cabin project.

II. LITERATURE REVIEW

II.1 SOUND PRESSURE

Sound is a form of energy transmitted by the collision of molecules, there is no permanent displacement, that is, there is no transfer of matter, only energy, sound is, therefore, a form of energy that flows through elastic means [7,8].

The sound pressure wave is the disturbance that occurs in the environment, where the sound vibration movement was transmitted from particle to particle without the migration of particles as shown in Figure 1 [8,9].

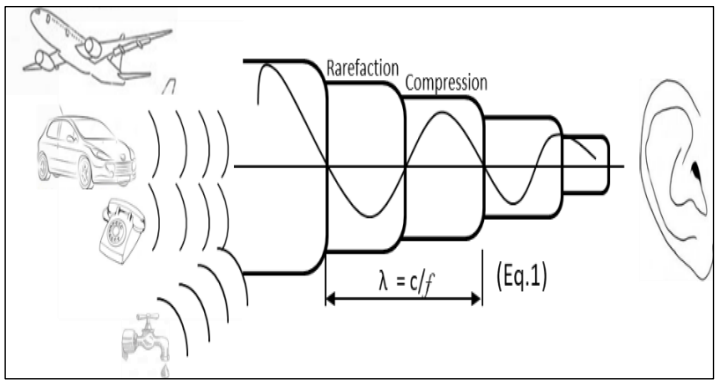

Figure 1: Propagation of sound waves.
Source: [10].

The wavelength and the speed of sound propagation are two factors that need to be taken into account the temperature and the medium, where the wavelength is represented by Equation 1, being the ratio between the speed of sound and the frequency in a time interval [9].

Nepomuceno [11] characterizes the propagation of sound through waves, depending on the medium and the temperature.

These waves that propagate, in a given instant, are repeated in different places with a lag equivalent to the necessary time of the travel of a wave, with the speed of sound [8, 9].

The speed of sound is according to Equation 2 [9] and Table 1 shows the comparison of the speed of sound in different materials [11].

Wavelength:

$$\lambda = \frac{c}{f} \tag{1}$$

Speed of sound:

$$c = \lambda f \tag{2}$$

Where:
λ = Wavelength in meters (m)
c = Speed of sound in meters per second (m/s)
f = Frequency over a given time interval in hertz (Hz)

Table 1: Speed of sound in different materials.

MATERIAL	PHYSICAL STATE	TEMPERATURE	VELOCITY
AIR	GASEOUS	20°C	340 m/s
HYDROGEN	GASEOUS	20°C	1.261 m/s
WATER	LIQUID	20°C	1.500 m/s
STEEL	SOLID	20°C	5.100 m/s

Source: [11].

II.2 SOUND INTENSITY, INTENSITY LEVEL AND SOUND PRESSURE

The sound quality is related to the energy carried by the wave, the energy intensity of the sound is the quotient of the power emitted by the source, by the area where the sound is found, as shown in Equation 3 [9]:

Energy intensity:

$$I = \frac{P}{S} \tag{3}$$

Where:
I = Energy intensity (physical) in watts per square meter (W/m2)
P = Sound source power in watts (W)
S = Area where sound is found instantly in square meters (m2)

Defines the intensity of sound energy as the average amount of energy that crosses an area perpendicular to the direction of propagation of the wave, in a certain unit of time [9].

Explains that the level of intensity and sound pressure are obtained through Equations 4 and 5, respectively [12].

Sound Intensity Level:

$$NI = 10 \log \frac{I}{I_0} \tag{4}$$

Sound Pressure Level:

$$NPS = 10 \log \frac{P^2}{P_0{}^2} = 20 \log \frac{P}{P_0} \tag{5}$$

Where:
I = It is the acoustic intensity in Watt/m2.
Io = It is the reference intensity = 10-2 Watt/m2.
P = It is the sound pressure in N /m2.
Po = It is the reference value of the hearing threshold in N /m2, P0 = √(ρI0 c) = √(415x10-12, that results in 0,00002 N/m2.

Informs that the unit to express the level of intensity or sound pressure is the decibel (dB), this unit was first used due to the loss of power in the telephone cables, but it was also observed that 1dB corresponded to the minimum variation audible sound [9].

II.3 ABSORPTION COEFFICIENT

The absorption coefficient as the ratio between the absorbed energy and the incident energy, shown in Equation 6 [9]. The energy produced by a sound source is called incident energy, when reaching an obstacle, part of the energy is reflected, transmitted or absorbed as shown in Figure 3 [8,9,13].

Absorption coefficient:

$$\alpha = \frac{W_a}{W_i} \tag{6}$$

Where:

W_a = Energy absorbed (W/m^2)
W_i = Energy incident (W/m^2)

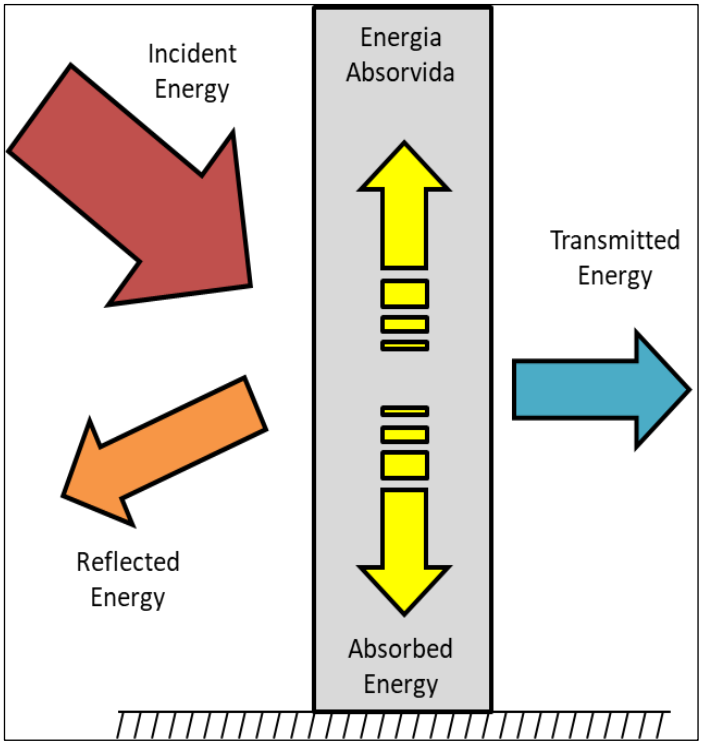

Figure 3: Incident energy behavior.
Source: [9].

II.4 NOISE EFFECT

The human ear is the best sound sensor there is. Prolonged exposure to a high level of noise causes deterioration of the auditory system, so it is important to understand the functioning and loss mechanism of this system [10].

It is customary to divide the effects of noise on men in two parts: those that affect people's health and well-being and the effects on hearing [1,2,4,14].

The hearing threshold, ie, where it is possible to detect sound pressure by the human ear is 20 x 10^{-6} N/m^2 at a frequency of 1 kHz and the range, or full frequency band audible to humans, is 20 Hz at 20 kHz, taking into account that the auditory sensitivity is not the same in the whole range [8,10].

According to [10] any reduction in sensitivity is considered hearing loss, the first frequency range that you lose is 4 to 6kHz, and usually accompanies the sensation of noise perception after the noise field is removed, and more critically the nerve cells inner ear are damaged by losing hearing (deafness).

Other effects can be associated with exposure to loud noises, [12] states that this exposure can cause on man: pupil dilation, increased production of thyroid hormone, increased heart rate; increased production of adrenaline and corticotrophin, contraction of the stomach, muscle reaction, contraction of blood vessels; and are shown by some behaviors, such as: nervousness; mental fatigue; frustration; low job performance; irritability; social conflicts [1,2].

The exposure to occupational noise is one of the biggest problems for employees, causing these non-auditory problems [3].

II.5 NOISE CONTROL

Noise is a sound characterized by a large number of acoustic vibrations, with amplitudes and phases, distributed at random [8,13]. Describes the noise intensities in a sequence from the inaudible to the one that causes auricular pain, according [3] to Table 2.

Table 2: Auditory sensations and sound sources.

Sensation	Noise source	Intensity (dB)
Ear pain/hearing damage	Rocket taking off	200
	Rifle Shot	150
	Airplane taking off close	140
	Airplane taking off - 30m	130
Uncomfortable	Police siren	110
Very intense	Motorcycle	90
Intense	Vacuum Cleaner	70
	Normal conversation	60
Audible	Peaceful office	50
	Leggy	40
Silent	Library interior	30
Very silent	Whisper	20
Inaudible	Silence	0

Source: [3].

The NR 15 [15], classifies noise into three types: 1) Continuous noises: variation in the level of sound intensity very small as a function of time (longer than 1 second); 2) Floating noises: large variations in level as a function of time; 3) Impulsive or impact noises: they present high levels of sound intensity, in a very short time (less than 1 second), which are those caused by explosions and impacts.

According to [9], in cases where noise problems were not addressed in the design phase, the control will be performed on the sound transmission path between the source and the receiver. The author lists some control methods: increasing the distance between the source and the receiver; isolation of machines, that is, confinement; installation of silencers; and/or surface treatment with sound absorbent materials [16,17].

II.6 NOISE ABSORPTION MATERIALS

As explained by [9], the waves of sound or noise, when indoors, suffer interference from other waves that are reflected by the wall, floor or ceiling. Part of the sound energy, according to the author, is reflected, another part disappears behind the surface, which are the sound energy dissipated and the sound energy transmitted.

According to [10], the materials used for noise control are:

- Sound absorbing materials (resistive mechanism): A part of the acoustic energy is transformed into thermal energy, this is due to the viscosity of the air [16,17].
- Reactive device: acoustic energy generates resonance in the device.
- Active device: the noise field is canceled by another field at 180º of lag.

High-sound-absorbing materials are usually porous and/or fibrous, says [12]. Nepomuceno [11] clarifies that absorption is a function of frequency and porosity, acting through viscous friction and absorbs up to 100% of the incident energy [16,17].

In porous materials, acoustic energy enters the pores, dissipating through multiple reflections and viscous friction, transforming into thermal energy, as shown in Figure 4 [10,13], [16,17].

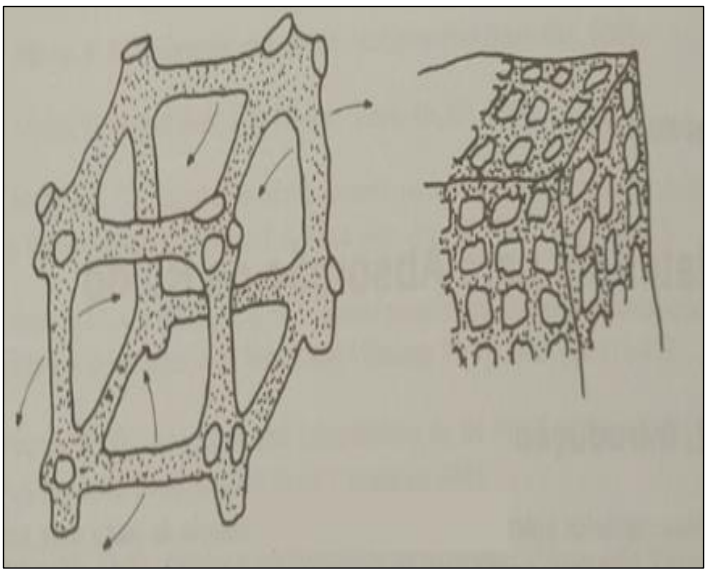

Figure 4: Porous material.
Source: [10].

In fibrous materials, the acoustic energy passes between the fibers, causing them to vibrate together with the air and is transformed into thermal energy by friction when it dissipates, as shown in Figure 5 [10] [13], [16], [17].

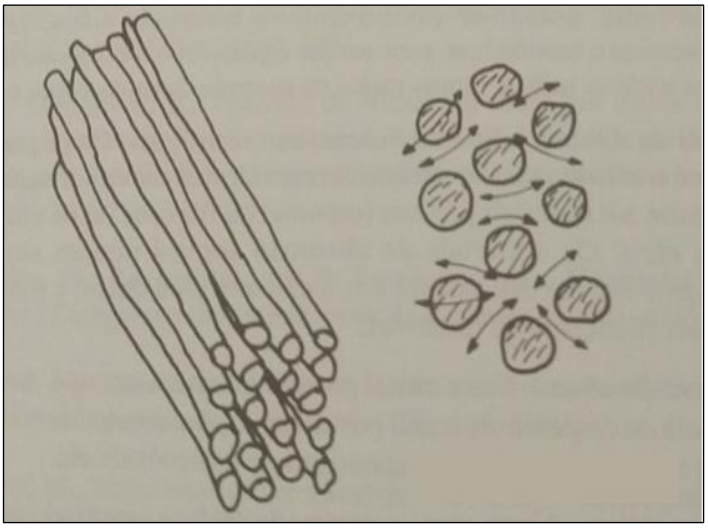

Figure 5: Fibrous material.
Source: [10].

According to [10] for all material used in sound absorption, it is necessary to admit the passage of an air flow, which will allow the propagation of acoustic waves. In addition, the author lists the characteristics necessary for choosing this material: Absorption coefficient [$\alpha = Wa/Wi$ (Equation 6), ratio between the absorbed and incident energy]; Noise frequency; High temperature characteristics; Weight and volume in relation to the available space; Fixing and maintenance; Appearance and painting; and Cost.

According to [10] the three most used types of materials for sound absorption are:

Polymer foam, shown in Figure 6, characterized by open pores, great for air flow, without erosion, but the risk of contamination with oils and other impurities tends to block the orifices, as they are flammable, additives are used that worsen the mechanical characteristics and its useful life, works in the temperature range of -40°C to 100°C [10].

Figure 6: Polyurethane foam.
Source: [10].

Glass wool, shown in Figure 7, for this case the author informs that it is available for use in many forms, such as panels, blankets, felts, cords or applied by blasting. To improve resistance to vibrations and fluid flow, resin is usually applied to seal, but the sealing makes the material become combustible, without the resin the glass wool resists up to 450°C, using a flame retardant additive. resist up to 540°C [10].

Figure 7: Sandblasted glass wool.
Source: [10].

Rock wool, shown in Figure 8, this material is obtained by melting different types of rock at a temperature of about 1500°C to obtain the fibers that are bonded by a resin to form a blanket or panel, this material is not fuel [10].

Figure 8: Rock wool panels.
Source: [10].

III. DEVELOPMENT

This case study was developed in the Product Testing Sector of a motorcycle industry at the Manaus Industrial Pole in 2019.

The methodological procedure is divided into two main parts: the noise level mapping; and the development of the proposed acoustic booth, as shown in Figure 9.

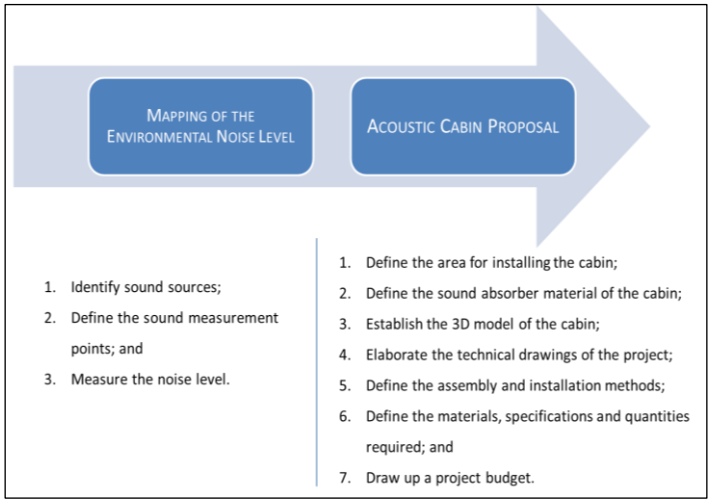

Figure 9: Steps of the methodological procedure.
Source: Authors, (2019).

III.1 MAPPING THE ENVIRONMENTAL NOISE LEVEL

The sound sources in the testing area were related through on-site verification.

The sound sources identified were:

- 7 industrial fans;
- 3 motorcycle test equipment (dynamometers);
- the motorcycle engine;
- the motorcycle horn.

The positioning of the sound sources found is as indicated in the layout of Figure 10.

The noise level measurement points were defined by observing the places of passage of employees and between the listed sound sources.

9 measurement points were defined in the motorcycle testing sector, according to the layout in Figure 10. Between points 1, 2, and 3 is 5 meters apart, between the other points is 2 meters and approximate height of 1.5 m (corresponding to the human ear according to NR 15 [15]).

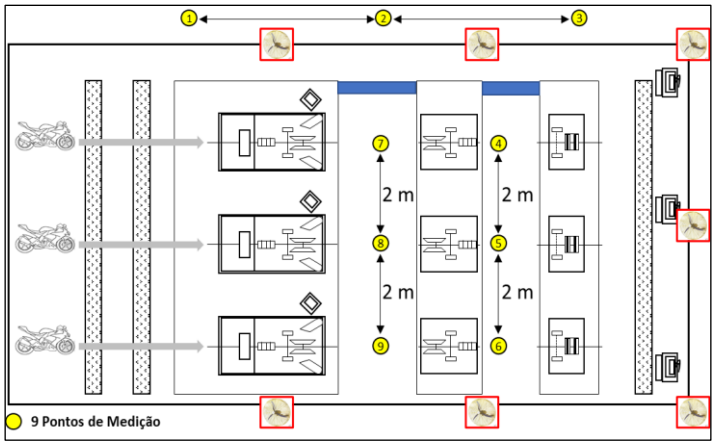

Figure 10: Sound pressure level measurement sources and points.
Source: Authors, (2019).

The noise level was measured at each defined point, using the sound pressure measurement instrument of the manufacturer Brüel & Kjaer, as shown in Figure 11. The instrument is calibrated and has a valid certificate giving reliability to the measurement performed.

Figure 11: Sound pressure gauge (left side). Verification of the sound pressure gauge measurement (right side).
Source: Authors, (2019).

The sound pressure meter has: 1) a windshield as shown in Figure 11, so that the action of the wind does not interfere with the capture of sound vibrations; 2) a microphone as shown in Figure 11, responsible for capturing the sound vibrations and transforming it into an electrical signal as a result of the decibel measurement; and 3) a calibrator was used before the measurements started.

The measurement of the pressure gauge was done in two steps, in the first the first level was selected, which is 94.01 ± 0.2 dB, the microphone was directly coupled to the calibrator as shown in Figure 11 (right side) and the result was 94.1 dB, in the second measurement step the second level was selected, which is 114.02 ± 0.2 dB, the result of 114.0 dB was found. With the results within the tolerance limit, the sound pressure meter is as specified, being able to consider the measurements valid.

With the sound pressure meter properly measured, 36 measurements were made, distributed in 9 points defined in Figure 10 (points of passage of people in the sector). The measurements are shown in Table 3 and in the graph of Figure 12. The normative reference value of NR 15 [15] of 85 dB is identified in Figure 12 by the blue dotted line. The noise levels presented in Table 3 were measured progressively and cumulatively from the 7 fans, 3 test equipment, 3 engines and 3 horns of the motorcycles under test. The test area is closed, in the same environment in continuity with the final assembly line of the motorcycles.

Table 3: Sound pressure level measurements at each point (dB).

Sound source	Motorcycle horn	Motorcycle engine	Test Equipment	Industrial fan
Point 1	98.4	91.3	78.1	73.2
Point 2	101.1	90.6	81.2	75.0
Point 3	97.3	88.9	77.9	76.5
Point 4	102.2	89.9	78.3	76.1
Point 5	101.4	88.2	77.8	71.0
Point 6	100.4	89.8	79.0	74.7
Point 7	102.3	92.3	80.5	73.4
Point 8	103.0	92.3	80.2	72.3
Point 9	102.1	90.1	81.1	78.8
Average	100.91	90.38	79.34	74.56

Source: Authors, (2019).

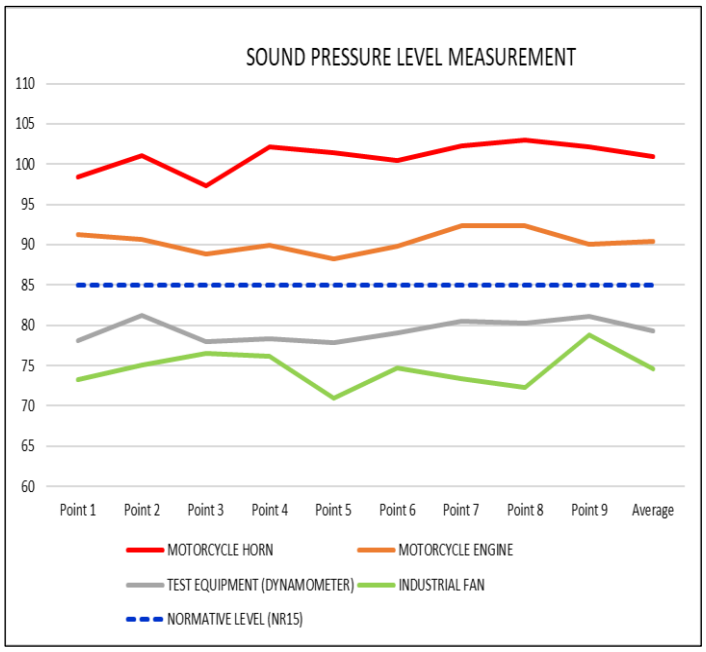

Figure 12: Graph of sound pressure measurements.
Source: Authors, (2019).

III.2 ACOUSTIC BOOTH PROPOSAL

The test site, necessary for the installation of the acoustic booth, was evaluated. Possible interferences, accesses and modifications were observed.

The project sought to adapt to the available area and perimeter so that significant changes were not necessary. So, the available area is 28.5 m2, as shown in Figure 13. With an available height of 3m, up to the luminaires, therefore, the final dimension is 3800mm x 7500mm x 3000mm. This space comprises 3 simultaneous test equipment as shown in Figure 13.

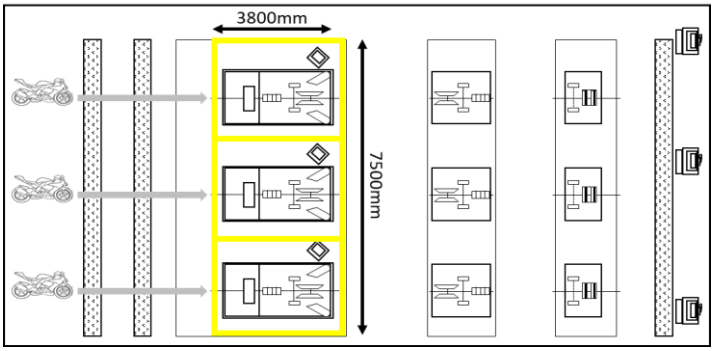

Figure 13: Location of the acoustic booth.
Source: Authors, (2019).

Decision is a choice between several alternatives and the decision-making process is a form of structuring the problem that aims to identify the best options. This structure must be constructed in stages, including problem definition, identification of alternatives, definition of criteria/objectives and their weights, and finally determine the best alternative [18]. The material alternatives with the highest potential for available and recommended sound absorbers (polyurethane foam; glass wool; and rock wool - Figures 6, 7 and 8 respectively) were compared in the Matrix of Table 4. The comparison criteria, among the indicated materials were: the sound absorption coefficient; resistance to temperature; the cost of the square meter; the useful life; maintainability; and availability in the national market. The weights and grades assigned to each material were recommended by a multidisciplinary team in the areas of projects, maintenance, quality, safety and purchases.

The criteria weights were established hierarchically from the most important (weight 7) to the least important (weight 2). Similarly, the comparison between the 3 material options, within each criterion, was hierarchically defined from the best evaluated (value = 4) to the least evaluated (value = 2). The criterion total is the product between the criterion weight and the value. The grand total is the sum of the total of all criteria.

The comparison matrix in Table 4 presents the evaluation and the results of the comparison, with rock wool being best evaluated.

Table 4: Evaluation matrix for sound absorbing materials.

COMPARISON MATRIX **EVALUATION OF THE SOUND ABSORBING MATERIAL OF THE ACOUSTIC CABIN**			 **POLYURETHANE FOAM**			 **GLASS WOOL**			 **ROCK WOOL**		
N	**CRITERIA**	**WEIGHT**	**NOTE**	VALUE	TOTAL	**NOTE**	VALUE	TOTAL	**NOTE**	VALUE	TOTAL
1	ACOUSTIC ABSORBING COEFFICIENT	7	0,8	2	14	0,85	3	21	0.98	4	28
2	TEMPERATURE	6	Up to 100º C	2	12	Up to 540º C	3	18	Non-combustible	4	24
3	COST	5	R$ 13.12/m²	2	10	R$ 6.8/m²	4	20	R$ 10.7/m²	3	15
4	DURABILITY	4	Low	2	8	Medium	3	12	High	4	16
5	MAINTENANCE	3	High frequency	2	6	Medium frequency	3	9	Low frequency	4	12
6	AVAILABILITY	2	High	4	8	High	4	8	High	4	8
G rand total			**58,0**			**88,0**			**103,0**		

Source: Authors, (2019).

A 3D acoustic booth was modeled using the Auto CAD software. The cabin has 3 doors at the front (entrance) and 3 at the rear (exit), for entry and exit of the test equipment motorcycles, as shown in Figure 14. The dimensions in detail are shown in the 2D drawings of Figures 15, 16, 17, 18 and 19 (measures in mm).

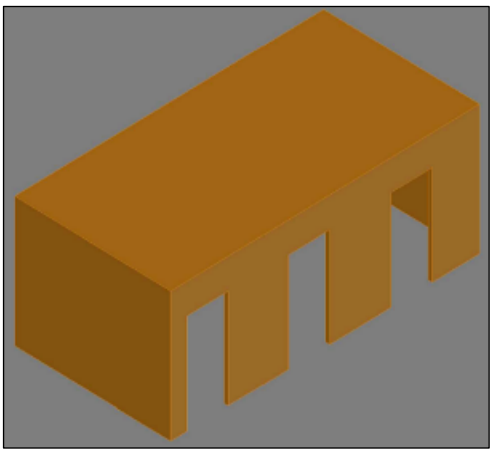

Figure 14: Acoustic cabin layout.
Source: Authors, (2019).

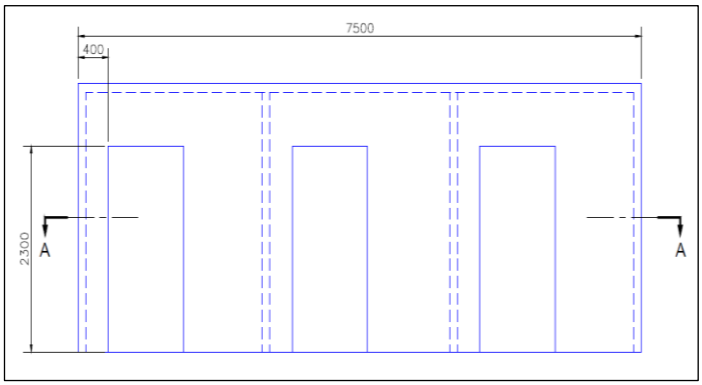

Figure 15: Front view, with the divisions between the 3 test equipment.
Source: Authors, (2019).

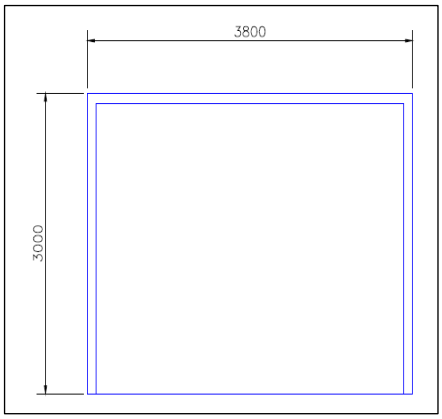

Figure 16: Left side view.
Source: Authors, (2019).

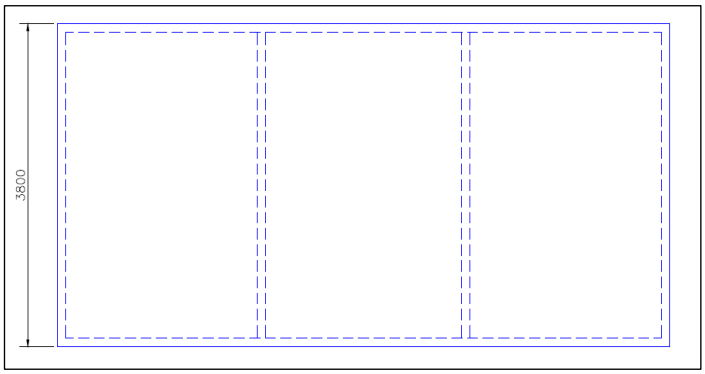

Figure 17: Top view.
Source: Authors, (2019).

Section A-A of Figure 15 shows the detail of the automated sliding doors that close and open automatically at the beginning and end of the test, respectively.

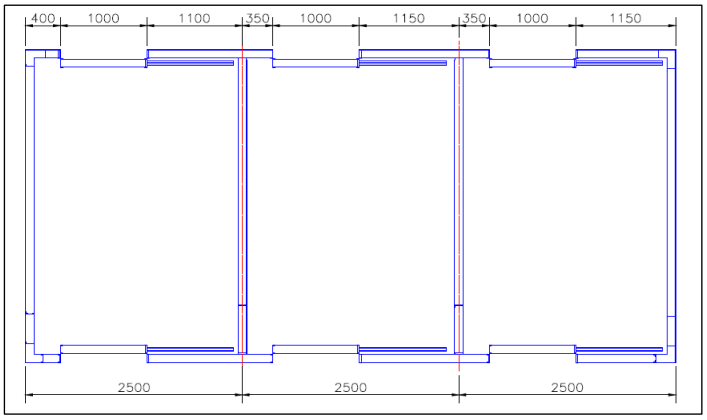

Figure 18: Section A-A (doors closed during testing).
Source: Authors, (2019).

The details of the constructive configuration, including the assembly, of the panels are presented through Figures 19, 20 and 21. The cabin consists of panels of 3 m by 3 m (total thickness of 100 mm), coated on both sides by steel sheets of 1.2 mm thick and filled internally with the selected sound absorbing material (rock wool).

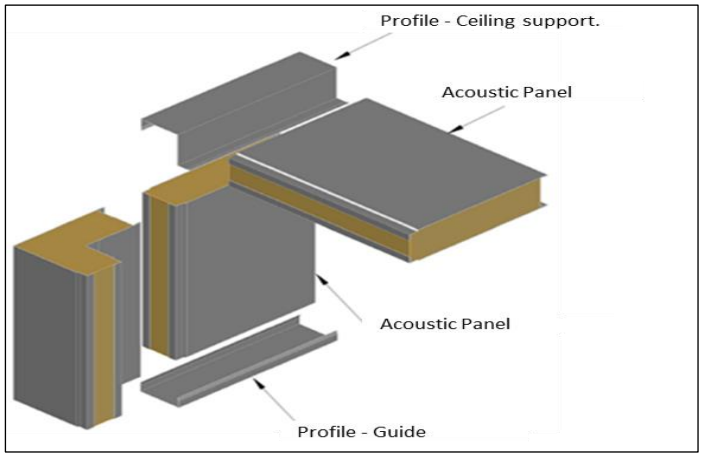

Figure 19: Construction and assembly details of the cabin panels.
Source: Authors, (2019).

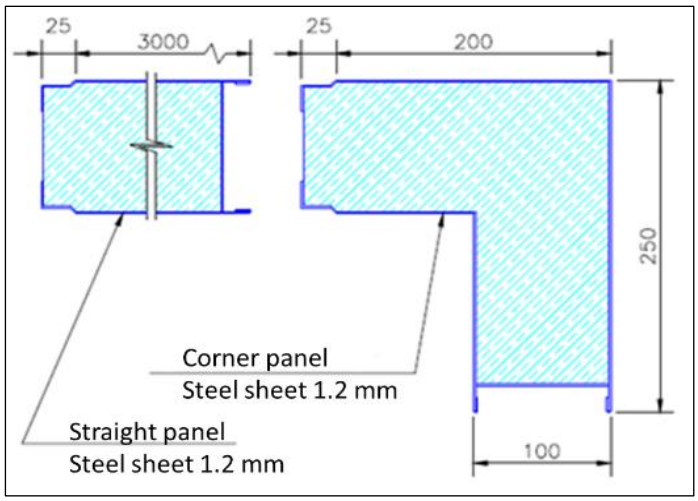

Figure 20: Constructive, dimensional and assembly details of the panels.
Source: Authors, (2019).

The steel plates of the cabin's internal panels have holes for the flow of sound energy (noise). This configuration improves the absorption of noise in the cabin (prevents sound reverberation - noise return). The schematic of the distribution and size of the holes is shown in Figure 21.

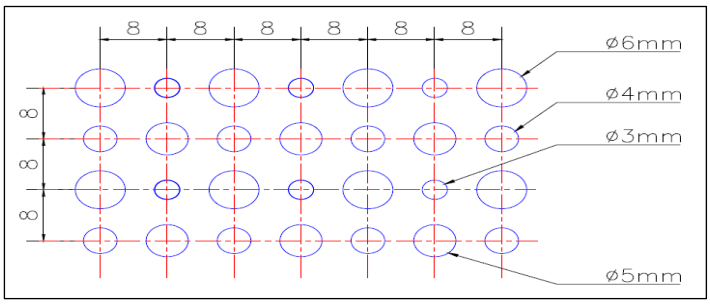

Figure 21: Scheme of distribution and dimension of the holes in the internal plate of the panel.
Source: Authors, (2019).

The Table 5 presents the project's bill of materials, describing specifications and quantities.

Table 5: Project´s bill of materials.

KIT	IT	DESCRIPTION/MATERIAL	TECHNICAL SPECIFICATIONS	QUANTITY
STEEL PANEL WITH ROCK WOOL NUCLEUS	01	SMOTHPLATE	GALVANIZED STEEL, 1.2 mm THICKNESS.	96.3 m²
	02	PERFORATED PLATE	GALVANIZED STEEL, 1.2 mm THICKNESS.	141.9 m²
	03	ACOUSTIC INSULATION OF ROCK WOOL	DENSITY OF 80 kg/m³	11.91 m³
SUPPORT STRUCTURE FOR ASSEMBLY	04	"U" PROFILE - GUIDE	CARBON STEEL 1020, HOT GALVANIZED, 101.6 mm SOUL, 4.67 mm THICKNESS.	30.2 m
	05	PROFILE – CEILING SUPPORT	CARBON STEEL 1020, HOT GALVANIZED, 101.6 mm SOUL, 4.67 mm THICKNESS.	30.2 m
SUPPORT STRUCTURE FOR FIXING	06	SLIDING DOOR GUIDE	SLIDING CAR OF STEEL, WITH TWO PULLEYS AND WITH BRAKE.	12 unit
	07	SLIDING DOOR RAIL	STEEL 1045, EXTRUDED.	12.6 m
	08	FIXING SCREW - GUIDE	SELF-DRILLING / LAMINATED STEEL / ZINCED SURFACE.	76 unit
	09	FIXING SCREW – SIDES AND CEILING	SELF-DRILLING / LAMINATED STEEL / ZINCED SURFACE.	220 unit

Source: Authors, (2019).

A price and budget survey was carried out with national suppliers, according to the bill of materials in Table 5. Table 6 presents the lowest value budget.

Table 6: Budget of the acoustic booth.

It	Description	Unit	Quantity	Price	Total (R$)
01	Steel panel with rock wool core.	m²	119.1	242.46	28876.99
02	Profile - Guide.	m	30.2	65.46	1976.89
03	Profile - Ceiling support.	m	30.2	44.45	1342.39
04	Guide for sliding door.	unit	12	65.8	789.60
05	Rail for sliding door.	m	12.6	17.91	225.67
06	Fixing screw - Guide.	unit	76	2.49	189.24
07	Fixing screw - Walls and ceiling.	unit	220	0.38	83.60
				Final Total	**33484.38**

Source: Authors, (2019).

IV. RESULTS AND DISCUSSIONS

The results of the work are listed below in accordance with the research objectives and the methodology:

The sound sources were identified and listed: Industrial fans; Test Equipment; motorcycle engine; and motorcycle horn;

Nine (9) noise measurement points, in the current layout of the motorcycle test area, were indicated considering the flow of people on these routes exposed to noise;

Thirty-six noise level measurements were made distributed over the 9 defined points. The motorcycle horn promoted the highest sound pressure level at 100.9 dB.

The installation area of the cabin was defined and delimited, comprising 3 test equipment simultaneously, without the need for significant changes or modifications of the location;

The sound absorbing material of the cabin was selected based on 6 comparison criteria. Rock wool stood out in the evaluation, being the material indicated as a sound absorber; and

The constructive, geometric and assembly specifications were defined, modeled and issued technical drawings. As well as, the project bill of materials and respective budget in the amount of R$ 33484.37.

This design can be applied to any noisy area, requiring only dimensional adjustments of the cabin.

V. CONCLUSIONS

The research objectives of mapping the sectorial noise level and establishing a proposal for an acoustic booth in the test process, which reduced the level of noise exposure of people traveling in this area were achieved. It is estimated that the level of environmental noise should be reduced between 40dB and 50dB with the implementation of the acoustic cabin in the test equipment. The greatest risk is related to employees in administrative areas who travel near the test areas without the use of hearing protection or who remain for a long period in this traffic. The hearing protector reduces noise intensity by about 15%, leaving acceptable levels for 8 hours of exposure. As well, considering the analysis of NR15, the mapped levels are acceptable up to 30 minutes of exposure. Process employees wear ear protectors. However, the cabin also promotes improvements in the inspection process allowing the inspector to concentrate on the noise inherent in the inspected motorcycle. It minimizes that the inspector hears noises from other motorcycles, environmental or sound reverberation. Furthermore, the lower the level of environmental noise, the more pleasant for people and productive for the company. In future works it is proposed to implement the acoustic booth, a new noise

mapping, comparison of productivity, quality and satisfaction of the people who work and travel through the test area.

VI. REFERENCES

[1] P. Roelofsen, "Evaluation of environmental noise based upon the percentage of dissatisfied," J. Facil. Manag., vol. 10, no. 2, pp. 133–139, Apr. 2012.

[2] A. Czyzewski and J. Kotus, "Universal system for diagnosing environmental noise," Manag. Environ. Qual. An Int. J., vol. 15, no. 3, pp. 294–305, 2004.

[3] A. Essien, Sound Sources: The Origin of Auditory Sensations, 1a ed. New York, NY: Michael Terence, 2019.

[4] R. Kumar, E. Madhu, A. Maan, S. Sinha, and N. Akhtar, "Estimation of combined exposure factor due to the impact of different transport related environmental pollutants air quality and noise level in Delhi city," World J. Sci. Technol. Sustain. Dev., vol. 12, no. 4, pp. 269–280, Oct. 2015.

[5] M. N. K. Saunders, P. Lewis, and A. Thornhill, Research methods for business students. Prentice Hall, 2009.

[6] J. A. Sharp, J. Peters, and K. Howard, The management of a student research project. Gower, 2002.

[7] P. Montanari, V.; Cunha, Nas ondas do som. São Paulo-SP: Moderna, 1996.

[8] R. F. Barron, Noise Control and Acoustics, 1a ed. Columbus, OH: CRC Press, 2003.

[9] S. R. Bistafa, Acústica aplicada ao controle do ruído. São Paulo-SP: Blücher, 2018.

[10] S. Gerges, Ruído: Fundamentos e Controle, Ed. 2a. Florianópolis-SC: NR Editora, 2000.

[11] L. A. Nepomuceno, Elementos de acústica física e psicoacústica. São Paulo-SP: Edigard Blücher, 1994.

[12] S. Gerges, Ruídos e vibrações veiculares, 1a ed. Florianópolis-SC: NR Editora, 2005.

[13] T. Ford, "Test improves accuracy of acoustic aircraft cabin model," Aircr. Eng. Aerosp. Technol., vol. 76, no. 6, pp. 284–289, Dec. 2004.

[14] A. A. Nudelmann, E. A. da. Costa, J. Seligman, and R. N. Ibañez, PAIR : perda auditiva induzida pelo ruído. Porto Alegre-RS: Revinter, 2001.

[15] BRASIL, Norma Regulamentadora do Ministério do Trabalho. NR 15 – Atividades e Operações Insalubres. BRASIL, 1978.

[16] "High-performance thermal and acoustic protection," Aircr. Eng. Aerosp. Technol., vol. 73, no. 1, pp. 93–100, Feb. 2001.

[17] "Researchers can reduce noise in aircraft cabins with 'active' trim panels," Aircr. Eng. Aerosp. Technol., vol. 80, no. 3, pp. 27–28, May 2008.

[18] J. C. Soares, S. D. Sousa, and A. Tereso, "A decision-making model for the rework of defective products," Int. J. Qual. Reliab. Manag, 2019.

Journal of Engineering and Technology for Industrial Applications, 2020. Edition. 23. Vol: 06
https://www.itegam-jetia.org
ISSN ONLINE: 2447-0228
DOI: https://dx.doi.org/10.5935/2447-0228.20200022

RESEARCH ARTICLE OPEN ACCESS

COMPARISON OF BRAZILIAN STANDARDS FOR THE QUALIFICATION OF THREE-PHASE INDUCTION MOTORS AGAINST A GLOBAL SCENARIO

Leandro Braz Sousa[1], Felipe Sass[2], Marcio Zamboti Fortes[3] and Guilherme Moreira Quintanilha[4]

[1, 2, 3, 4] Federal University Fluminense – UFF. Rio de Janeiro – Rio de Janeiro, Brazil.

Email: leandrobraz.sousa@hotmail.com, felipesass@id.uff.br, mzamboti@id.uff.br, guilherme.moreira@globo.com

Received: Apr 27th, 2020

Accepted: Jun 15th, 2020

Published: June 30th, 2020

ABSTRACT

Electric motors are considered the most important equipment among those that consume final electric energy in Brazil. It is estimated that the induction motors and the systems driven by them are responsible for approximately 70% of the energy consumption of the Brazilian industrial sector. Countries like Japan, members of the European Union, the United States, Australia, India, and Brazil have specific standards to qualify their equipment. These, among other countries, have regulatory or even mandatory regime mechanisms that classify the efficiency of three-phase induction motors, using specific standards and regulations. In this way, this article aims to compare the application of national standard methods with international methods, making it possible to qualify the national standard against a global scenario. This articles compares the test standards IEEE 112 Method B, IEC 60034-2-1, JEC 37 and ABNT NBR 17094-3, these standards have different methodologies, so that when the same engine is tested by them their efficiency can present different results, generating large discourses among international committees on which standard is the most appropriate for this type of trial.

Keywords: Electric motors, Energy efficiency, Induction motor standards, Energy policies.

I. INTRODUCTION

The growing demand for electricity to sustain global development requires significant investments in power generation. However, these investments depend on increasingly scarce natural resources due to the constant degradation of the environment. The best strategy for maintaining power supply in the short term is to avoid waste and increase energy efficiency [1,2].

Electric motors play an important role in this strategy, as around 40% of global energy consumption is related to the application of this equipment [1]. Because of this need to reduce energy consumption and greenhouse gas emissions, governments in various countries around the world are establishing minimum energy efficiency requirements, also known as Minimum Energy Performance Standards (MEPS) for several devices, including electric motors [1].

In 2014, about 45.8 million low-voltage motors (LVM) were sold around the world. This amount is estimated to increase to 51.6 million in 2019, representing an annual growth rate of 2.5% [3]. In 2014, LVM sales were classified according to International Efficiency (IE) standards as Standard Efficiency (IE1) 44% of the units sold, High Efficiency (IE2) 34%, Premium Efficiency (IE3) 14% and Super Premium Efficiency (IE4) 1%. As presented in Figure 1, considerable transition to more efficient motors is expected until 2019. This result was partially driven by the MEPS.

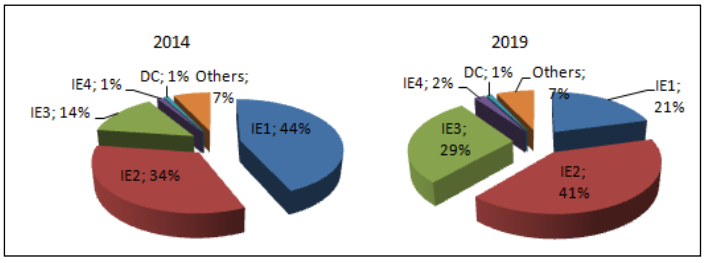

Figure 1: Classification of low voltage motors sold around the world according to international efficiency index.
Source: Adapted from [3].

The electric motor and motor-driven systems contribute significantly to the demand for energy consumption. In the European Union Industry, it is estimated that this equipment represents about 70% of all energy consumption [4].

When an old motor fails, it will probably be an IE0 or IE1 class equivalent motor, and this situation provides an opportunity for replacing the old motor with a properly sized IE3 or IE4 class motor, which offers significantly higher efficiency for a wide range of loads [5].

Some countries adopt strategies to reduce the electricity consumption of motors include the application scope of MEPS, the industrial electricity price, the load factor, and installation of a variable-speed drive (VSD) [6]. Since motors are the major energy consumers in industry and buildings, most economies have some kind of voluntary or mandatory regulatory scheme regarding the efficiency of the power equipment. Some of these economies also have mandatory minimum levels of efficiency for electric motors sold in their respective countries and labeling recommendations for the manufactures of higher efficiency machines. Motor efficiency regulations around the world are to date limited to AC induction motors, which represent by far the largest share of the motor market [7-9].

The strategy to implement the policies to improve efficiency in Brazil is similar to most of the countries around the world. The initiatives are usually government oriented and go through education initiatives, equipment regulation, labeling programs, project and R&D funding, rebate programs, and an Energy Efficiency Law. The government's National Energy Plan 2030 proposed a strategy for expansion of the energy supply, however, current Brazilian market mechanisms are not sufficient to promote desirable efficiency improvements in end-use of energy [10,11].

In 1993, the PROCEL Label of Energy Economy, or simply the PROCEL label, was introduced with the objective of informing the consumer about better equipment and reinforcing the value of more efficient products [12]. Complementary to the qualifying labels of PBE, this endorsement label emphasizes the most efficient products which mean class A equipment, according to the efficiency label and presents additional quality attributes, such as safety, low noise, and lower water consumption. The concession of this label is the responsibility of PROCEL, which essentially uses the same equipment performance database as PBE (Brazilian labelling program) [13].

This paper reviews the Brazilian experimental procedures for determining the efficiency level of electric motors, compare them with international standards and qualify the results against the world scenario. In section Efficiency Policies, the application of efficiency policies will be presented, where over the years it is possible to observe the reduction of the sales of IE1 electric motors and the increase of sales of IE2 and IE3 electric motors. In section Analysis of the Brazilian Standard, an analysis of the NBR 17094-3 through a type test in the three-phase induction motor is presented. In sequence, there are two sections showing how to compute induction motor losses, and making a comparison between the standards IEE 112, IEC 60034-2-1 and JEC 37 indicating the main differences in the test methods. Finally, the last section presents conclusions about the main differences in the presented measurement procedures.

II. EFFICIENCY POLICIES

Several strategies can be used to increase the efficiency of induction motors: advances in motor design, smaller tolerances, use of best magnetic materials, a greater cross-section of copper/aluminum in stator and rotor to reduce resistance among others [13].

To accelerate the market penetration of efficient motors, the implementation of minimum efficiency standards is being discussed by the European Commission (EC). Motors belonging to the same group size must fit specific eco-design requirements [14].

MEPS are legislative instruments used by national governments and the EU to remove the most inefficient electric motors and Power Drive Systems (PDS) from the markets. The change, however, takes some time because it usually lasts from 4 to 6 years for the transition from a new MEPS to be completed [11].

Overall, the regulations on electric motors were first introduced in North America. The United States implemented standards through the Energy Policy Act of 1992, but only in 2007 that the standards were applied. The so-called EPAct (Energy Policy Act) 92 standard was comparable to the IE2 class, but the US has already begun moving the IE3/NEMA Premium Motors in 2010. In Canada, the first requirements came into force in 1997 and Mexico adopted the standard EPAct in 1998 [15]. Brazil and China issued the first MEPS in 2002, but these referred to standard efficiency electric motors. MEPS for the IE2 level came into force in Brazil in 2009 and in China in 2011 and Brazil implemented higher minimum efficiency values going from IR2 to IR3 level on August 30, 2017. On this date was signed the Ministerial Ordinance No. 1, dated June 29, 2017, where the maximum levels of specific energy consumption or minimum energy efficiency of energy consuming machines and appliances in Brazil are established [13]. Australia and New Zealand have placed MEPS at the IE2 level since 2006. Other countries with MEPs at the level of at least IE2 include Chile (2011), Israel (2008), South Korea (2013, IE2 / 2015, IE3 level), Switzerland (2011, level IE2 / 2015, same level as Eco-design in Europe), Taiwan (2015) and Turkey (2015, same level of Eco-design in Europe).

In addition, several countries have implemented requirements at the IE1 level [13]. In India, an IE1 standard motor was first adopted in 2004 and was revised for IE2 and IE3 in 2011, covering the IE2 and IE3 electric motors. The MEPS at the level of IE2 were adopted in 2016. At present, IE1 or less efficient electric motors cannot be commercialized in the Brazilian market, however, they are sold abroad and returned applied in finished products [16-20].

Figure 2 shows the impact of energy efficiency policies on the volume of electric motors sold per efficiency class, where we can see the growth in the number of more efficient electric motors sold after the implementation of policies in the countries and the decrease in the sale of inefficient electric motors [3]. The horizontal axis represents the year of the analyses and the vertical axis the amount of the units (motors) sold [21].

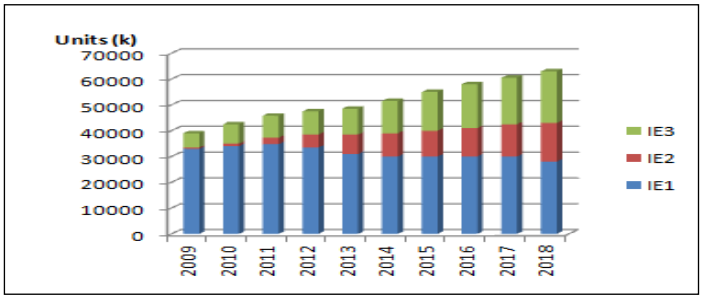

Figure 2: Impact of energy efficiency policies on the volume of electric motors sold per efficiency class.
Source: Adapted from [3].

II.1 ANALYSIS OF THE BRAZILIAN STANDARD

NBR 17094-3: 2018 [22] which recently replaced NBR 5383-1 [23] prescribes test methods for determination of the performance a compliance characteristics of the three-phase induction motor, where the efficiency values found must meet the minimum values required by NBR 17094-1: 2018 [24]. The use of an ABNT NBR is voluntary and is based on the consensus of society, becoming mandatory when established by the public power, in the form of laws, decrees, ordinances, and etc. [23,25].

According to item VIII of Article 39 of the Consumer Protection Code in Brazil, it is prohibited to place on the consumer market any product or service that does not comply with the standards issued by the competent official bodies or, if there are no specific rules, by the Brazilian Association of Technical Standards or another entity accredited by Conmetro (National Council of Metrology, Standardization and Industrial Quality) [22].

Table 23 of NBR 17094-1: 2018 separates the tests from NBR 17094-3-2018 into three classes: Routine, Type, and Special Tests. Routine tests are applied to all induction motors, during or after their manufacture, to verify that it meets defined criteria. Type tests are applied to one or more electric motors, manufactured according to a particular design, to prove that the design meets certain specifications. Special tests are those not considered as routine or type tests and are performed only by agreement between the manufacturer and buyer [26].

In Brazil there are procedures to obtain the characteristics of the three-phase induction motor according to NBR 17094-3. The electric motor tested presented on Table 1 has a great application in the Brazilian industries and therefore know its characteristics and determine its efficiency is relevant.

The methods for determining the characteristics of the three-phase induction motor are presented in NBR 17094-3 and described in the procedures of method 2, dynamometric test with indirect measurement of additional losses and direct measurement of the stator, rotor, core, friction and ventilation losses.

The initial test considers that the motor is cool and in thermal equilibrium with the environment, the ambient temperature and the average line resistance must be measured. To measure the ambient temperature, thermocouples or other types of sensors can also be installed, also for temperature measurement on the motor, coil heads or slots (outside the cooling air circulation path), to have a good average winding temperature. It is necessary to choose the method that will perform the resistance measurement, where the method used in this article is the Kelvin bridge because according to NBR 17094-3 is the most accurate to perform the direct measurement of resistance. Measurement results are presented in Table 2 [22, 24-26].

Table 1: Motor Data.

Model	132S	Power (CV)	5
Rotation (rpm)	3495	Voltage (V)	220
Current (A)	12.2	Insulation class	F
Frequency (Hz)	60	Relation IA/IN	5.9
Regime	S1	Power Factor	0.91
Index protection (IP)	55	Category	N
Number of phases	3	Service factor	1
Number of poles	2	Efficiency (%)	87.5

Source: Authors, (2020).

Table 2: Measure of The Initial Electric Motor Resistance.

R-S (Ω)	0.715	S-T (Ω)	0.714
T-R (Ω)	0.709	Room temperature(°C)	24.6

Source: Authors, (2020).

After performing the resistance measurement with the cold electric motor, the temperature rise test is done, the motor is running continuously at nominal load until it reaches the thermal stability, in order to obtain the temperature at which the stator and rotor losses will be corrected. When the thermal equilibrium is reached, the power supply is switched off and the winding resistance measurement is checked. The results are presented in Table 3 [26].

Table 3: Temperature Rise Test.

Measurement Time	08:54	09:24	09:54	10:24	10:54
Housing (Middle - Right Side) (K)	12.1	15.1	13.7	13.5	13.8
Housing (Middle - Left) (K)	11.2	13.9	12.6	12.5	12.8
Room temperature (° C)	25.5	26.1	26.2	26.1	26.2
Torque (N.m)	12.1	10.0	10	10.0	10.0
Power (W)	5037	4150	4141	4145	4144
Current (A)	14.6	12.0	12.0	12.1	12.0
Voltage (V)	219.9	220.2	220.0	219.6	219.9
Speed (rpm)	3490	3512	3513	3513	3512

Source: Authors, (2020).

Temperature measurement after an electric motor shutdown is evaluated considering changes in the resistance value, according to Equation 1. The equations in this article are based on [22].

$$\frac{R_2}{R_1} = \frac{t_2 + K}{t_1 + K} \quad (1)$$

Where:

t_2 is the winding temperature at the end of the test, expressed in degrees Celsius (°C);

t_1 is the winding temperature (cold motor with stabilized temperature) at the moment of measuring resistance R_1, expressed in degrees Celsius (°C);

R_2 is the winding resistance at the end of the test, expressed in ohms (Ω);

R_1 is the winding resistance at temperature t_1, expressed in ohms (Ω);

K is equal to 234.5 for electrolytic copper with 100% conductivity or 225 for aluminum with 62% IACS (International Annealed Copper Standard) conductivity. The measured resistance value after the temperature rise test is presented in Table 4.

Table 4: Measure of Resistance After Temperature Rise.

Measurement of resistance after temperature rise (Ω)	0.771	Room temperature (°C)	26.4
Read time (s)	11		

Source: Authors, (2020).

If the resistance reading is obtained within the time interval indicated in Table 5, this reading should be used to compute the winding temperature [24].

Table 5: Time Interval with the Initial Reading of Resistance Adopted as Temperature Measurement.

Rp ≤ 37.5 kW	0 -30
37.5 < Rp ≤ 150 kW	0-90
150 < Rp ≤ 5050 kW	0 -120
5000 kW< Rp	By agreement

Source: Authors, (2020).

The next step is to perform a load test, applying rated voltage and frequency to the motor, and placing load at four different operational points: 25%, 50%, 75%, and 100% of the rated load. In addition, the tests must be performed with two load operational points above 100 % of the rated load, but without exceeding 150%. In this work, tests were performed with 125% and 150%. The electric motor loading must be done in descending order and considering a point with the dynamometer turn off to determine the dynamometer correction.

For each load point, it is necessary to measure: the output torque (Nm), the input power (kW), the average line current (A), the motor speed (rpm), the winding temperature and the ambient temperature (°C), and the applied midline voltage (V). It is possible to replace direct winding temperature measurement with resistance measurement. In this case, the winding resistance shall be measured at the beginning and end of the load test according to Table 6. The test is valid if the ratio between the two values does not exceed 3.5% for electric motors up to 15 kW and 3.0% for electric motors above 15 kW. The mean value of the measured resistances should be used to compute electrical losses [24]. The load test is shown in Table 7.

The next step is to perform the no-load test and determine the friction and ventilation losses, according to NBR 17094-3. If the dynamometer is still coupled to the motor under test, it must be disengaged, leaving the motor shaft completely free. Before starting data acquisition, it is necessary to ensure that the power source is stable.

Table 6: Measurement of Resistance in Load Test.

Resistance before test (Ω)	0.775	Resistance after the test (Ω)	0.765
Temperature before test (°C)	26.4	Temperature after test (°C)	26.4

Source: Authors, (2020).

Table 7: Load Test.

Torque (%)	150	125	100	75	50	25	0
Torque (N.m)	14.9	12.5	10.0	7.5	5.0	2.5	0.7
Power (W)	6342	5250	4203	3168	2164	1183	477
Current (A)	18.3	15.13	12.21	9.38	6.8	4.54	3.4
Speed (rpm)	3451	3482	3507	3531	3554	3574	3587
Voltage (V)	220	220	220	220	219	220	221

Source: Authors, (2020).

Voltage and current readings must be performed, the motor must initially be fed with a nominal voltage. Then the voltage must be varied in a decreasing way between the points of 110 to 20% [22] of the nominal voltage. However, in this case, for over-voltage forces on the motor, the voltage variation was 125 to 20% of the nominal voltage. After each decrease, with stable signals, voltage and current readings shall be recorded. The tests results are shown in Table 8.

Table 8: No Load Test.

Voltage (%)	125	100	80	60	40	20
Voltage (V)	275.3	220.4	176	132.4	88.2	44.5
Current (A)	4.0	3.2	2.5	1.9	1.5	2.0
Power (W)	245.9	201.2	175.6	152.9	137	126

Source: Authors, (2020).

In this test, it is also possible to estimate the winding temperature using the measured resistance values measured at the beginning and end of the no-load test, as shown in Table 9.

Table 9: Measurement of Resistance Before and After No-load Testing.

Resistance before test (Ω)	0.766	Resistance after the test (Ω)	0.752
Temperature before test (°C)	26.4	Temperature after test (°C)	26.3

Source: Authors, (2020).

III. LOSSES DETERMINATION

Based on standard the NBR 17094-3: 2018 and adopting method 2, the losses used to compute the electric motor performance are friction and ventilation losses, core losses, stator losses, rotor losses, and Supplementary losses.

III.1 FRICTION AND VENTILATION LOSSES

The value of the input power minus the I^2R loss on the stator versus the voltage is plotted, and the curve obtained is extended to zero voltage. The intersection with the zero-voltage axis is equal to the friction and ventilation losses. For the low voltage range, the intersection can be determined more precisely if the input power values subtracted by the I^2R losses in the stator are plotted in function of the squared voltage (Figure 3).

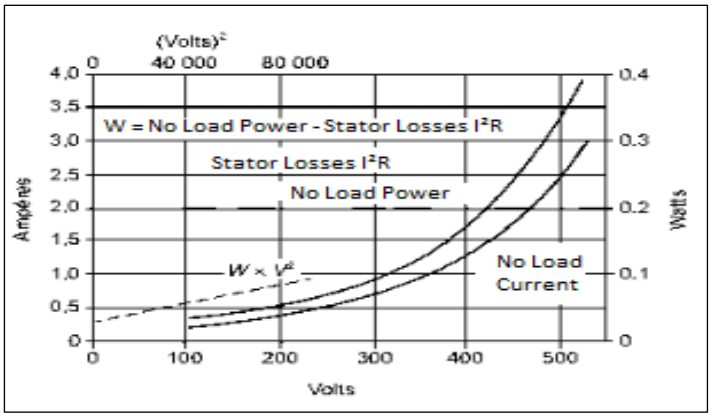

Figure 3: Friction and Ventilation Losses.
Source: Adapted from [18].

III.2 CORE LOSSES

The core losses in the no-load test at rated voltage is obtained by subtracting the friction loss and the loss of the sum of the losses obtained from the no-load losses.

III.3 STATOR LOSSES

Calculate the loss (I²R) of the stator expressed in watts, according to Equation 2.

$$1.5\ R.I^2 \qquad (2)$$

for three-phase motors, where:

I is the measured or calculated effective current per line terminal at a specified load (A);

R is the direct current resistance between any two line terminals, corrected to the specified temperature (Ω).

III.4 ROTOR LOSSES

Compute the loss of the rotor for each load point. This loss, which includes the brush contact losses for motors with the winding rotor, must be determined by sliding in decimal fraction using Equation 3.

$$P_{rot} = (P_{in} - P_{est} - P_{cor}.S) \qquad (3)$$

Where:

P_{rot} is the Rotor Loss (W);

P_{in} is the Input power (W);

P_{est} is the Stator Loss (W);

P_{cor} is the Core Loss (W);

S is the slip.

Correcting the slip to the temperature measured at the point.

III.5 SUPPLEMENTARY LOSSES

The determination of the additional loss for each load point is obtained by the methodology:

a) Calculate the apparent total loss, such as input power minus output power (with corrected output torque);

b) Subtract from the apparent total loss the sum of the corrected conventional losses to the temperature of the laden test, obtaining the additional losses;

c) Adjust the additional loss data using the linear regression method, considering Equation 4.

$$P_s = P_{sn}\ \left(\frac{I_2}{I_{2n}}\right)^2 \qquad (4)$$

Where:

P_s is the supplementary loss (W);

P_{sn} is the nominal supplementary loss (W);

I_2 is the operational current (A);

I_{2n} is the nominal operational current (A).

If the slope is negative or if the correlation factor γ is less than 0.95, suppress the worst point and recalculate the slope of the line and the intersection with the zero conjugate line. If, after this procedure, the correlation factor increases to values equal to or greater than 0.95 and the slope is positive, use this calculation; otherwise, the test is unsatisfactory. Possible instrumentation errors and readings should be present. The source of errors should be investigated and corrected, and the trials should be repeated.

d) The corrected value of the supplementary loss to be used is obtained for each point with A, by Equation 5.

$$P_s = A.T^2 \qquad (5)$$

Where:

P_s is the supplementary losses (W);

A is the slope obtained in item C;

T is the torque (Nm).

Recalculate the I²R stator loss for each load point, correcting the resistance to the final temperature rise test temperature and considering the ambient temperature of 25 °C.

Recalculate the I²R losses of the rotor for each load point, correcting the slip to the final temperature of the temperature rise test and considering the ambient temperature of 25 °C.

Calculate the corrected output power for each load point according to Equation 6.

$$P_{oc} = P_{in} - P_{core} - P_{fv} - P_{stc} - P_{rotc} - P_{sc} \qquad (6)$$

At where:

P_{oc} is the corrected output power (W);

P_{in} is the measured input power (W);

P_{core} is the nucleus loss (W);

P_{fv} is the friction and ventilation losses (W);

P_{stc} is the I²R corrected stator loss for the final temperature (W);

P_{rotc} is the I²R corrected rotor loss for the final temperature (W);

P_{sc} is the corrected supplemental loss (W).

Determine the efficiency for each loading point of the test using the following Equation 7.

$$\eta = \frac{P_{out}}{P_{in}} \qquad (7)$$

Where:

η is the efficiency;

P_{out} is the corrected output power (W);

P_{in} is the measured input power (W).

To determine the efficiency at precise points of charge, an efficiency curve versus corrected output power was obtained and the desired values are obtained as shown in Figure 4.

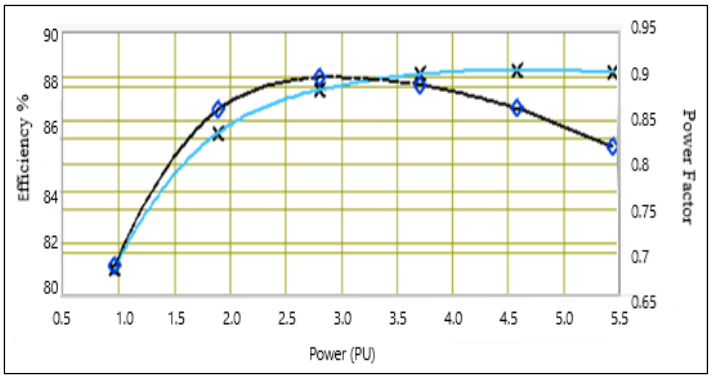

Figure 4: Efficiency X Output Power.
Source: Authors, (2020).

Table 10 shows the synthesis of the results obtained in the three-phase induction motor test.

Table 10: Synthesis of Results Output X Output Power.

Torque (%)	**150**	**125**	**100**	**75**	**50**	**25**
Frequency (Hz)	60	60	60	60	60	60
Speed (rpm)	3452	3482	3507	3531	3554	3574
Slip (rpm)	148.1	117.2	92.5	68.7	46.3	26
Voltage (V)	219.9	220.	220.0	220.	220	220.7
Current (A)	18.4	15.1	12.2	9.4	6.8	4.5
Input power (W)	6342.5	5250	4203.	316	2164	1183
Core losses (W)	66.2	66.2	66.2	66.2	66.2	66.2
Stator loss(W)	19.0	11.4	7.3	4.3	2.7	4.5
Power through the air gap (W)	6257	5173	4130	309	2095	1113
Rotor losses (W)	257.5	168.4	106.1	59.0	26.9	8.0
Friction and windage losses (W)	123.5	123.5	123.5	123.5	124	123.5
Total Conventional Losses (W)	466.3	369.6	303.2	253.2	219.2	202.4
Conjugate (N.m)	14.9	12.49	10.01	7.5	5.0	2.5
Correction of the dynamometer (N.m)	0.03	0.03	0.03	0.03	0.03	0.03
Corrected Conjugate (N.m)	15	12.5	10.0	7.5	5.0	2.5
Output power (W)	5422	4566	3687.8	2792	1876	946.9
Total apparent losses (W)	920.1	684.3	515.3	376.6	288.2	236.5
Supplementary Losses (W)	453.8	314.8	212.11	123.4	68.9	34.1
Intersection with the axis (B)		0.01	Correlation Factor (g)		1	-
Stator loss corrected (W)	389.7	263.4	171.5	101.2	53.2	23.7
Corrected power through air gap (W)	5887	4921	3965	3001	2045	1093
Corrected sliding (rpm)	141.5	112.	89.8	67.1	45.5	25.7
Speed Corrected (rpm)	3458	3487	3510	3532	3555	3574
Loss of rotor (W)	242.2	160.1	101.9	57.22	26.3	7.9
Supplementary losses corrected (W)	87.3	60.8	39.1	22.1	9.9	2.5
Total corrected losses (W)	908.4	674.1	502.3	370.3	279	223.9
Corrected output power (W)	5435	4577	3701	2798	1885	959.5
Output Power (CV)	7.4	6.2	5.03	3.8	2.6	1.3
Efficiency (%)	85.7	87.2	88.1	88.3	87.1	81.1
Power factor	0.91	0.91	0.9	0.89	0.84	0.68
Index of income removal - IAR (%)	-	-	-24	-	-	-

Source: Authors, (2020).

The Brazilian standard NBR 17094-3 for motor testing determines a methodology for acceptance of the results of the test performance uncertainty of electric motors of an informative nature, where the test compliance tolerance limits vary according to the performance range of the electric motor which is defined by the results deviation index, which represents how the electric motor tested is far from the declared value of the electric motor. The tolerance applied to the performance evaluation is represented as a zone of acceptable values. Its border limits are called the lower limit of tolerance (LIT) and an upper limit of tolerance (LST). Electric motors that exhibit their characteristics within these limits must be considered approved. The uncertainty of the performance should be considered.

And for the efficiency's located in the uncertainty zone, the electric motor tested may or may not respect the established tolerance. In this case, it is recommended to test the sample, review the uncertainty or the tolerance applied in the measured range.

Motors with efficiency within the rejection zone should be reproved in this test. Figure 5 shows the results for the electric motor tested in this work where its data are within the acceptance zone with an IAR of -24%.

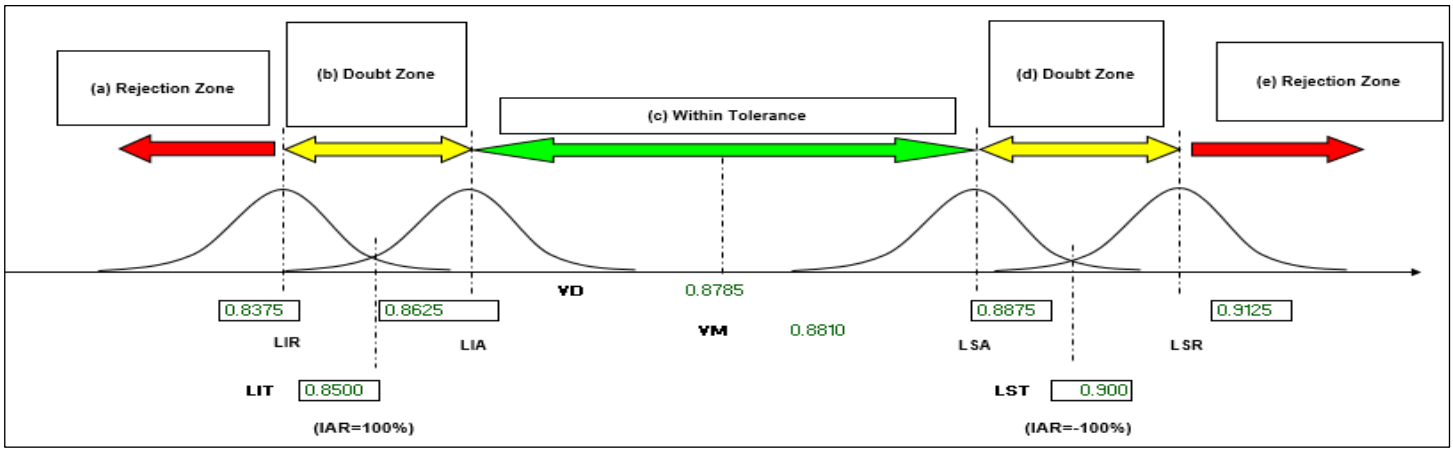

Figure 5: Compliance Zone.
Source: Adapted from [22].

At where:
LIT - Lower Limit of Tolerance;
LST – Upper Limit of Tolerance;
IM – Measurement Uncertainty;
LIA – Lower Limit of Acceptance;
LSA – Upper Limit of Acceptance;
LIR – Lower Rejection Limit;
LSR – Upper Limit of Rejection.

IV. COMPARISION BETWEEN THE MAIN STANDARDS

The energy efficiency of the electrical equipment is today one of the main factors that influence the competitiveness between industries. The convenient choice and dimensioning of the equipment are therefore one of the challenges that the industries in general face. To do this, it is important that strong regulation that establishes national procedures to determine the efficiency of electric motors are implemented.

IV.1 MAIN STANDARDS

The efficiency values provided by the manufacturers are determined according to the specifications of minimum efficiency values through the different energy efficiency standards of three-phase induction motors adopted by each country in the world. This work highlights:

• IEEE 112 (Institute of Electrical and Electronics Engineers) - method B (American standard);

• IEC 60034-2-1 (International Electrotechnical Commission) - (International standard);

• JEC 37 (Japanese Electrotechnical Commission) - (Japanese standard);

• NBR 17094-3 (Brazilian standard).

IV.2 TESTS METHODS

There are currently some standards for testing electric machines, and for three-phase induction motors. Different electric motor test methodologies leads to significantly different efficiency values. This is due to the fact that different considerations and treatment were given to the losses that occur during the energy conversion process inside the electric motor. The IEEE 112 standard test method A, B, and C determines the motor efficiency directly from electrical power input measurements and mechanical output power under load operating conditions. The IEEE 112, E and F test method and the JEC standard use different techniques to determine the input and output power, or both, when a direct measurement is not available. The main difference between the different methods is the treatment of dispersion losses under load. The IEEE 112 method E and F requires a separate test for the on-load dispersion losses while the old IEC 34-2 assumes a percentage value at full load for these losses, where the current standard 60034-2-1 already performs a test to determine dispersion losses. The JEC standard 37 uses a circular diagram as the main method for calculating efficiency and does not include a direct measurement of on-load dispersion losses. Since the load dispersion losses are about 8-15% of all the loss, the accuracy in dispersion losses computations can be compromised in these methods [27].

There are several procedures for conducting tests in electric motors, which establishes the methods to be adopted during the tests so that the characteristics of the motors can be determined and the minimum values for their acceptance. The test methods can be divided into two groups, named by Direct Method and Indirect Method.

In the direct method, both input and output mechanical power is measured. In the indirect method, one or both are not measured directly. Within the same norm, it is difficult to compare the values obtained by the direct and indirect methods, since they start from different hypotheses.

In addition, the choice between several methods depends on factors such as equipment availability, cost and time to perform the tests, the precision required, the amount of power involved, etc. Analyzing in terms of energy conservation, it is important that the method chosen it's the one that more accurately assesses the actual electric motor performance. The input-output with loss segregation method, described by IEEE-112 - Method B, is the most suitable for this. This is because of the estimation of dispersion losses that are difficult to quantify. One of the main differences between these procedures is in the form of how the dispersion loss in charge is determined. The test methods of the abovementioned standards are given.

IV.3 IEEE 112-METHOD B

It is the most important standard in the industrial field because polyphase squirrel cage induction motors with power in the range of 0.16 to 370 kW are tested on the horizontal axis. Method B requires three tests:

• Temperature rise test - The machine operates at nominal load until the main motor winding temperature stabilizes), measurements are taken every 30 minutes, where the machine is considered stabilized if the measured value of the temperature does not exceed 1 °C within 1 hour, this test is performed to establish the temperature at which stator and rotor losses will be corrected. At the end of this test, the stator winding resistance must be measured.

• No-load test - The no-load test must be carried out in an uncoupled machine immediately after the load test. Six different voltage values are applied, including the nominal voltage. The suggested voltage are: 125%, 100%, 80% and 60% 40% and 20% of the nominal voltage. This test aims to determine the iron losses and friction and ventilation losses. The test should be performed as soon as possible with the readings performed in descending voltage sequence. The winding resistance is measured and after the test. The validity of this test depends on the difference observed between the first and second measure of the winding resistance.

The maximum allowable difference for machines up to 15kW is 3.5%. Machines with power higher than 15kW the maximum allowable difference is 3.0%.

• Variable load test under nominal conditions - Four load points are applied approximately equally spaced between 25% and 100% (including 100%) and two equally spaced values above 100% and not exceeding 150% of the rated load. Classification and partial load application tests are performed from the highest load to the lowest in descending order. These tests should be performed as soon as possible to minimize electric motor temperature changes.

The maximum allowable difference for machines up to 15kW is 3.5%. Machines with power higher than 15kW the maximum allowable difference is 3.0%. It is necessary to add to this test a specific point with the dynamometer turned off to determine the dynamometer correction.

IV.4 IEC 60034-2-1

This test method is similar to [22]. Temperature rise test – After performing the resistance measurement with the cold machine is initiated to the temperature elevation test. The motor is driven in a continuous regime with nominal load until it reaches the thermal stability, so get the temperature for which the stator and rotor losses will be corrected. The thermal equilibrium is achieved, when in the interval of 30 min, the temperature does not vary more than 1°C then the power supply is switched off and the measurement of the winding resistance is done.

Load test - This test should be performed immediately after the temperature rise test with the motor at the operating temperature. A controlled load is applied to the machine in different six points. It is suggested to use loading points close to 125%, 115%, 100%, 75%, 50% and 25% of the nominal load. These tests should be performed as quickly as possible to minimize the temperature changes in the machine during the test and it is necessary to measure the winding resistance (before and after the test). The procedure aims to determine the stator and rotor losses.

No-load test – The no-load test must be carried out immediately after the load test. Eight different voltage values are applied, including the nominal voltage. The suggested voltage is: 110%, 100%, 95% and 90% of the nominal voltage. These values are used for the determination of the iron losses; the values of approximately 60%, 50%, 40% and 30% of the nominal voltage are used for the determination of friction and ventilation losses; the test should be performed as soon as possible with the readings performed in descending voltage sequence.

The winding temperature is determined by direct measurement in the nominal load test using the shortest time possible by the extrapolation procedure. After the lowest loading point is processed, another reading the winding temperature is recorded. Both readings are used to predict winding resistances for all other loads. Alternatively, the winding temperature can also be measured with temperature sensors, similar to IEEE procedures.

IV.5 JEC 37

This standard is less restrictive than that of the USA and Europe. The evaluation of efficiency by the Japanese standard can be considered as an indirect method. JEC 37 neglects parasitic load losses. For this reason, the efficiencies obtained are generally higher. In addition, no thermal correction of Joule losses is specified. Since it is very difficult to find the measurement procedures used in the Japanese standard, it is practical to evaluate the efficiency of the machine using the test results required by the other standards.

V. CONCLUSIONS

In this manuscript, standards NBR 17094-3, IEEE 112-B, IEC 60034-2-1 and JEC 37 were considered for the evaluation of the efficiency of the induction motor. Differences in the prescribed procedures of each standard were discussed. This work also supports the evaluation of the insertion of three-phase induction motors in the Brazilian market in front of the national standard.

Previous studies according to reference [24] have verified the efficacy of IEC 60034-2-1, which may offer similar efficiency values to IEEE method B, provided that the procedures are followed strictly. It can also be said that the IEC 60034-2-1 standard is well aligned with the IEEE 112 due to the values presented. However, the two standards present some distinctions in procedures adopted to determine stator conductor loss, core loss, and load losses. However, there are no differences in the determination of rotor conductor loss, friction and ventilation losses. The differences in conductor stator losses are virtually within tolerance measurement, while those in core loss and parasitic head loss are relatively significant.

Compared to IEEE 112 method B and NBR 17094-3, the IEC standard can provide more accurate but smaller loss values and thus higher values of dispersion load loss. Clearly, the nominal efficiency values for the two standards are approximately the same.

Direct Methods (IEEE 112-B) consider that speed measurement is a relatively simple procedure requiring equipment to achieve accurate results (± 1 RPM), torque measurement requires elaborate setup and much more expensive equipment to provide accurate results. Torque measurement usually requires the coupling of the motor to a dynamometer, which has the possibility of creating a controllable variable load, equipped with a torque transducer.

It is important to highlight that if the instruments used are not correctly calibrated the tests may show significant deviations due to instrumentation errors, then it is concluded that for this analysis the reason of discrepancies could be caused by wrong procedures or mistaken readings of some equipment.

In the Japanese standard JEC 37, the error is greater, since the load losses are totally ignored in the indirect measurement of the efficiency. Due to the way the losses are evaluated, the tests to determine the characteristics of the induction motor generate efficiency values that can be several points above the measured values with direct efficiency methods.

The electric motor tested had a higher efficiency than the minimum required by standard NBR 17094-1 for class IR2, 5CV, 2 poles, with efficiency of 88.1% where the efficiency standard of the induction motors determines 87.5% for this type of engine, even with a results deviation index of -24%, the project showed itself within the conformity zone, approving the lot to be marketed.

Finally, comparing the no-load test of IEC 60034-2-1 with NBR 5383-1, it is observed that the procedures present differences in the application of the variation of percentages of nominal voltage but according to [28], and the comparative analysis of the standards can be observed that the final result of efficiency undergoes small variations.

The goal of this article was to present a comparison of the test methods of the mentioned standards in order to determine the best procedure to be applied for the three-phase induction motors tests, the results show that ABNT NBR 17094-3: 2018 and IEC 60034-2-1 present advantages compared to JEC 37 because their final result of efficiency levels is more accurate.

VI. REFERENCES

[1] WEG S.A.. Regulamentações Globais de Eficiência para Motores Elétricos de Baixa Tensão – v 2017. Available at:< https://static.weg.net/medias/downloadcenter/h62/hb8/WEG-regulamenta-es-globais-de-eficiencia-para-motores-eletricos-de-baixa-tensao-50065222-brochure-portuguese-web.pdf. Accessed 31 March 2019.

[2] Pérez-Lombard, L.; Ortiz, J.; Velázquez, D.. Revisiting energy efficiency fundamentals. Energy Effic., vol.6, pp.239-254, 2013. doi: 10.1007/s12053-012-9180-8.

[3] Reine, P. (2015). Industrial Motors and Drives: Global Market Update. EEMODS'15 Conference Helsinki, 2015. doi: 10.2790/903731.

[4] EMSA. Policy Guidelines for Electric Motor Systems, Part 2: Toolkit for Policy Makers. IEA 4E Implementing Agreement, 2014. Available at: <https://nachhaltigwirtschaften.at/resources/iea_pdf/iea_4e_policy_guidelines_for_electric_motor_systems.pdf. Accessed 31 March 2019.

[5] Ferreira, F.J.T.E.; Cisneroz-González M.; Almeida A.T.. Technical and economic considerations on induction motor oversizing, Energy Effic., vol.9, pp.1-25, 2016. doi: 10.1007/s12053-015-9345-3.

[6] Han, J.; Yun, S.J.. An analysis of the electricity consumption reduction potential of electric motors in the South Korean manufacturing sector. Energy Effic., vol.8, pp.1035-1047, 2015. doi:10.1007/s12053-015-9335-5.

[7] Waide, P.; Brunner, C. U.. Energy-efficiency policy opportunities for electric motor systems, 2011. Available at: < https://www.oecdilibrary.org/docserver/5kgg52gb9gjden.pdf?expires=1554118240&id=id&accname=ocid54025470&checksum=B0F0E72C5913D8FDFEAC63ED8C2215C6. Accessed 31 March 2019.

[8] Sauer, I.L.; Tatizawa, H.; Salotti, F.A.M.; Mercedes, S.S.. A comparative assessment of Brazilian electric motors performance with minimum efficiency standards. Renew Sustain Energy Rev, vol.41, pp.308–18. 2015. doi: 10.1016/j.rser.2014.08.053.

[9] Almeida, A.T.; Fong, J.; Falkner, H Bertoldi, P.. Policy options to promote energy efficient electric motors and drives in the EU, Renew Sustain Energy Rev,, vol.74, pp.1275-1286, 2017. .doi:10.1016/j.rser.2017.01.112.

[10] de Castro Andrade, C. T.; Pontes, R. S. T.. Economic analysis of Brazilian policies for energy efficient electric motors. Energy Policy, vol.106, pp.315-325, 2017. doi: 10.1016/j.enpol.2017.03.029.

[11] Macedo, P.P.; Mota, C.M.M.; Sola, A.V.H.. Meeting the Brazilian Energy Efficiency Law: A flexible and interactive multicriteria proposal to replace non-efficient motors. Sustainable Cities and Society, vol.41, pp. 822-832, 2018. doi: 10.1016/j.scs.2018.06.020.

[12] Bortoni, E.C.; Nogueira, L.A.H.; Cardoso, R.B.; Haddad,J.; Souza, E.P.; Dias, M.V.X.; Yamachita,R.A.. Assessment of the achieved savings form induction motors energy efficiency labeling in Brazil. Energy Conversion and Management, vol.75, pp.734-740, 2013. .doi:10.1016/j.enconman.2013.08.034.

[13] Nogueira, L.A.H.; Cardoso, R.B.; Cavalcanti, C.Z.B.; Leonelli, P.A.. Evaluation of the energy impacts of the Energy Efficiency Law in Brazil. Energy for Sustainable Development, vol. 24, pp. 58-69, 2015. Available at: < https://www.academia.edu/20128586/Evaluation_of_the_energy_impacts_of_the_Energy_Efficiency_Law_in_Brazil. Accessed 31 March 2019.

[14] Almeida, A. T.; Ferreira, J.T.E.F.; Fong, J.. Standards for efficiency of electric motors permanent magnet synchronous motor technology, IEEE Industry Applications Magazine, vol.17, pp.12–19, 2011. doi: 10.1109/MIAS.2010.939427.

[15] Jardot, D.; Eichhammer, W.; Fleiter, T.. Effects of Economies of Scale and Experience on the Costs of Energy-Efficient Technologies – Case Study of Electric Motors in Germany. Energy Efficiency, vol.3, pp.331–346, 2010. doi: 10.1007/s12053-009-9074-6.

[16] MME (Ministério de Minas e Energia). Portaria no. 1, de 29 de junho de 2017, 2017. Available at: <http://pesquisa.in.gov.br/imprensa/jsp/visualiza/index.jsp?jornal=1&pagina=50&data=30/08/2017. Accessed 21 July 2018.

[17] Siemens AG. Minimum Energy Performance Standards, MEPS regulations worldwide, 2-15. Available at: < https://pt.scribd.com/document/352001568/SIEMENS-Meps-Regulations-En. Accessed 31 March 2019.

[18] UNIDO (United Nations Industrial Development Organization) Energy efficiency in electric motor systems: Technical potentials and policy approaches for developing countries. Working paper 11/2011, 2011. Available at: < https://open.unido.org/api/documents/4818324/download/Energy%20efficiency%20in%20electric%20motor%20systems%20-%20Technology,%20saving%20potentials%20and%20policy%20options%20for%20developing%20countries. Accessed 31 March 2019.

[19] IEA (International Energy Agency). Energy-Efficiency Policy Opportunities for Electric Motor-Driven Systems, 2011. Available at: <https://www.energiestiftung.ch/files/downloads/energiethemen-energieeffizienz-industriegewerbe/ee_for_electricsystems-2-.pdf. Accessed 31 March 2019.

[20] de Almeida, A. T.; Fong, J.; Falkner, H.; Bertoldi, P.. Policy options to promote energy efficient electric motors and drives in the EU, Renewable and Sustainable Energy Reviews, vol. 74, pp. 1275-1286, 2017. doi: 10.1016/j.rser.2017.01.112.

[21] Boglietti, A.; Cavagnino, A.; Lazzari, M.; Pastorelli, M.. International standards for the induction motor efficiency evaluation: a critical analysis of the stray-load loss determination. In 38th IAS Annual Meeting on Conference Record of the Industry Applications Conference, vol.2, pp. 841-848, 2003. doi: 10.1109/IAS.2003.1257626.

[22] ABNT (Associação Brasileira de Normas Técnicas). NBR 17094-3: Parte 3: Motores de indução trifásicos – Métodos de ensaio, 2018.

[23] ABNT (Associação Brasileira de Normas Técnicas). NBR 5383: Parte 1: Motores de indução trifásicos – Métodos de ensaio, 2002.

[24] ABNT (Associação Brasileira de Normas Técnicas). NBR 17094-1: Parte 1: Motores de indução trifásicos – Requisitos, 2018.

[25] Kumar, H. International Copper Association India.Interview5February2016, 2016. Available at: <.https://copperindia.org/india-copper-forum. Accessed 31 March 2019.

[26] CDC (Código de Defesa do Consumidor). Art.39, inc.VIII do Código de Defesa do ConsumidorLei8078/90, 1990. Available at: .https://www.jusbrasil.com.br/topicos/10602565/inciso-viii-do-artigo-39-da-lei-n-8078-de-11-de-setembro-de-1990?ref=serp-featured. Accessed 15 June 2018.

[27] Yamachita, R.A. Determinação de perdas e rendimento em motores elétricos empregando termografia infravermelha, Doctorate Thesis, Universidade Federal de Itajubá, Brazil, 2013. Available at: < https://repositorio.unifei.edu.br/xmlui/handle/123456789/736. Accessed 31 March 2019.

[28] Cao, W.. Comparison of IEEE 112 and New IEC Standard 60034-2-1. IEEE Trans on Energy Conversion. Vol. 24, pp.802-808, 2009. doi: 10.1109/TEC.2009.2025321.

Journal of Engineering and Technology for Industrial Applications, 2020. Edition. 23. Vol: 06
https://www.itegam-jetia.org
ISSN ONLINE: 2447-0228
DOI: https://dx.doi.org/10.5935/2447-0228.20200023

RESEARCH ARTICLE OPEN ACCESS

DEVELOPMENT OF ANTI-THEFT OFFLINE GPS TRACKER

Sourav Kumar Ghosh[1], Mamunur Rashid[2], Nazmus Sama Tuba[3], Mehbubul Mukaddem Akash Neerjhor[4], Anika Kader[5], Tahiya Nuzhat Peata[6] and Pritom Biswas[7]

[1, 2, 3, 4, 5, 6, 7] Bangladesh University of Textiles (BUTEX), Tejgaon, Dhaka-1208, Bangladesh.

Email: sourav@butex.edu.bd, mamunrashid@butex.edu.bd, nazmusssama@gmail.com, akashneerjhor@gmail.com, anika.kader.butex@gmail.com, tahiya.peata@gmail.com, pritombiswas2020@gmail.com

Received: May 19th, 2020

Accepted: Jun 18th, 2020

Published: June 30th, 2020

ABSTRACT

Anti-Theft Offline GPS Tracker has been introduced in this paper to meet up the demand for secure use of important technological gadgets i.e. laptop, mobile phone, etc. It is developed in a way so that if any gadget gets stolen or gets lost, it can track even if it is offline. The tracker will be connected with the battery of the device where it is installed. So, even the device is switched off, it can gain power from the recharged battery from the device. Anti-Theft Offline GPS tracker is designed to locate the place of location offline, of the object with which the GPS Tracker will be attached. It will send a text message containing the Google Map link of the location to a given phone number when asked. By this, the gadget can be identified with its location point. We have followed almost all the procedures of the product development process from getting customer preferences to designing and finalizing the product. Material selection and cost analysis have also been done based on the mass production of the product. This product features exact location & real-time tracking, quick and continuous reply, rechargeable battery, easy to carry and cost efficient.

Keywords: GPS, Arduino, Offline tracking, Real-time response, Product Development.

I. INTRODUCTION

Laptops and other portable IT devices i.e. smartphones, tablets, etc. are often lost or stolen frequently nowadays. In a crowded city like Dhaka, stealing laptops and mobile phones is a common issue. However, it is assumed that 98% of the stolen laptops are hard to be recovered. So, there is a huge economic loss due to this type of crime. Mostly these devices lost or stolen at the airport, other places like shopping malls, left in transport, or even stolen sometime by company employees or other people. One will need to level up his or her security, to prevent this loss of devices, and the information stored within. Stolen IT devices can include proprietary information such as reports, contact lists, important sales-related documents, financial records, and the like. This data can cause great damage if it goes to the wrong hands, such as a competitor or anyone who might want to make a quick buck out of selling the information in the black market. When these devices are stolen, they are immediately turned off and cannot be tracked mostly for being offline. As such, there is a need to protect and track these devices. Understanding the emerging demand of the current scenario, a real-time "Anti-Theft Offline GPS Tracker" can track important devices when it is offline and solve the problems. By doing this, the protection of the devices and the safety of information will be ensured. The product is basically a GPS (Global Positioning System) tracker, made with a micro controller (Arduino Mega) and GSM module and some other equipment to track the devices when they are turned off. We powered our micro controller by a power-bank and our GSM module by a lithium polymer battery. When GPS is fixed, we will automatically receive a message with latitude, longitude, and a Google map link on the number that is given in the Arduino code. The objectives of this paper are stated below.

i. To design the prototype.
ii. To develop a tracker that is easy to carry and that contains a rechargeable battery.
iii. To ensure the security of the device and the valuable information within
iv. To track the exact location of the device.
v. To check the reply from the tracker to the smartphone with a google map link.

II. LITERATURE REVIEW

Among many approaches, the well-known approaches to product design are the systematic approach, axiomatic design, and quality engineering [1]. In the product design phase, everything required to develop a working prototype [2]. Design decisions determine 70% of product costs and that early design decisions are much more significant than later manufacturing decisions [3]. Huimin Jiang showed in detail that Quality function deployment (QFD) is commonly used in the product planning stage to define the engineering characteristics and target value settings of new products [4]. Hlaing proposed a device where GPS & GSM have been used for vehicle tracking by installing the device inside a vehicle [5]. Omar developed a Realtime tracking system based on Arduino intel galileo which acts on GPS, GSM, and GPRS which are utilized for vehicle tracking and monitoring. The SIM908 Module is applied which incorporates three technics to be specific GPS, GPRS, and GSM [6]. Dhanya prepared an Anti-Theft Vehicle Tracking System is developed to track vehicles all the time and it can also predict the location of the vehicle if the GPS fails. The Time series prediction algorithm is used for the prediction [7]. Mounika presented vehicle tracking and monitoring using GPS and GSM which is based on the Internet of Things [8]. Poonam implemented a child tracking system using GPS and GSM based on Arduino [9]. Gullipalli proposed a GPS live tracking of buses and fuel monitoring system using Arduino [10]. Kaur developed A smart vehicle designed for mishap location detection, an anti-collision system where shock ultrasonic, the temperature sensor is used along with GPS and GSM for real-time analysis [11]. Asianuba designed the anti-theft control system which adopts GSM technology in form of AT command to notify the user through SMS once there is an intruder. It also consists of the inclusion of a database of security agencies so that the SMS is also sent to the nearest security agency [12]. Mohiuddin et al. proposed a smart Anti-Theft vehicle system based on the Internet of Things (IoT) for monitoring the movement of any equipped vehicle from anywhere in real-time. At the implementation of this system, (GPS), (GSM)/ (GPRS) and microcontrollers are used to enable users for monitoring their vehicles in a convenient manner [13]. Paing et al. propose a personal use VAT system using the IoT platform that can be easily introduced due to the very low cost [14]. Light Dependent Resistor (LDR) and motion sensor is used to develop a cost-efficient automatic street light control system [15]. A low cost solar water purifier is designed and embodied using product development theory [16]. Advanced air purifier facial mask is developed using Arduino Nano and air pump [17].

The tracking system has been mostly using for locating vehicles. There were a few systems for other reasons. But there was no GPS tracking system developed to locate a tech gadget. In daily life, people lose these items. These items get stolen. In order to retrieve these tech gadgets, first we need to know about its location in real-time and that is where our developed product serves its purpose.

III. METHODOLOGY

The development of the product starts with the customer survey. Then prioritization of their preferences, develop the quality function deployment (QFD), consist the black box model, analyze the functional decomposition, material and manufacturing process selection, cost analysis, prototype development, testing the prototype and finally the final product is build following all these steps. In figure 1, the full process flowchart is depicted. Customer satisfaction is our main target so that a survey was conducted among people from stages (urban & rural residential sector) through questionnaires using google response form and face to face interview.

QFD is a process and set of tools used to effectively define customer requirements and convert them into detailed engineering specifications. We converted these customers' needs to technical requirements & perform QFD (Figure 2).

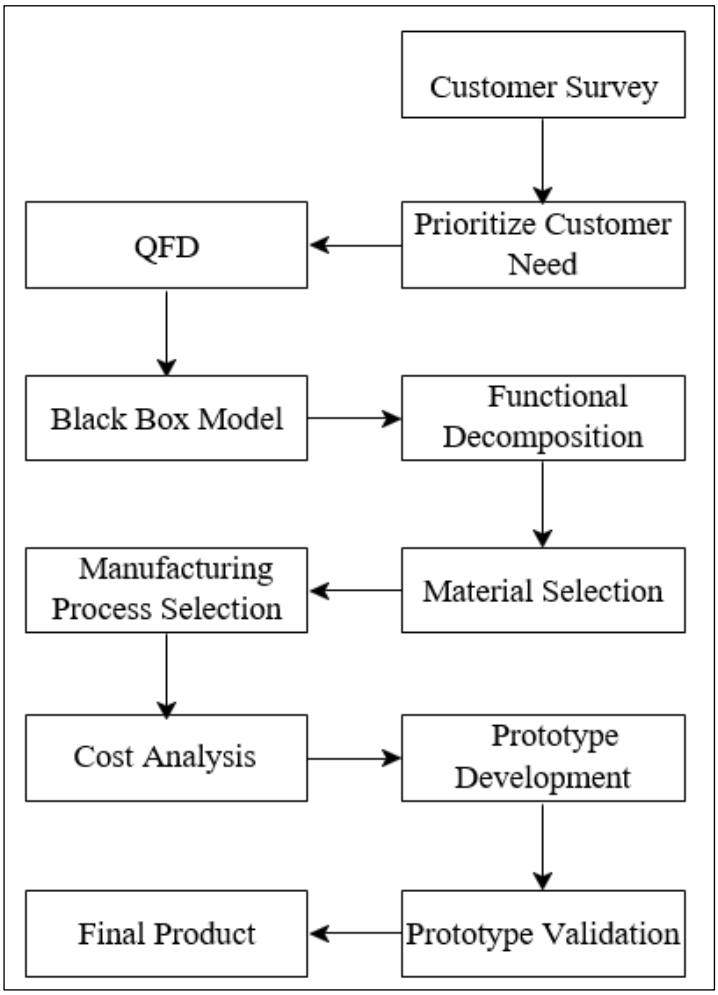

Figure 1: Process flowchart of product development.
Source: Authors, (2020).

According to their response, customer needs are classified into three groups that are presented in Table 1.

Table 1: Customer requirements with preference.

High Preference	Low Cost
	Effective Mechanism
	Real-time tracking
	Device weight
	Using for textile purpose
Medium Preference	The life period of the device
	Power supply process
	Effortless maintenance
	Additional features
Low Preference	Manufacturing Material
	Location messaging response time range

Source: Authors, (2020).

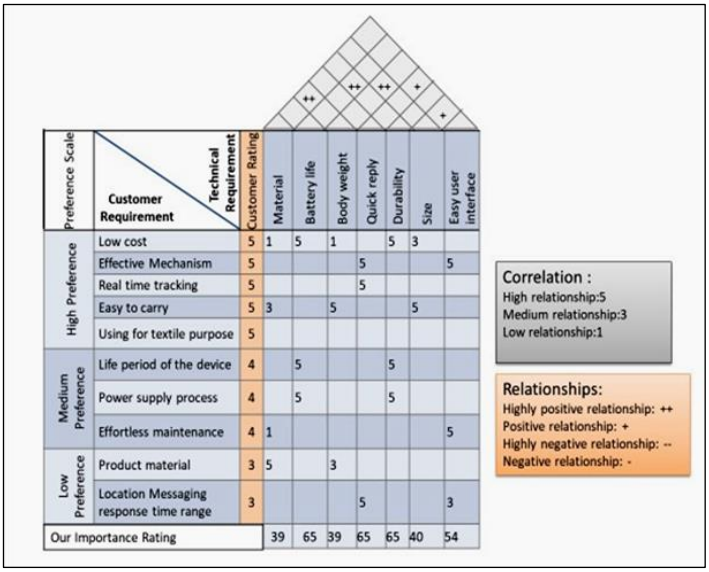

Figure 2: Product Planning Diagram (House of Quality) for Anti-Theft Offline GPS Tracker.
Source: Authors, (2020).

From Figure 2 we see that battey life, quick reply & durability are the main technical requirements for our product. Then we performed functional decomposition where we broke our product into smaller parts. We also conduct a black box design. After planning we have developed the prototype of our product successfully.

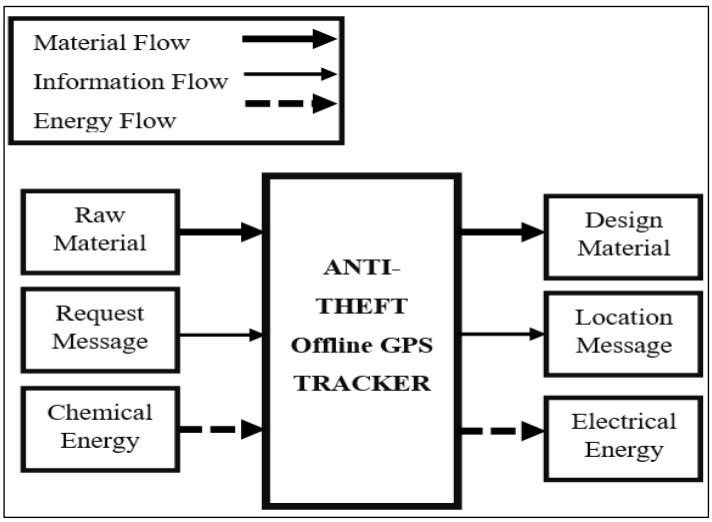

Figure 3: Black Box Model of the Anti-Theft GPS Tracker.
Source: Authors, (2020).

From the black box model (Figure 3), we can see that, raw material has been used as an input of raw material & we got design material as output. Request message has been used as an input of information & we got location message as output & chemical energy has been used as an input chemical energy & we got electrical energy as output from it.

From the cluster function diagram (Figure 4), we see that, chemical energy has been transformed into electrical energy through the energy conversion system which includes mobile battery,9V adapter, Arduino mega & GSM module. Raw material has been converted to design material using cover, Arduino mega, GSM module, SIM & connection wire.

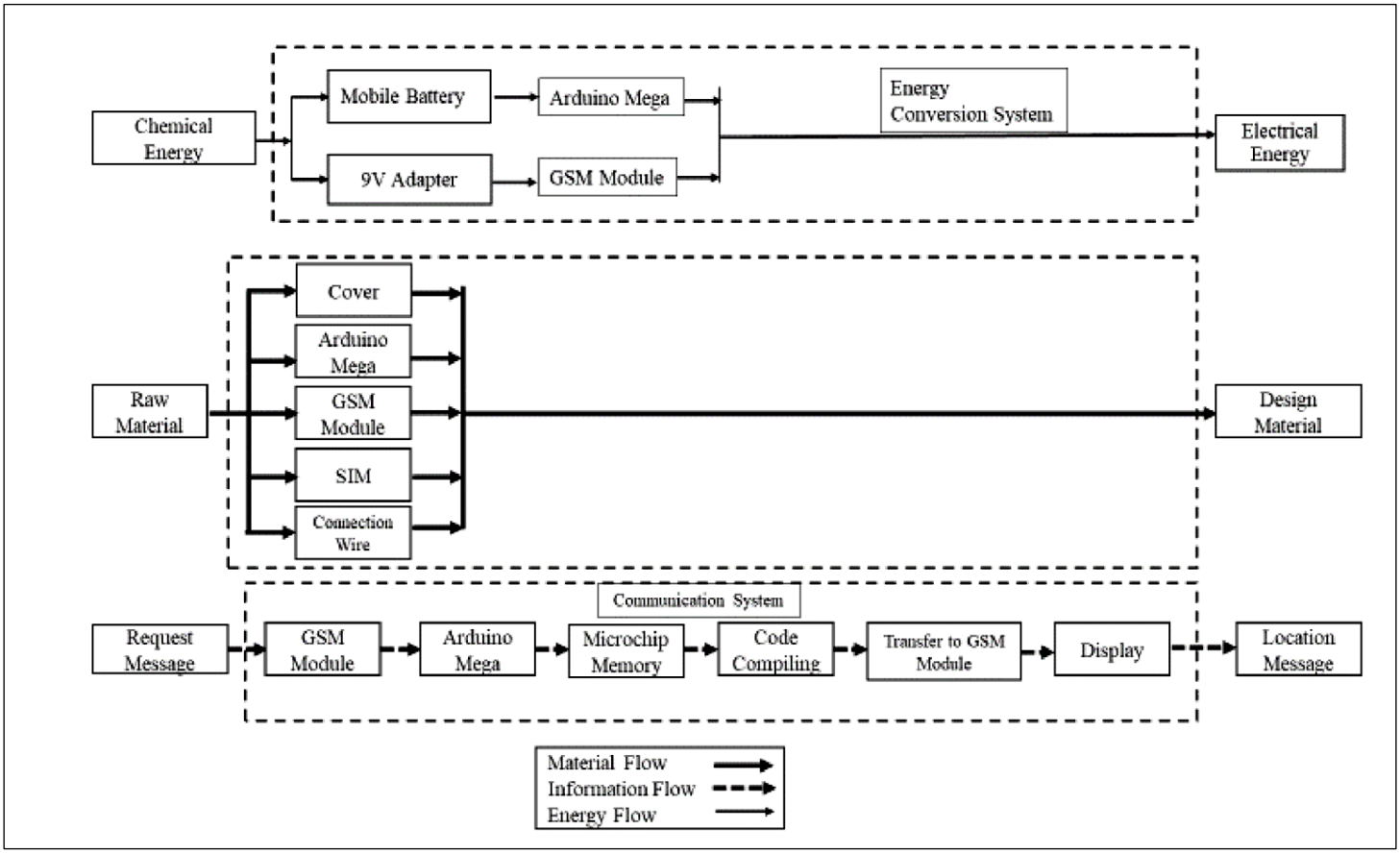

Figure 4: Cluster Function of Anti-Theft GPS Tracker.
Source: Authors, (2020).

This part mainly built the physical portion of the product which we call hardware system. It also sets up some parts to fulfill the software system implementation by Arduino mega, GSM module, SIM & connection wire. Request for message has been converted into location message as output through the process of communication system which includes GSM module, Arduino mega, microchip memory, code compiling, transfer to GSM module & display. After getting a command it goes to GSM module. Then to microchip memory then according to coding it responds with a location reply & after that it is displayed on the screen. After that material and manufacturing process selection were done by weighted average method. Afterwards the cost analysis was employed, and cost breakdown is shown in Table 2.

Table 2: Cost breakdown for Anti-Theft Offline GPS Tracker.

Component Name	Quantity	Unit Price (USD)	Total cost (USD)
Arduino Mega 2560	1	7	7
GPS Module	1	25	25
Battery	1	0.71	0.71
9V Adapter	1	1.77	1.77
Jumper wire	24	0.02	0.48
SIM	1	0.35	0.35
Total			35.31

Source: Authors, (2020).

III.1 HARDWARE SYSTEMS

1) Arduino Mega 2560: Arduino mega 2560 is a microcontroller board which is based on ATmega2560.It possesses more memory space and me/O pins compared to other boards. There are 16 analog inputs and 4 Hardware serial ports. Tx indicates the transmission of information whereas the RX indicates receive data Power can be connected through DC supply and AC supply. Mega 2560 has a power supply of 3.3v and 5v. It has a reset button if anyone wants to erase programs or memory. It is helpful for making many automatic machines.

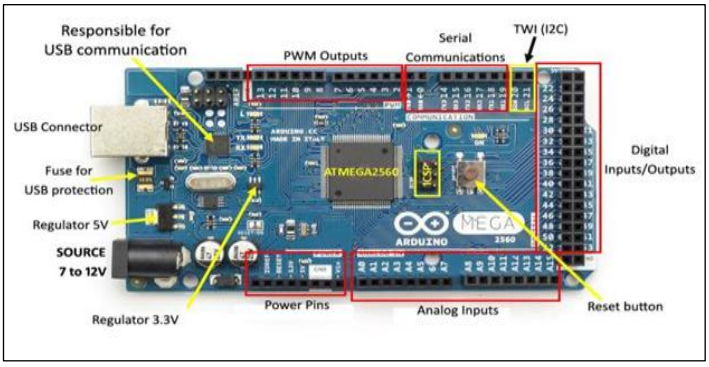

Figure 5: Arduino Mega2560.
Source: Authors, (2020).

2) SIM808 Module: Sim 808 module is850/900/1800/1900 MHz quad-band GSM/GPRS module. It has a global position system technology for satellite navigation module having internal TCP/IP stack to able to connect with the internet through GPRS. It possesses on board SMA connector for GSM antenna and UFL connector to connect GPS antenna. It has a sim socket including antistatic protection with a micro sim card connector, 3 LEDs to provide module status. SIM 808 module consists of cellular serial ports allows to configure and communicate with GPS receiver for the purpose of calling data for geographical positioning and satellite status through Arduino mega controller. All GPS function is controlled by AT command serial ports.

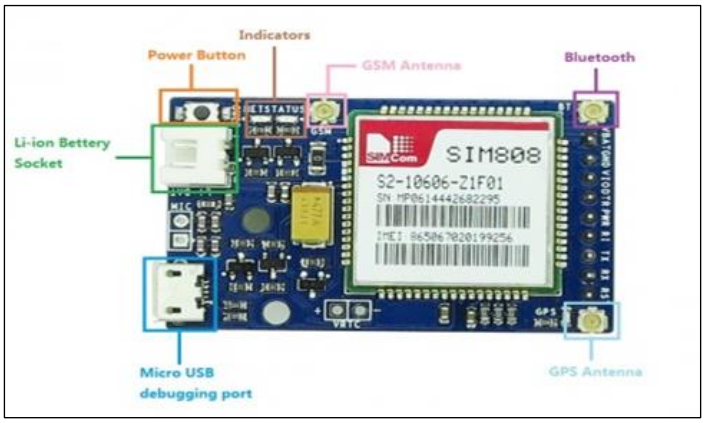

Figure 6: Sim 808 module.
Source: Authors, (2020).

3) GPS Antenna: GPS is a spaced navigation system. It can provide location and time information in all weather conditions. This technology detects latitude and longitude of the position and sends data to the microcontroller (Arduino Mega). Normally it needs three satellites to give exact position. So, for that antenna must be sky facing.

Figure 7: GPS antenna.
Source: Authors, (2020).

4) GSM Antenna: GSM (Global System For Mobile Communication) is a second-generation digital mobile telephone standard using time division multiple access. GSM provides basic to advanced voice and data services including roaming service. GSM antenna is an antenna that transmits GSM signal in a certain frequency of 850, 900, 1800, 1900, 2100MHz. GSM antenna boosts the signal strength in receiving and transmitting.

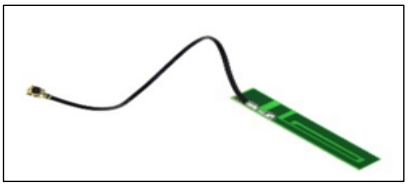

Figure 8: GSM antenna.
Source: Authors, (2020).

5) Battery: A Lithium Polymer battery power of 2200 mAh is used for the system. It is used to give the system power.

III.2 SOFTWARE SYSTEM

1) ARDUINO IDE: IDE stands for "Integrated Development Environment". It is a software introduced by Arduino .cc. It is mainly used for editing, compiling, and uploading the code to Arduino device. Almost all the modules and libraries are compatible with the software. IDE is cross-platform application written in JAVA. It has features such as syntax highlighting, brace matching, and automatic indentation. Arduino IDE comes with a c/c++ library called wiring that helps operations many users friendly. IDE has 2 parts one is Editor and Another one is Compiler.

2) Messages: Messages is an application that is popular among phone users. Android SMS is allows you to receive (SMS) messages and send messages to other phone numbers. Standard carrier rates may apply. This requires the IFTTT app. In the tracking system location is sent to phones through the messages. It contains longitude and latitude

3) Google Maps: Google Maps is a web mapping. It gives us satellite images, street maps, 360° interactive panoramic views, real-time traffic conditions. It also gives us a route to go from one place to another place. In the tracking system, a link of google Maps is sent so that it becomes easy to find the exact location of the tracker.

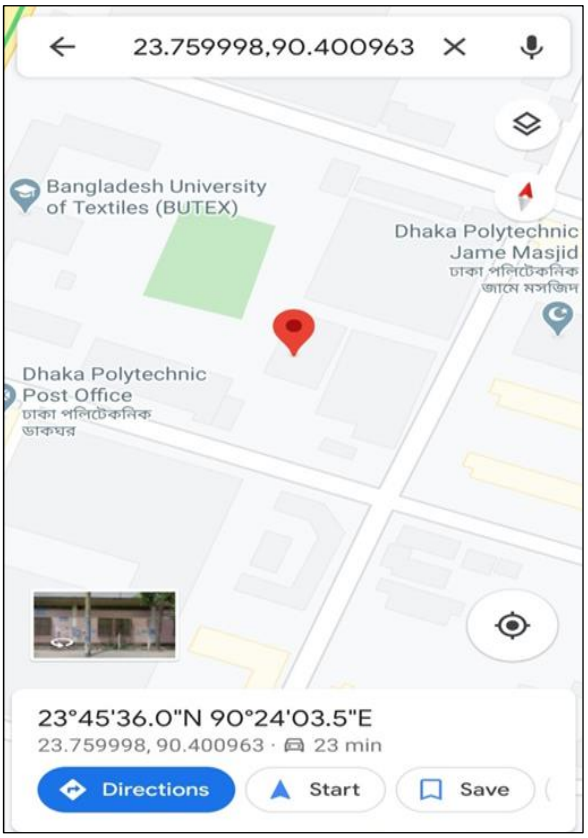

Figure 9: GPS tracking location on Google map.
Source: Authors, (2020).

III.2.1 System Implementation

In the system we have Arduino mega, sim 808 modules, GSM antenna, GPS antenna, and battery. To assemble the system we connect Arduino and sim 808 modules through jumper wires. Those are connected through transmitter pins and receiver pins of the microcontroller and sim 808 modems. GSM antenna and GPS antenna be connected to the GPS and GSM points of the module. After that, we connect battery on the power socket of Arduino Mega. Through the circuit diagram hardware, connections are shown easily.

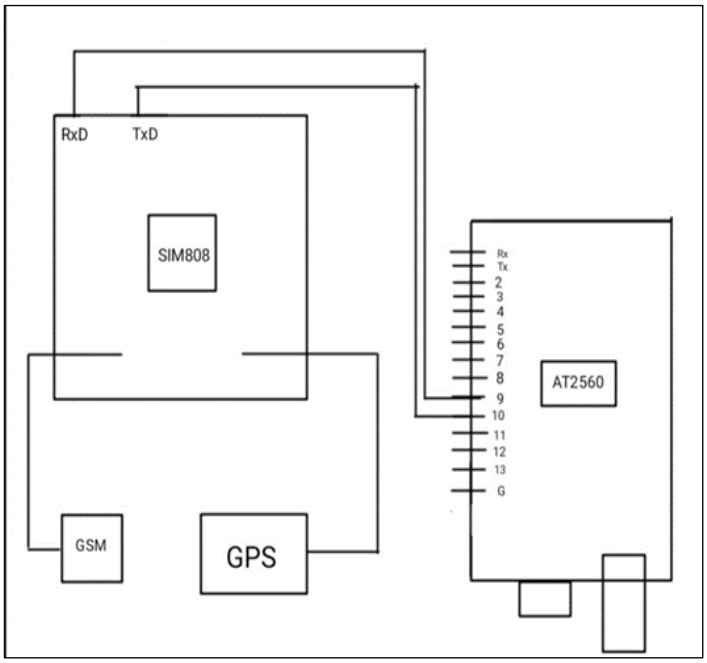

Figure 10: Circuit Diagram of the system.
Source: Authors, (2020).

Arduino Ide is the compiler where the code is uploaded to the Arduino mega so that system can run properly. To run the GSM module accurately can need to perform some attention command. GSM is the technology for mobile communication and it is used to connect the computer system over a network cause the GSM module is connected with Arduino. Receiver pin of Arduino is wired with transmitter pin of sim 808 modems. and transmitter pin of Arduino is wired with the receiver pin of sim 808 modems. Both are attached to the modem's shield. System needs attention command for selecting a mode for transfer and receive messages.

Table 3: Command information.

Command	Purpose
AT+CMGF	Text Mode
AT+CMGS	Send Message
AT+CMGD	Delete Message
AT+CMGSS	Send stored Message
AT+CMGA	Answer the call

Source: Authors, (2020).

After compiling the program, the system is ready to go. So, regarding knowing the position we need to call or send a message to the sim located to the module. After that the GPS antenna will try to connect three satellites to give position After connecting with three satellites it will reply with the longitude and latitude value and google links to the person's phone. Anyone can see the location of the system by inputting longitude and latitude on converter or google map link. Smartphone users can use google map to see the location after clicking the Gmap link. GPS receiver measures the distance between itself and the satellite. Receiver also measures time means exactly how long it takes each satellite's message to arrive. In this process, anyone can know the location.

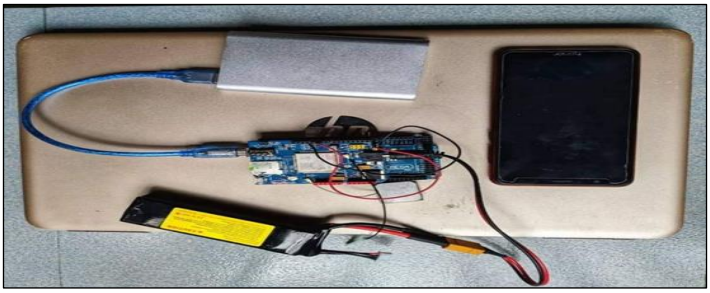

Figure 11: Anti-theft offline GPS tracker.
Source: Authors, (2020).

IV. CONCLUSION

The main aim of developing this product is to track technological gadgets when they are in offline mode. A command will be sent asking for the location of the device through SMS or phone call & the system will reply with its location in the form of longitude & latitude and link of Google map to a given phone number .The response will come shortly after command with real time location. It will help to retrieve lost or stolen devices that occurs almost every day in our lives.

Now we have developed a prototype of the product. In future this product can be modified heavily. Products shape and size can be manipulated for this usage of nano technology can be implemented. A high powerful GPS tracker will increase location accuracy. Response time can be accelerated. For location storage cloud system can be implemented. In future it can be useful for all types of tech gadgets and precious items. Further development will also decrease its price which will make it an affordable product.

V. REFERENCES

[1] S. Yamaguchi and H. Morita, "Efficient product design using functional equations," Journal of Advanced Mechanical Design, Systems and Manufacturing, vol. 12, no. 6, pp. 1–12, 2018, doi: 10.1299/jamdsm.2018jamdsm0114.

[2] M. A. Levin, T. T. Kalal, and J. Rodin, "Product Design Phase," Improving Product Reliability and Software Quality, pp. 273–297, 2019, doi: 10.1002/9781119179429.

[3] J. A. Barton, D. M. Love, and G. D. Taylor, "Design determines 70% of cost? A review of implications for design evaluation," Journal of Engineering Design, vol. 12, no. 1, pp. 47–58, 2001, doi: 10.1080/09544820010031553.

[4] H. Jiang, C. K. Kwong, and X. G. Luo, "Intelligent Quality Function Deployment," Intelligent Decision Making in Quality Management, vol. 97, pp. 327–362, 2016, doi: 10.1007/978-3-319-24499-0_11.

[5] N. N. S. Hlaing, M. Naing, and S. S. Naing, "GPS and GSM Based Vehicle Tracking System," International Journal of Trend in Scientific Research and Development, vol. 3, no. 4, pp. 271–275, 2019, doi: 10.31142/ijtsrd23718.

[6] O. A. Mohamad, R. T. Hameed, and N. Ţăpuş, "Design & implementation of real time tracking system based on Arduino Intel Galileo," in Proceedings of the 8th International Conference on Electronics, Computers and Artificial Intelligence, Ploiesti, ROMÂNIA., 2017, doi: 10.1109/ECAI.2016.7861114.

[7] N. M. Dhanya, "Anti-Theft Vehicle Tracking System using GPS and Location Prediction," International Journal on Advanced Science, Engineering and Information Technology, vol. 8, no. 6, pp. 2584–2589, 2018, doi: 10.18517/ijaseit.8.6.2847.

[8] A. Mounika and A. Chepuru, "IoT based vehicle tracking and monitoring system using GPS and GSM," International Journal of Recent Technology and Engineering, vol. 8, no. 2 Special Issue 11, pp. 2399–2403, 2019, doi: 10.35940/ijrte.B1275.0982S1119.

[9] P. Patel, S. K. Rauniyar, T. Singh, B. Dwivedi, and P. H. Tripathi, "Arduino Based Child Tracking System Using GPS and GSM," International Research Journal of Engineering and Technology (IRJET), vol. 5, no. 3, pp. 4137–4140, 2018.

[10] S. Gullipalli, Y. Karri, and S. Kota, "GPS Live Tracking of Buses and Fuel Monitoring System using Arduino," International Journal for Research in Applied Science and Engineering Technology, vol. 6, no. 3, pp. 2278–2285, 2018, doi: 10.22214/ijraset.2018.3362.

[11] P. Kaur, A. Das, M. P. Borah, and S. Dey, "Smart Vehicle Safety System Using Arduino," ADBU Journal of Electrical and Electronics Engineering (AJEEE), vol. 3, no. 1, pp. 20–25, 2019, [Online]. Available: www.tinyurl.com/ajeee-adbu.

[12] I. B. Asianuba and R. O. Okeke, "Gps/Gsm Technology for Anti-Theft Control System," American Journal of Engineering Research (AJER), vol. 7, no. 10, pp. 189–195, 2018, [Online]. Available: www.ajer.org.

[13] M. S. Uddin, M. M. Ahmed, J. B. Alam, and M. Islam, "Smart Anti-Theft Vehicle Tracking System for Bangladesh based on Internet of Things," in 4th International Conference on Advances in Electrical Engineering, Dhaka, Bangladesh., 2017, pp. 624–628, doi: 10.1109/ICAEE.2017.8255432.

[14] S. Paing, M. Oo, M. Othman, and N. Funabiki, "A Personal Use Vehicle Anti-Theft Tracking System Using IoT Platform," International Journal of Computer & Software Engineering, vol. 4, 2019, doi: 10.15344/2456-4451/2019/141.

[15] M. S. Ahmmed, T. Z. Chowdhury, and S. K. Ghosh, "Automatic Street Light Control System using Light Dependent," Global Journal of Research In Engineering, vol. 18, no. 1, 2018, [Online]. Available: https://engineeringresearch.org/index.php/GJRE/article/view/1781.

[16] S. K. Ghosh, M. Rashid, N. Zoha, F. K. Torsha, and I. Z. Era, "Development of A Low- Cost Solar Water Purifier Using Metaheuristic Process," in 10th International Conference on Industrial Engineering and Operations Management, Dubai, UAE., 2020, pp. 1268–1277.

[17] M. Rashid, S. S. Tushan, and S. K. Ghosh, "Development of Portable Electromagnetic Radiation Protective E-Textile," in 10th International Conference on Industrial Engineering and Operations Management, Dubai, UAE., 2020, pp. 337–344.